

Unmanned Aerial Vehicles for Vegetation Mapping: Opportunities and Challenges

Zur Erlangung des akademischen Grades eines

Doktors der Naturwissenschaften

von der KIT-Fakultät für Bau-, Geo- und Umweltwissenschaften

des Karlsruher Institut für Technologie (KIT)

genehmigte

Dissertation

von

Javier Lopatin Fourcade

aus Santiago de Chile

Karlsruhe, 2019

Tag der mündlichen Prüfung: 08. Juli 2019

Referent: Prof. Dr. Sebastian Schmidlein

Korreferent: Dr. habil. Angela Lausch



This document is licensed under a Creative Commons Attribution-ShareAlike 4.0 International License (CC BY-SA 4.0): <https://creativecommons.org/licenses/by-sa/4.0/deed.en>

Acknowledgments

I would like to thank the people who make this Ph.D. journey possible and enjoyable. Firstly, I thank Jaime Hernández and Mauricio Galleguillos to encourage me following the path of science: I will be in eternal debt for that. Secondly, I thank my laboratory fellows; Teja Kattenborn, Michael Ewald, Ulrike Merkel, Johannes Schmidt, for sharing their experiences and knowledge. You made the journey fun, even in times when the ship seemed to sink due to high sea-level rising and storms. Thirdly, special thanks to Fabian E. Fassnacht, who worked with me closely during the whole period, and was therefore guilty of most of my learning process. Likewise, I specially thank my supervisor, Sebastian Schmidlein, for teaching me the relevance of science accuracy and for giving my wife, Rocío, a place to stay and work at the institute: you allowed us to stay together when we scaredly arrived to a strange and foreign country, for that I will be always thankful.

My sincere gratitude to the Graduate School for Climate and Environment (GRACE) of the KIT, for supporting me with my scholarship, and for covering the travel costs of all those conferences, summer schools, and the research stay abroad. Those exchanges made my journey dynamic and allowed me to expand my scientific horizon. Similarly, I have to thank Gregory Biging and Iryna Dronova for hosting me in a very fruitful stay at the University of California Berkeley. You made me feel at home, and showed me whole new branches of research topics. I hope that our collaborations endure in time. How can I forgot Pablo Flores and Sle-gee Lee, my companions in that adventure.

I thank my family, who always supported my every decision and pushed me to follow my hart. You teach me the soft skills needed to survive every challenge. Finally, my infinite gratitude

to Rocío Araya, my wife and partner, who supported me during all difficulties, commented my every draft and pushed me to do better. I would not have done this without you.

Contents

Summary	vii
Zusammenfassung	ix
List of Figures	xi
List of Tables	xvi
Acronyms and Abbreviations	xix
1 Introduction	1
1.1 Estimating vegetation properties	1
1.2 Remote sensing of vegetation	2
1.3 Very-high resolution remote sensing and the concept of scale	6
1.3.1 Unmanned aerial vehicles (UAVs)	7
1.3.2 Opportunities and challenges of UAV applications	10
1.4 Research questions and list of publications	14
2 Mapping plant species in mixed grassland communities using close range imaging spectroscopy	17
2.1 Abstract	17
2.2 Introduction	18
2.3 Methods	21
2.3.1 Study area	21
2.3.2 Complexity gradient	22

2.3.3	Spectral data	24
2.3.4	Species classification and cover estimation	25
2.4	Results	29
2.4.1	Model performances	29
2.4.2	What causes the differences in model quality?	29
2.4.3	Impact of spatial resolution, canopy complexity, species cover and functional types on cover estimates	32
2.5	Discussion	33
2.5.1	Model performances	33
2.5.2	Impact of spatial resolution, canopy complexity, species cover and functional types on cover estimates	36
2.5.3	Semi-automatic field survey: strength, limitations and future considerations	38
2.5.4	Transferring the present approach to UAVs	39
2.5.5	Suitable environments and applications of the model	40
2.6	Conclusions	41
3	How canopy shadow affects invasive plant species classification in high spatial resolution remote sensing	43
3.1	Abstract	43
3.2	Introduction	44
3.3	Materials and methods	47
3.3.1	Study sites and target species	47
3.3.2	UAV data acquisition and derivation of presence data for the target species	48
3.3.3	Shadow detection	49
3.3.4	Derivation of independent variables from the UAV data	50
3.3.5	Modeling and validation	51
3.3.6	Species occurrence maps	53
3.3.7	Shadow fraction simulation analysis	53

3.4	Results	54
3.4.1	Model performances and independent variable selection	54
3.4.2	Model predictions	57
3.4.3	Shadow fraction simulation analysis	59
3.5	Discussion	60
3.5.1	Shadows effects in MaxEnt models	60
3.5.2	Variable importance	63
3.5.3	Classification approach	65
3.6	Conclusions	65
4	Using aboveground vegetation attributes as proxies for mapping peat- land belowground carbon stocks	67
4.1	Abstract	67
4.2	Introduction	68
4.3	Materials and methods	70
4.3.1	Study site	70
4.3.2	In-situ / reference data	71
4.3.3	UAV data acquisition	72
4.3.4	Selected aboveground vegetation attributes	73
4.3.5	Algorithms used	75
4.3.6	Modeling and validation	76
4.3.7	Maps	80
4.4	Results	80
4.4.1	Model performances	80
4.4.2	Spatial extrapolation of belowground C stocks	83
4.5	Discussion	83
4.5.1	Linkages between vegetation attributes and belowground C stocks	83
4.5.2	Model performances	85
4.5.3	Variable importance	89

4.5.4	Belowground C stocks extrapolations	90
4.6	Conclusions	91
5	Synthesis	93
5.1	How structural and community plant attributes impair the success of woody and herbaceous species mapping with UAVs?	93
5.2	How very-high resolution data can be used to obtain reference data for subsequent species classifications?	94
5.3	How aboveground vegetation structure and composition estimated from UAV relate to peatland belowground carbon stocks?	95
5.4	Potentials for future research	97
	References	118
	A Appendices	119
	Appendix 1	119
	Appendix 2	128
	Appendix 3	131

Summary

Plants are closely linked to a range of ecosystem processes and services, providing food and fresh water, climate regulation, and support soil formation and carbon storage. Therefore, vegetation attributes, such as species abundance, biodiversity, and plant traits, can be used to evaluate and monitor ecosystem processes. Accurately assessing recent vegetation changes is thus crucial to understanding current and future ecosystem dynamics.

The use of remote sensing data has been ascribed with high potential to spatially map vegetation attributes and processes. Whilst the advantages of coarse grain remote sensing to understand regional and global processes is well known, the study of fine-scale processes has increased in the last decades due to the growing availability of very-high resolution data. Methods developed using coarse grain data are often not able to fully harness the full potential of fine-scale data, due to differences in data properties. Therefore, new approaches are needed for very-high resolution data. Advantages of fine-scale data includes the direct detection of species crowns, and matching between field and remotely sensed data. These foster the use of very-high resolution data to e.g. map species occurrences at the level of individuals, and predict community-level attributes such as plant biodiversity, aboveground biomass and floristic compositions with high spatial detail. Unmanned aerial vehicles (UAVs) are ascribed to be a cost-efficient platform to obtain very-high resolution data, specially for small areas. However, their use for methodological development and ecological experimentation in small scale areas is relatively unexplored. The aim of this thesis was to assess the strengths and limitations of UAVs for vegetation mapping. The thesis focused in two main topics: plant species, and detailed ecosystem process mapping. Here, a case study showed that the use of very-high resolution data to classify grasslands individuals is constrained by the canopy mixture within different species. This suggests that the

use of remote sensing to directly map grassland species could be of operational value only in environments with low species cover and structural complexity, such as stress-prone dunes. A second case study revealed that shadows significantly affect the success of UAV-based classifications when mapping the invasive woody species *Ulex europaeus*, *Acacia dealbata* and *Pinus radiata*. This remained true using all sort of variables, such as optical, textural and canopy structural data. By means of simulations, it was depicted that each species creates shadows differently due to their specific canopy architecture. Therefore, the optimal UAV acquisition windows during the day differ among species.

A third case study showed that aboveground community attributes can be used as proxies to improve mapping accuracies of peatland belowground carbon stock. Here, a plot-level empirical model was fitted to assess the aboveground–belowground interdependencies. The aboveground variables included vegetation height, biomass, species richness, and species occurrences in continuous gradients. UAV-based data was then used to map the significantly depicted aboveground variables. Belowground carbon stock was then mapped by parameterizing the plot-based model with the UAV extrapolations. This suggests that ecosystem attributes with low direct influences on reflectance data can be mapped using vegetation parameters as proxies. Because the coupling of empirical models may induce unknown bias into each modeling steps, such approach is only recommended when strong empirical links are found between the plot-based variables. This thesis demonstrates that the use of very-high resolution data obtained from UAVs is useful to semi-automatically acquire field reference data, to develop new methodologies to decrease classification uncertainties on very-high resolution products, and to link plant community attributes with ecosystem processes. The thesis further make recommendations and suggestions to improve future research of fine-scale vegetation processes.

Zusammenfassung

Pflanzen sind eng mit einer Reihe von Ökosystemprozessen und -dienstleistungen wie die Bereitstellung von Lebensmitteln und Trinkwasser, die Klimaregulierung sowie die Bodenbildung und Kohlenstoffspeicherung verbunden. Deshalb können Vegetationseigenschaften wie Artenreichtum, Biodiversität und Pflanzenmerkmale zur Bewertung und Überwachung von Ökosystemprozessen genutzt werden. Die genaue Beobachtung von Vegetationsveränderungen ist daher entscheidend für das Verständnis der aktuellen und zukünftigen Ökosystemdynamik.

Fernerkundungsdaten haben hohes Potenzial Vegetationseigenschaften und -prozesse räumlich abzubilden. Die zunehmende Verfügbarkeit von sehr hochauflösenden Fernerkundungsdaten ermöglicht auch die Untersuchung von feinskaligen Prozessen. Die für niedriger aufgelöste Fernerkundungsdaten entwickelten Auswertungsverfahren sind häufig nicht auf sehr hochaufgelöste Daten übertragbar. Daher werden neue Verfahren benötigt, um das volle Potenzial auszuschöpfen. Die Vorteile von sehr hochauflösenden Daten liegen unter anderem in der Erkennung von einzelnen Pflanzen und der besseren räumlichen Feinabstimmung mit Felddaten. Diese Vorteile ermöglichen die genaue Kartierung von Pflanzenarten auf der Ebene einzelner Individuen und Vegetationseigenschaften auf der Ebene von Pflanzengesellschaften, wie die Biodiversität, oberirdische Biomasse oder Artenzusammensetzung. Unbemannte Luftfahrzeuge (UAVs) werden als kostengünstige Plattform zur Gewinnung von Daten mit sehr hoher Auflösung, insbesondere für kleine Gebiete, verwendet. Daher ist ihr Einsatz gut zur Entwicklung neuer Methoden geeignet.

Das Ziel dieser Arbeit war die Feststellung von Vorteilen und Limitierungen der Nutzung von UAVs zur Vegetationskartierung. Der Fokus der Arbeit lag auf zwei Hauptthemen, die Kartierung von Pflanzenarten und kleinräumigen Ökosystemprozessen. Eine der Fallstudien

zeigte, dass die Verwendung von sehr hochauflösenden Daten zur Klassifizierung von Pflanzenarten durch die Überlappung verschiedener Arten erschwert wird. Daher ist Nutzung solcher Daten zur direkten Kartierung von Grünlandarten nur für Habitats mit geringer Vegetationsbedeckung und einfachen Strukturen, wie beispielsweise Dünenhabitats, vielversprechend. Eine zweite Fallstudie ergab, dass der Schattenwurf von Baumkronen den Erfolg von UAV-basierten Klassifikationen der invasiven Baumarten *Ulex europaeus*, *Acacia dealbata* und *Pinus radiata* erheblich beeinflusst. Dabei machte es keinen Unterschied ob optische Daten oder Informationen über die Textur oder Kronenstruktur verwendet wurden. Anhand von Simulationen wurde dargestellt, dass jede Art aufgrund ihrer spezifischen Kronenarchitektur unterschiedliche Schatten erzeugt. Die optimalen Zeitfenster zur Klassifikation im Verlaufe eines Tages unterscheiden sich daher zwischen den einzelnen Arten.

In einer dritten Fallstudie wurde gezeigt, dass Merkmale der oberirdischen Vegetation als Proxy genutzt werden können um Kartierungen von unterirdischen Kohlenstoffvorräten in Mooren zu verbessern. Ein empirisches Modell wurde genutzt um unter- und oberirdische Merkmale zu verknüpfen. Dafür wurden kontinuierliche Daten mit Informationen über Höhe, Biomasse, sowie den Artenreichtum und die Artenzusammensetzung der Vegetation verwendet. UAV Daten wurden genutzt um die relevanten oberirdischen Merkmale zu kartieren. Der unterirdische Kohlenstoffvorrat wurde dann durch die Parametrisierung des plotbasierten Modells mit den UAV-Extrapolationen kartiert. Dies deutet darauf hin, dass auch Ökosystemeigenschaften mit geringem direkten Einfluss auf die Reflektanz mit Hilfe von Vegetationsmerkmalen als Proxies kartiert werden können. Da bei Kopplung empirischer Modelle in jedem Modellierungsschritt fehlerbehaftete Voraussagen entstehen können, wird ein solcher Ansatz nur empfohlen, wenn starke empirische Verbindungen zwischen den feldbasierten Variablen vorliegen.

Diese Arbeit zeigt, dass mit UAVs erhobene Erdbeobachtungsdaten geeignet sind, um die technischen und umweltbedingten Voraussetzungen für eine erfolgreiche Kartierung von Pflanzenarten zu erforschen, um neue Methoden zu entwickeln, welche die Genauigkeit von Klassifikationen aus sehr hochaufgelösten Daten erhöhen und um Vegetationseigenschaften mit unterirdischen Gradienten zu verknüpfen. Die Arbeit enthält außerdem Empfehlungen und Vorschläge für die zukünftige Erforschung von feinskaligen Vegetationsprozessen.

List of Figures

1.1	Optical characteristics of remotely sensed data. a) The electromagnetic spectrum, where the visible portion is highlighted; b) Sensor measurement of vegetation reflectance; c) Spectral sensor types.	4
1.2	a) Typical vegetation spectral signature with typical wavelength absorption interpretations (Jones and Vaughan, 2010); b) Sensitivity of plant traits in the optical range of the electromagnetic spectrum according to radiative transfer model simulations (PROSAIL). This shows that vegetation traits shape the spectral behaviors in intricate ways.	5
1.3	Typical Structure-from-Motion processing pipeline. a) UAV flight plan, including flight line separation depending on sensor field of view (FOV) and flight altitude; b) alignment of UAV tiles by common ground object identification; c) create dense mesh of 3D point clouds, and d) create the orthomosaic.	8
1.4	Effects of UAV characteristics on species classification. a) Schematic where UAV acquisitions with low tile density result in larger data gap (dark gray) around closely spaced canopies (Hendrickson et al., 2016); b) examples of UAV ortomosaics on different forest types with their respective canopy shadows; and c) theoretical example of reflectance within-class variation in images with course (top) and fine (bottom) spatial resolution. Coarser grains have less reflectance extream values due to mixed sunlit–shaded canopies.	12
1.5	Example of belowground attribute predictions by using UAVs and pre-existing deterministic feedbacks. a) UAVs are used to estimate aboveground vegetation parameters, such as biomass and species richness, and b) aboveground–belowground linkages are studied empirically by e.g. independent or nested regressions.	13

2.1	Experimental setup. A: image of the AISA+ sensor scanning a plot; B: plot structure (i), species occurrence and location recording at sub-plot level (ii) and the pin-point density grid to estimate species covers at the sub-plot level (iii); C: complexity gradient hypothesis, and D: location of the examined plots on the KIT Campus.	22
2.2	Schematic work flow of the analysis.	26
2.3	Bootstrap distribution of classification results using all sub-plots. In (A), the overall accuracy and Kappa of the SVM classification are presented, while in (B-D) the prediction accuracies (r^2 , RMSE and bias) of the measured against the predicted species covers are displayed. Beanplots show the relative distribution of the bootstrap results with the width indicating the frequency of a given value, while black horizontal lines indicate the median values of the distribution.	30
2.4	Model covers predictions. A: scatter plot of observed versus predicted species cover values; B: frequency distribution of false negative, false positive and correctly classified species (presence detected) at the sub-plot level are displayed.	31
2.5	Examples of prediction maps at the sub-plot level for the four complexity categories. Images obtained with a RGB color composition of the AISA+ scan, the classification results and the coefficient of variation map of the bootstrap procedure are presented. For the classification, the mode class of the bootstrapping procedure is drawn in each pixel.	32
2.6	Per pixel variability in the classification results. Zoom-ins within two sub-plots (A and B) are presented with the RGB compositions (left) and the Shannon Index maps (right). Main sources for high variabilities are shadows and structural edges (mixed pixels).	33
2.7	Impact of different sources of variation on the predicted cover. The sources of variation are: (A) the spatial resolution of the scans, (B) the complexity gradient of the plots, (C) the species cover within the sub-plots, and (D) the species functional types. All analyses (except for the spatial resolution) were performed with ~ 3 mm pixel size. The beanplots show the distribution of model performances for all sub-plots, where wider areas represent a higher frequency. Black dots show the mean distribution value and horizontal lines the standard deviation.	34

3.1	(A) Study areas in central-south Chile. (B–D) show the UAV-based RGB imageries. Blue polygons indicate the presence of the invasive species.	50
3.2	Model performances for sunlit (a) and shaded (b) canopies using models that include (incl.) and exclude (excl.) shadows in the calibration data. The median iterative values are presented, with dot size scaled to the values. A.d. = <i>Acacia dealbata</i> ; U.e. = <i>Ulex europaeus</i> ; P.r. = <i>Pinus radiata</i> . * depicts significant ($\alpha = 0.05$) improvements of the models: (a) shows significant improvements of models excluding shaded canopies. Contrary, (b) shows significant improvements of models including shaded canopies.	55
3.3	Variable importance based on MaxEnt permutation for the models including and excluding shaded canopies in the calibration data. Median and standard deviation values of the iterative validation are represented by barplots and error bars, respectively.	58
3.4	Relative likelihood predictions using different independent variables. Models including and excluding shadows during calibration are presented.	58
3.5	Comparison of species occurrence maps between models including and excluding shaded canopies in the calibration data. Models presented: <i>A. dealbata</i> and <i>P. radiata</i> = strctttextrgb, <i>U. europaeus</i> = hyper.	59
3.6	Shadow simulation using the digital surface models (DSM) and the sun elevation and zenith angles corresponding to beginning, middle and end of the summer season (i.e. 21-12-2017, 04-02-2018 and 20-03-2018 of each study site: (a) shows the simulated shadow fractions between 9:00 hrs - 18:00 hrs; (b) shows an RGB subsample of the target species canopies; and (c) shows the number of times (in percentage) that the pixels of the target canopies were under shadow for the daily period of the middle summer day (04-02-2018).	60
4.1	(a) Location of the study area in Chile; (b) UAV false color composite (R = 765 nm, G = 665 nm, B = 565 nm) of the study area with plot locations scaled with the measured belowground C stock (blue points). The dashed line shows the border between the conservation area (bottom) and the managed area (upper); (c) detailed sampling design.	71

4.2	The hypothesized model for the plot-based PLS-PM. Solid black lines represent expected effects obtained from literature. Examples are (1), (2), (3), (4), (5) and (6) Lawson et al. (2014); (7) Rocchini et al. (2018); (8) Dorrepaal et al. (2007); (9) and (10) Dorrepaal et al. (2005); (11) and (12) Lange et al. (2015) and (13) Lawson et al. (2014), Akumu and McLaughlin (2014) and Draper et al. (2014).	77
4.3	Methodological workflow of the predictive models. In (a) and (b) belowground C stocks independent predictive models using RF and PLS-PM were applied using the plot-based and UAV-based predictors, respectively; and (c) the hybrid models combining the SEM plot-based information with the RF UAV estimations.	78
4.4	(a) Resulting PLS-PM model using plot-based information. Arrows represent unidirectional relationships among LVs. Solid and dashed arrows denote positive and negative relationships, respectively. Arrows with non-significant coefficients ($\alpha = 0.05$) were not drawn. The thickness of the paths is scaled based on the magnitude of path coefficient (β). Path coefficients and internal R^2 correspond to mean bootstrap values of the internal PLS-PM validation. (b) Bar plot showing the variable importance (direct + indirect effects) of the vegetation attributes to predict belowground C stocks. Asterisks (*) indicate a significant ($\alpha = 0.05$) influence over belowground C stocks.	81
4.5	Scatterplots of observed versus predicted values of belowground C stocks for: (a) the direct use of random forests using UAV-based predictors, and (b) the hybrid model combining PLS-PM plot-based information and RF UAV predictions. The dots and the error bars represent the median and the standard deviation of the values generated in the iterative validation, respectively. (c) Bootstrapping distribution of accuracies. Asterisks (*) indicate a significant differences ($\alpha = 0.05$)	84
4.6	Belowground C stocks prediction maps using random forests (RF) with UAV-based predictors (left) and the hybrid model combining PLS-PM plot-based information and RF UAV estimations (right). The maps represent the median (top) and the coefficient of variation (CV; below) of the 500 bootstrapping iterations.	86

- 4.7 Spatial distribution of the PLS-PM LV scores produced by RF regressions (Figure 3 iii). RGB map representations using only aboveground peatland characteristics (a), and a mix of above with belowground variables (b). The variables were normalized (0-255) and plotted with a 20–80 % percentiles linear stretching. BM = vascular aboveground biomass, FC = floristic composition, SR = vascular species richness and Depth = soil depth. The dashed line is the border between the conservation (southern) and the managed (northern) areas. 87
- A.1 Bootstrap distribution of classification results using all sub-plots. In (A), the overall accuracy and kappa of the SVM classification are presented, while in (B-D) the prediction accuracies (r^2 , RMSE and bias) of the measured against the predicted species covers are displayed. Distributions for the pot (black) and the isolation (gray) methods (for collecting training data) are depicted. Beanplots show the relative distribution of the bootstrap results with the width indicating the frequency of a given value, while black horizontal lines indicate the median values of the distribution and * indicates a significant difference of the distributions ($\alpha = 0.05$; Lopatin et al., 2016). 122
- A.2 MRPP wavelength distance analysis of single spectral bands. Results using all species, only graminoids and only forbs are presented. A describes the proportion of the distances explained by group identity. Values of A over 0.3 are shown as black areas. In the presented spectral signatures, the 5, 25, 50, 75 and 95 percentiles of all analyzed spectra are displayed. 124
- A.3 Bootstrap distributions of classification and cover prediction (%) accuracies of all models. Model symbols (\circ , \triangle , \square , $+$) shows the mean value of the bootstrap distribution while the vertical line depict the standard deviation of the bootstrap distribution. Wider areas represent a higher frequency. Spectra = spectral bands as input; MNF = minimum noise fraction transformation as input; bn = preprocessing using brightness normalization of the spectral (Feilhauer et al., 2010). 128

A.4	Model performances for sunlit (A) and shaded (B) canopies using models that include (incl.) and exclude (excl.) shadows in the calibration data. The coefficient of variation (CV) iterative values are presented, with dot size scaled to the values. A.d. = <i>Acacia dealbata</i> ; U.e. = <i>Ulex europaeus</i> ; P.r. = <i>Pinus radiata</i> . * depicts significant ($\alpha = 0.05$) improvements of the models excluding shaded canopies over the models including shaded canopies (A) and of the models including shaded canopies over the models excluding shaded canopies (B).	130
A.5	Significant differences in terms of model performance among models using models excluding shadows in the calibration data.	131
A.6	PLS-PM structural model for the estimation of vegetation proxies, soil depth and belowground C stock using UAV-based predictors (Fig. 3b).	132
A.7	Results of the floristic gradient. (a) Distribution of plots (sample points) in the two-dimensional ordination space of NMDS, showing the distribution of the belowground C stock (left) and the management types (right) along the gradients. Close plots feature a similar species composition, while remote plots are more dissimilar. Vectors illustrate the correlations of the axes with the PLS-PM latent variables (H = vascular vegetation height, BM = vascular aboveground biomass, Rich = vascular species richness and Depth = soil depth). (b) Typical species identified with the isopam clustering algorithms in the NMDS first axis. Underlined species names indicate exotic species. (c) Floristic gradient obtained in the NMDS first axis with the plot locations (black dots) and the placement of the commons species on it. . .	133
A.8	Variable importance of the random forest models using the UAV-based predictors . . .	135

List of Tables

2.1	Summary of plot characteristics.	23
2.2	Summary of accuracies per functional types. The percentiles (P) 5 %, 25 %, 50 %, 75 % and 95 % are depicted.	31
3.1	Datasets for each invasive species. Texture corresponds to the GLCM variables while Structure corresponds to the CANUPO 3D variables. All datasets were tested at ~0.1 m pixel size.	51
3.2	Significant differences in terms of model performance between evaluations in sunlit and shaded canopies. Model including (incl.) and excluding (excl.) shadows during calibration are shown. Marks depict for which variable combinations and calibration data the performance was significantly better for sunlit than in shaded areas. A.d. = <i>Acacia dealbata</i> ; U.e. = <i>Ulex europaeus</i> ; P.r. = <i>Pinus radiata</i>	56
4.1	Plot-based variables included in the modeling.	75
4.2	Prediction accuracies of belowground <i>C</i> stocks applying plot-based information with random forests (RF) and PLS path modeling (PLS-PM). The median values of the iterative validation are shown. Asterisks (*) indicate a significant difference ($\alpha = 0.05$) between PLS-PM and RF.	82
4.3	Variable importance of the random forests plot-based model (Figure 3a).	82
4.4	Prediction accuracies of peatland characteristics (latent variables) using PLS-PM and RF with solely remote sensing information. Vegetation height was obtained directly from the UAV photogrammetric point cloud. All values are the median of the bootstrapping validation.	83
A.1	List of species along with respective producer (PA) and user (UA) accuracies and their r^2 , RMSE and bias from the cover estimation. Median values of the bootstrap iteration procedure are listed.	119

A.2 Parameterization of Agisoft Photoscan. Settings not included in the table were set as default. 129

A.3 PLS-PM outer model specifications. The weights correspond to the outer model coefficients while the loading are similar to the correlations in regression analysis. Non-significant predictors (n.s.) are highlighted in gray. 132

Acronyms and Abbreviations

AISA+	An airborne imaging spectroscopy sensor system.
DCM	Digital crown model, also known as normalized DSM, is the digital representation of the terrain's surface including all objects on it in elevation units aboveground. Is calculated as DSM minus DTM.
DSM	Digital surface model, a digital representation of the terrain's surface including all objects on it in elevation units above sea level.
DTM	Digital terrain model, a digital representation of the terrain's surface excluding all objects on it in elevation units above sea level.
Kappa	Measure of accuracy used in classifications. Kappa takes into consideration the probability that a sample was correctly classified by chance.
LAI	Leaf area index, a dimensionless measure of plant canopy density, calculated as one-sided green leaf area per unit ground surface area.
MNF	Minimum Noise Fraction, a feature extraction technique which combines a noise filter with a data transformation similar to the principle of the Principle Component Analysis.
NDVI	Normalized Difference Vegetation Index, a commonly used vegetation index calculated as the normalized difference of the bands the near-infrared and the red portion of the electromagnetic spectrum.
NIR	Near Infrared, refers to the spectral range between 700-1400 nm.

nRMSE	Normalize root mean square error, is the normalized form of the RMSE, where the error of the regression model is presented in percentage instead than in the target variables unit.
OA	Overall Accuracy, calculated in a confusion matrix as ratio of number of correctly classified pixels to total number of reference pixels.
PA	Producer's Accuracy, also known as omission error, calculated in a confusion matrix as ratio of number of correctly classified pixels of a category to the total number of pixels known to be of that category (column total).
PCA	Principle Component Analysis, a linear transformation method which searches for linear combinations of the predictors (bands) that capture a maximum amount of the variance inherent in the full dataset.
PLSR	Partial least squares regression, a statistical regression method that maximize the predictor information into less correlated components.
PLS-PM	Partial least square path modeling, a structural equation modeling component-based algorithm.
RF	Random Forest, an ensemble based machine learning method which can be used for classification and regression problems.
RMSE	Root mean square error, a frequent measure of error or difference between the predicted and observed values of a regression model. Is in the same units than the target variable.
RS	Remote sensing, the acquisition of information about an object or phenomenon through a device that is not in physical contact with the object.
SEM	Structural equation modeling, a family of regression methods that can test multiple relations at the same time. Used for hypothesis testing and prediction.

SVM	Support Vector Machines, a machine learning method which can be used for classification and regression problems.
SWIR	Short Wave Infrared, refers to the spectral range between 1400-3000 nm.
UA	User's Accuracy, also known as commission error, calculated in a confusion matrix as ratio of the number of correctly classified pixels to the total number of pixels that were classified in that category (row total).
VHRRS	Very high resolution remote sensing, remote sensing data that has equal or less than 5 m spatial resolution.
VI	Vegetation Index, a normally dimensionless measure of vegetation-related properties, normally calculated by a mathematical combination of a few bands of a remote sensing dataset.
VIS	Visible, refers to the spectral range between 390-790 nm.

1 Introduction

1.1 Estimating vegetation properties

Terrestrial plants are crucial to maintaining the Earth's ecological processes, which include carbon and water cycling, bio-geochemical interactions, and climate regulation. Vegetation characteristics, such as species abundance, biodiversity and biomass, are closely linked to a range of ecosystem processes and services that operate across scales. These provide us with food and fresh water, regulate Earth's climate, and support soil formation and carbon storage.

Our society and economy both depend on the healthy functioning of plants and the resilience of the ecosystems they constitute. Yet, despite international commitments, such as the Convention on Biological Diversity CBD2010, global plant biodiversity and biomass continue to decline at unprecedented rates (TEEB, 2010). Ecosystem degradation and the loss of vegetation structure undermine ecosystem functioning and resilience, threatening the ability of ecosystems to continuously supply ecosystem services for present and future generations (de Groot et al., 2012). These threats are expected to grow as our planet's climate changes and humans consume ever more resources.

Vegetation characteristics are often used for evaluating ecosystem processes and functioning. The most commonly used characteristics are species composition and abundance, biodiversity, canopy structure or architecture, and plant traits or functional attributes (Thackway and Lesslie, 2008). For example, the occurrence and coverage (i.e., abundance) of certain species or plant functional types are often used to assess threats to biodiversity caused by invasive plant species (Binggeli, 1996) or to monitor sub-surface soil properties such as carbon stocks (Dorrepaal et al., 2005; Ma et al., 2017). Accurately assessing vegetation attributes is thus crucial to un-

derstanding current and future ecosystem dynamics across scales. These assessments are often measured locally through field surveys.

Field surveys are used to measure structural and compositional attributes of plant communities either visually, by exhaustive methods or by a mixture of both. Selecting a method is often a trade-off between accuracy and speed: exhaustive methods are accurate but time consuming, allowing the monitoring of smaller plots (e.g., the pin-point method of Levy and Madden, 1933); meanwhile, visual interpretation is faster but may introduce observation bias into the results, either by incompleteness of the listed flora or by inconsistency between surveyors (Klimeš et al., 2001; Vittoz and Guisan, 2007). Vittoz and Guisan (2007) found that only 45 % – 63 % of the species presences were seen by all observers surveying grassland ecosystems, and that a pair of observers missed 10 % – 20 % fewer species than a single observer. Vegetation surveys are often restricted to point observations, involve copious field-work, and are dependent on accessibility. Hence, they are often biased toward areas of easy access (Whittaker et al., 2005). Moreover, it is hard to generalize *in-situ* observations spatially or to scale them to larger areas (Kattge et al., 2011). Consequently, cost-efficient methods are needed to assess changes in vegetation attributes in a spatially continuous way.

The use of remotely sensed vegetation data represents an alternative to unravel global and local processes that could not be explained before using traditional local measurement (Ustin et al., 1991). The increasing availability of remote sensing products and technological advancements has fostered a new era of earth observation data. These are characterized by depicting detailed information of the Earth's surface, creating new opportunities and challenges that need to be addressed.

1.2 Remote sensing of vegetation

In nature, electromagnetic waves of all frequencies coexist, such as X-rays, visible light and radio waves. This continuum is referred to as the electromagnetic spectrum, which is usually divided up into regions (Figure 1.1a): The visible (VIS) region, to which the human eyes responds, covers only a small portion that partially corresponds with the photosynthetic active

region. The ultraviolet (UV), the X- and γ -ray regions occur in high-frequencies, while the infrared (IR) and the microwave regions occur in longer-wavelength of the spectrum. Portions of this electromagnetic spectrum are measured by optical remote sensing sensors and used to derive spatial-explicit information of the Earth's surface (Jones and Vaughan, 2010).

Optical sensors have considerable potential as a objective source of spatially continuous information of vegetation attributes, by measuring the solar radiance [W/m^2] that is reflected from the earth's surface at different portions of the electromagnetic spectrum (Figure 1.1; Ustin et al., 1991). The reflected portion of solar radiation is always smaller than the incoming radiation as some energy is absorbed by the earth's surface. The reflected radiance can thus be normalized into reflectance values [%] by comparing the incoming–reflected relation, either by simultaneous measurements of incoming solar radiance or by using a reference surface with known reflection properties. Optical sensors typically measure information comprised between the VIS and the IR (400 nm–2500 nm) in a spatial-explicit manner. This is done by dividing a 'picture' of a portion of the Earth's surface into smaller sections or 'pixels'. Each pixel has a multiple reflectance measurements covering a certain area on the ground. The 'picture' with all pixel-reflectance values altogether provide the spatial context that makes remote sensing data appealing to enhance vegetation-based studies. Reflectance relates to plant properties according to physical behaviors occurring between the plant and incoming radiation at the leaf and canopy level.

Due to the absorption characteristics of plants, reflectance data derived from optical sensors have been widely used to characterize vegetation attributes directly linked to structural and biochemical plant traits (Ollinger, 2011, Figure 1.2). These traits shape plant reflectance in different ways: the visible range (VIS, 400 nm–700 nm) depicts overall low reflectance as pigments absorbs the major part of the incident radiation (e.g., chlorophyll and carotenoids); the near-infrared range (NIR, 700 nm–1300 nm) shows high reflectance as the absorption by leafs is low due to cell mesophyll and other cell-structure characteristics; while light in the shortwave infrared (SWIR, 1400 nm–2500 nm) is predominantly absorbed by different leaf constituents (e.g., proteins, lignin, carbohydrates and waxes) and water content. Because water vapor is also

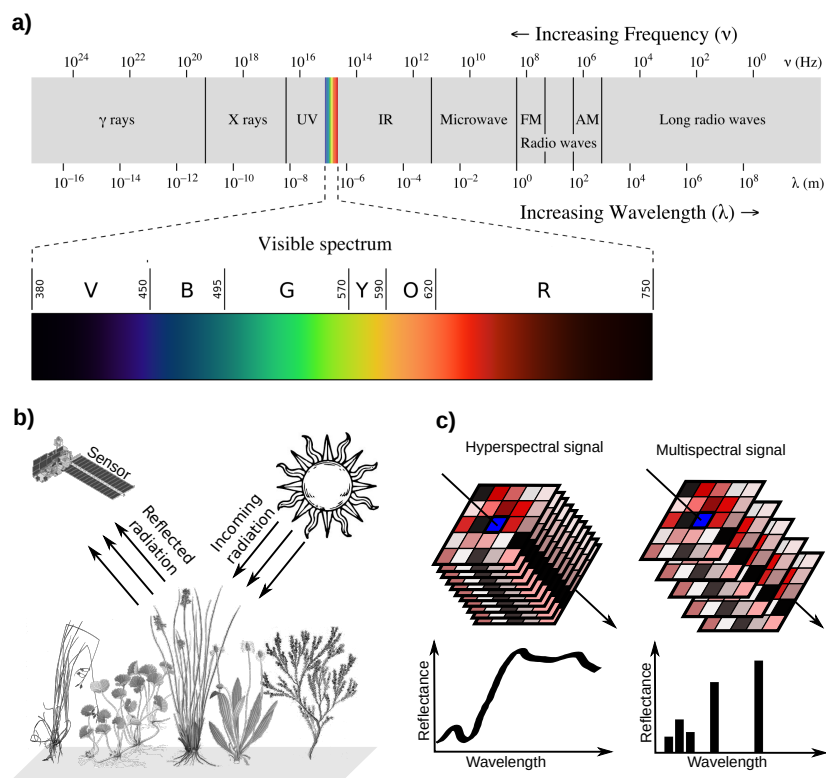


Figure 1.1: Optical characteristics of remotely sensed data. **a)** The electromagnetic spectrum, where the visible portion is highlighted; **b)** Sensor measurement of vegetation reflectance; **c)** Spectral sensor types.

one of the main components of the atmosphere, some SWIR portions are often worthless for analyses as are continuously undermined by strong noise.

Spectral resolution is defined as ‘*the ability of a sensor to define fine wavelength intervals and hence to discriminate between different component wavelengths in the scene, and is determined by the number and width of the individual spectral bands that are recorded*’ (Jones and Vaughan, 2010, Figure 1.1c). Sensors measuring discrete and relatively small portions of the electromagnetic spectrum are called multispectral sensors, while those measuring continuous portions of the electromagnetic spectrum in narrow bands are called hyperspectral sensors. The spectral resolution becomes important when detailed spectral information is needed, for example for mapping invasive species with similar morphological characteristics as the native species (He et al., 2011), mapping complex community mixtures (Schmidtlein and Sassin, 2004) or to retrieve canopy biophysical parameters that are sensitive only to specific narrow areas of the electromagnetic spectrum (Kattenborn et al., 2018a).

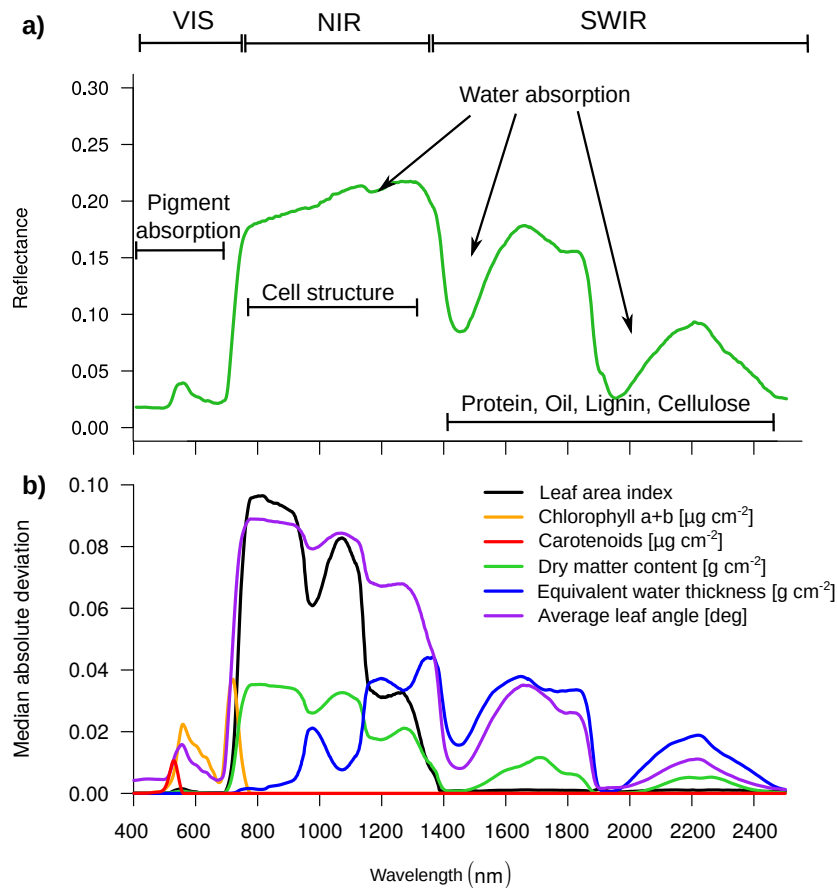


Figure 1.2: a) Typical vegetation spectral signature with typical wavelength absorption interpretations (Jones and Vaughan, 2010); b) Sensitivity of plant traits in the optical range of the electromagnetic spectrum according to radiative transfer model simulations (PROSAIL). This shows that vegetation traits shape the spectral behaviors in intricate ways.

The spatial resolution, or the pixel size, of remote sensing products is also an important characteristic to map plant attributes. Fine-scale spatial and spectral data is often best suited to reveal underlying vegetation mechanisms or plant traits (Anderson, 2018). At larger scales, vegetation functions are the combination of many fine-scale properties and processes that may combine in complex ways due to nonlinear responses and intricate feedbacks. Hence, the selected remote sensing spatial resolution determines to some extent which vegetation processes are detectable and how. Consequently, remotely sensed observations of vegetation functions and properties should consider carefully the scale, paying special attentions to possible underlying mechanisms at finer scales that may influence the emergent properties at larger scales (Gamon et al., 2019).

1.3 Very-high resolution remote sensing and the concept of scale

In ecological and remote sensing applications, the scale need to be selected carefully depending on the study aims. Commonly, the selected plot size in field surveys determine the amount of variations within measurements (Levin et al., 2007; Wiens, 1989). For example, large plot measurements of community patterns are expected to contain higher species richness per observation than smaller plots. This often leads to the inclusion of more rare species and environmental variation per measurement, therefore lowering the species turnover (Keil et al., 2015; Rosenzweig, 1995). Multiple ecological processes often drive vegetation patterns, acting across multiple spatial and organismal scales (Chase and Knight, 2013). Hence, there is rarely a single scale that best identifies how specific vegetation processes drive patterns (Anderson, 2018).

Remote sensing data at varying spatial resolutions can thus be used independently or in combination to assess different vegetation processes. Traditionally, moderate or coarse grain remote sensing products have been used more often than fine grain data due to their longer trajectory, lower price and ease implementation (Ustin et al., 1991). Yet, moderate and coarse grain systems often have the problem of scale mismatches with the field data. In such cases, the size of field plots (i.e., response data) are smaller than the grain size of the remote sensing product (i.e., predictors or feature data), which can obscure key patterns and processes operating between these scales (Anderson, 2018). For this reason, very-high resolution (VHRRS; here < 5 m) sensors and platforms have gained much interest in the scientific community, as their products share the same scale as field ecologists.

VHRRS allows the direct study of a large number of ecological properties that were not possible before with regional-scale sensors (Turner et al., 2003), such as detail forest structures for inventory purposes (Fassnacht et al., 2017), mapping of biodiversity indicators in species rich environments like tropical forests (Nagendra et al., 2010) and grasslands (Möckel et al., 2016), floristic mapping (Schmidtlein et al., 2007), tree species detection (Fassnacht et al., 2016), and urban management assessments (Agarwal et al., 2013). Satellite-based VHRRS data can be obtained nowadays from a varying range of sensor types and platforms (Figure 1.3). Multispectral

data with pixel sizes below 5 m are available from satellite-based platforms like Worldview-2 and -3, Pleiades, GEOEYE-1 and the recently launched Venus. While some of these sensors have a relatively high spectral resolution (e.g., Worldview-3 has 16 bands), the general rule is that sensors with high spatial resolution present low spectral resolution. Satellite-based VHRRS is often operationally constrained by: 1) high cost per scene for relatively small areas; 2) repetitive acquisitions are often only possible if oblique view angles are used; and 3) cloud contamination could obscure features of interest. Alternatively, airborne remote sensing can be used with a larger range of sensor types for fine-scale ecological studies, such as full-range hyperspectral. These systems usually obtain high qualities, but are very expensive which also hamper their use for mapping small areas. Therefore, the use of unmanned aerial vehicles (UAVs) in remote sensing applications has increased as consequence of the technical and economical gaps of airborne and satellite-based platforms.

1.3.1 Unmanned aerial vehicles (UAVs)

Unmanned aerial vehicles (UAVs), commonly known as drones, are aircrafts without a human pilot onboard. UAVs were created in a military context, yet their mapping potential was understood already in the late nineteen-seventies (Przybilla and Wester-Ebbinghaus, 1979). Any type of aerial vehicle able to carry a sensor is potentially a UAV, including balloons, kites or zeppelins. However, nowadays most UAVs used for scientific purposes are either rotopters (type of helicopter) or fix-wings (type of airplane). Rotopters usually cover relatively small spatial areas, are cheap, can flight at different speeds and are flexible in their deploy because they include vertical takeoff and landing. Fix-wings, however, cover bigger areas due to longer flight autonomy, but are often more expensive and need large areas for takeoff and landing. Recent advances in technology have developed hybrid UAVs, where rotopter characteristics are used for vertical takeoff–landing and fix-wing frames are used to maximize flight time and area cover (e.g., <https://www.altiuas.com/>). UAVs can carry all sort of payload, such as RGB consumer grade cameras (de Sá et al., 2018), multi- and hyperspectral optical sensors (Malenovský et al., 2017). Data obtained from these sensors are often processed in photogrammetric software's to create both 3D canopy data and orthomosaics with optical information.

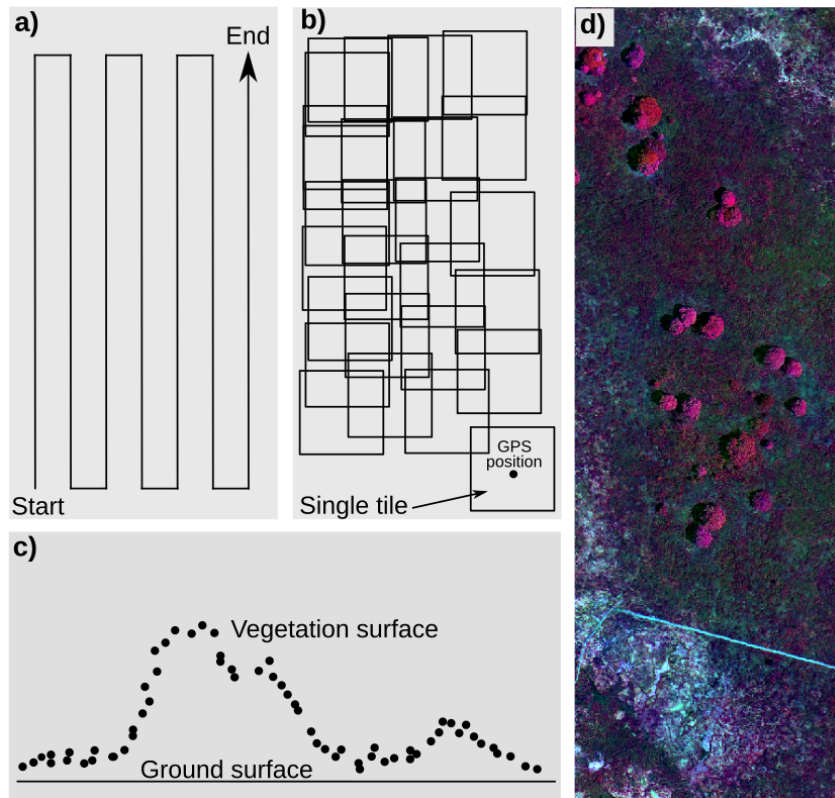


Figure 1.3: Typical Structure-from-Motion processing pipeline. **a)** UAV flight plan, including flight line separation depending on sensor field of view (FOV) and flight altitude; **b)** alignment of UAV tiles by common ground object identification; **c)** create dense mesh of 3D point clouds, and **d)** create the orthomosaic.

User-friendly photogrammetric software with Structure-from-Motion (SfM) capabilities are available to process UAV data (Dandois and Ellis, 2010). SfM algorithms resolve the alignment of camera positions, generating orthorectified aerial imagery and 3D models (i.e., point cloud and/or raster models) without the allocation of ground control points (Westoby et al., 2012, Figure 1.4.). Here, typical steps include the alignment of sensor frames, the creation of a dense mesh of 3D information, and the creation of orthomosaics (Figure 1.4). Some sensors, however, may need other type of processing pipeline, such as hyperspectral pushboom-based sensors. Snapshot-based sensors have the advantage of ease of implementation due to the large availability of processing software's, including proprietary and open source alternatives (e.g., <https://www.opendronemap.org/webodm/>), and the ability to create 3D information without the need of alternative sensors, such as light detection and ranging (Colomina and Molina, 2014). Such implementation makes the processing of UAV data attractive for natural management practitioners with basic knowledge in geomatics.

The increasing usage of UAVs created a strong economical niche, which forced the governments to rapidly adapt and create new laws to constrain their use to safe areas and conditions (Stöcker et al., 2017). From the legal perspective, UAVs can be divided into two main groups: systems below and over 5 kilos of takeoff including payloads. UAVs weighting less than 5 kilos have less restrictions: flight permissions are needed only when flying inside governmental areas, such as national parks, in urban areas and in the proximity of power towers, airports and military bases. Contrary, UAVs weighting more than 5 kilos always need permissions to flight. Such permissions are either free or not depending on the country. Bigger UAVs may carry heavier sensors and are often able to cover larger areas than low-weight systems, but their deployment restrictions may hamper spontaneous acquisitions due to e.g. good weather conditions. UAV pilots need certifications in most countries when the aircraft weight more than one kilo.

UAVs have been increasingly used in vegetation science because are often less expensive and more flexible than satellite or airborne-based VHRRS in their acquisitions when mapping relatively small areas (Anderson and Gaston, 2013), allowing the optimization of revisit times to the phenological cycle of the target species or community. However, UAV measurements could be very expensive when mapping large extents as repetitive field labor is often needed (Ørka and Hauglin, 2016). UAVs have been found useful to complement field labor as interference and disturbances of the study area are reduced (Jones et al., 2006; Sardà-Palomera et al., 2012). For example, Getzin et al. (2012) demonstrated how the fine spatial resolution data provided by UAV photography (7 cm pixel size) is useful for describing canopy-gap metrics relating to the floristic biodiversity of a forest understory. Meanwhile, de Sá et al. (2018) commented on the benefits of using the low aboveground altitude flight capabilities of UAVs to avoid contamination of image data by clouds. Flight planning need site-specific considerations, as low densities of UAV-tiles overlap may result in large image areas without information around closely spaced shrubs or trees (Figure 1.5a; Hendrickson et al., 2016).

UAVs have been used to obtain detail information of a large range of vegetation applications at the individual- and community-level. Studies to classify species at the level of individual have been performed in tree (Nevalainen et al., 2017; Franklin et al., 2017), shrub (de Sá et al., 2018; Breckenridge et al., 2011) and wetland species (Cao et al., 2018), where many of the tree

species applications relate to the detection of invasive species (Baena et al., 2017; Dvořák et al., 2015; Müllerová et al., 2013; Mafanya et al., 2017; Michez et al., 2016). Likewise, community-level studies have been performed to estimate biodiversity (Getzin et al., 2012), aboveground biomass (Husson et al., 2014; Dandois and Ellis, 2013; Zahawi et al., 2015), and photosynthetic pigments (Hernández-Stefanoni et al., 2012). Temporal revisits to study vegetation dynamics are further possible using UAVs due to the (relatively) nadir acquisitions of the photogrammetric data (Torres-Sánchez et al., 2014).

1.3.2 Opportunities and challenges of UAV applications

As remarked in the previous sections, remote sensing technologies have been used extensively to understand vegetation dynamics across scales (Ustin et al., 1991). Nevertheless, there is still room for improvements and the deploy of new methods and approaches, specially for very-high resolution technologies such as UAVs. The small pixel size of UAV-based data is beneficial for mapping plant attributes for two reasons: **A**) it allows for plant species detection at the level of individuals, and **B**) it reduces spatial mismatches between field and remote sensing data.

Concerning **A**), UAVs have been used extensively to map tree plant species (Lu and He, 2017; Alvarez-Taboada et al., 2017; Michez et al., 2016). However, most studies focused only in mapping the species without searching for possible technical and environmental factors hampering their classification performance. Technical factors hampering species classification have been more commonly studied using airborne and satellite-based data, such as the spatial (Nagendra, 2001), spectral (Dalponte et al., 2012) and temporal (Key et al., 2001) resolutions, and data type (Puttonen et al., 2010). For example, grain sizes smaller than the target species canopies are recommended, where pixels below 1 m are usually suggested as a rule of thumb (Nagendra, 2001). Nevertheless, the ideal pixel size will depend upon the crown size and the canopy closure, which can vary widely within and between species and vegetation types. However, the effects of vegetation attributes on the classification success have been less studied. For example, Korpela (2004) found that crown density and size, the influence of neighboring tree and the composition of the understory are likely to contribute to the success of tree species classification from any sensor type.

Further problems relate to the high bias towards woody species mapping compared to species of other growth forms, such as herbaceous plants encounter in grassland ecosystems. Only few studies have been focusing on such vegetation types, where usually only one or two species are studied simultaneously (Lu and He, 2017; Skowronek et al., 2017b; Gebhardt et al., 2006; Silva et al., 2014; Booth and Cox, 2008; Kumar and Sinha, 2014). This bias could be due to the small size of the herbaceous individuals and the high environmental heterogeneity of grassland ecosystems (Möckel et al., 2016), which may further hamper the proper detection of the individuals. However, the high spatial resolution of UAV-based data may allow for the direct detection of small-sized herbaceous species. The requirements regarding sensor resolution and community properties to ensure the successful species classifications in such environments are needed.

UAV-based data often have pixel sizes in the centimeter-range, causing that canopy characteristics such as branching and gaps are directly visible from the image. Because of this detail level, the information captured from UAVs differ from other sources of VHRRS, such as satellites and airborne. Therefore, approaches developed for general VHRRS data may not be directly applicable to UAV-based data. Hence, new methodologies are needed to exploit their full potential. For example, UAV data increases the within-class reflectance variability in species classification caused by extreme values in sunlit and shaded canopies (Figure 1.5c). Shadows result from the obstruction of light, causing a decrease of reflectance. In vegetated areas, cast shadows receive diffuse radiation (mostly Rayleigh scattering) from light scattered within the atmosphere or surrounding objects (Gu and Robles-Kelly, 2014). In practice, shadows can lead to either a reduction or a total loss of the spectral signal of a canopy (Zhang et al., 2015), affecting the success of classification tasks (Saha et al., 2005; Liu and Yamazaki, 2012). This is particularly harmful in forested areas where shadows may reduce the understory information. Therefore, careful considerations regarding acquisition time of the day are needed to reduce shaded canopies.

Finally, an efficient collection of reference data to train and validate UAV models is needed to efficiently map plant species. The quantity and quality of the training data are known to impact the accuracy of mapping products and hence play a key role in any operational approach (Foody,

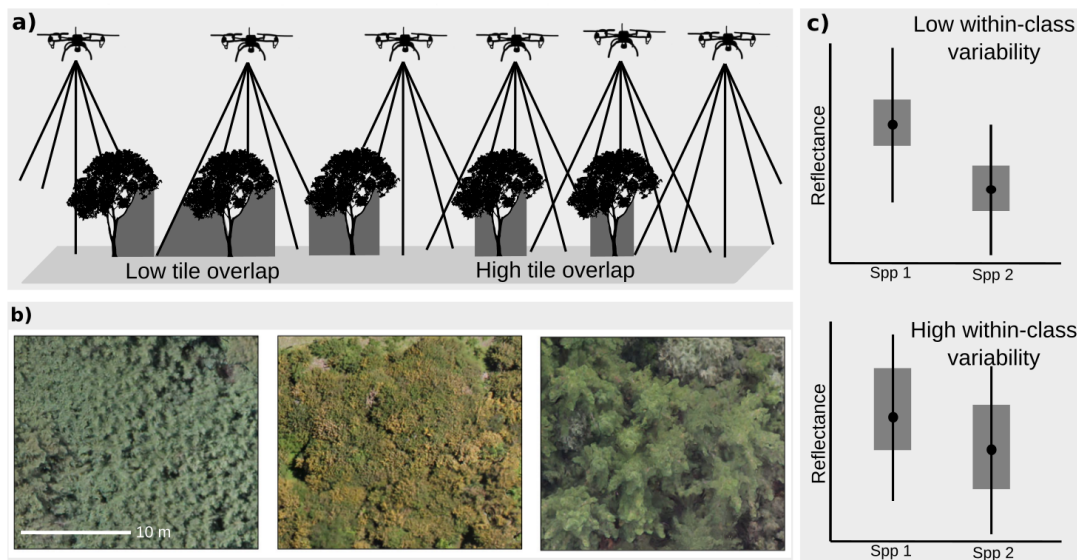


Figure 1.4: Effects of UAV characteristics on species classification. **a)** Schematic where UAV acquisitions with low tile density result in larger data gap (dark gray) around closely spaced canopies (Hendrickson et al., 2016); **b)** examples of UAV ortomosaics on different forest types with their respective canopy shadows; and **c)** theoretical example of reflectance within-class variation in images with coarse (top) and fine (bottom) spatial resolution. Coarser grains have less reflectance extreme values due to mixed sunlit–shaded canopies.

2010; Immitzer et al., 2018). Reference data for remote sensing applications are often acquired on the ground using GNSS-devices, which presents several limitations (Kaplan et al., 2014; Anderson, 2018): 1) the quantity of references is usually constrained as field campaigns are laborious and costly; 2) the quality and representativeness of observations is often impaired by GPS inaccuracies resulting from dense canopy cover in forested ecosystems (Valbuena et al., 2010), while accessibility often induce biases toward data obtained in areas of easy access. Visual estimation methods of species cover is challenging from below the canopy in forested ecosystems (Lepš and Hadincová, 1992), while species occurrences are often miss-represented in grasslands (Klimeš et al., 2001; Vittoz and Guisan, 2007); and 3) field data are often measured as discrete point observations or plots, which are not explicitly matching the continuous representation of earth observation data and its spatial scales (Turner, 2014; Anderson, 2018). Therefore, new approaches are needed to increase the quality and quantity of reference data for both woody and non-woody species mapping.

Concerning **B)**, the reduced errors caused by scale mismatches between field and UAV data is particularly important to accurately predict community-level attributes. For example, above-

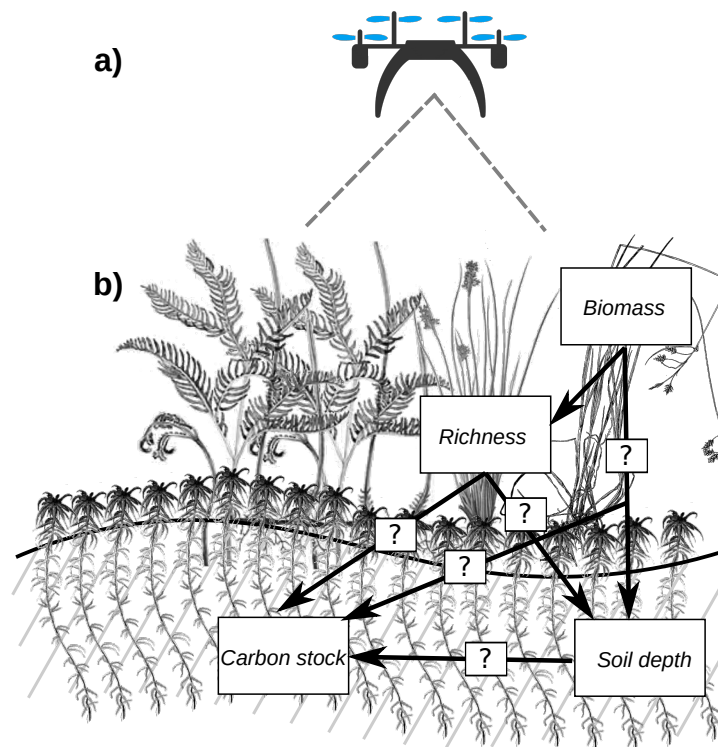


Figure 1.5: Example of belowground attribute predictions by using UAVs and pre-existing deterministic feedbacks. **a)** UAVs are used to estimate aboveground vegetation parameters, such as biomass and species richness, and **b)** aboveground–belowground linkages are studied empirically by e.g. independent or nested regressions.

ground properties such as biodiversity and biomass predictions have been estimated with high spatial detail using both spectral and 3D UAV-based information (Getzin et al., 2012; Husson et al., 2014; Dandois and Ellis, 2013; Zahawi et al., 2015). This level of detail is already a step-forward for spatial ecology and vegetation science, specially in highly-heterogeneous ecosystems such as grasslands and wetlands. However, the use of such highly detailed data for subsequent analysis is still rare. Aboveground vegetation properties could thus be used to estimate ecosystem processes that are less correlated with the UAV data, such as belowground carbon stocks. Predicting belowground carbon stocks solely with remote sensing data is often challenging as the links between aboveground (i.e., what is measure by remote sensing sensors) and belowground properties have usually non-linear or complex interdependencies (Dorrepaal et al., 2007). Nevertheless, field ecologists have studied deterministic linkages between aerial plant properties and belowground processes, such as carbon storage, for decades (Figure1.6;

Dorrepaal et al., 2007; Fenner and Freeman, 2011; Ma et al., 2017). Therefore, UAV-based remote sensing could directly investigate such relations spatially without scaling problems.

1.4 Research questions and list of publications

By analyzing the research gaps described in Chapter 1 section 3.2, the present thesis approached specific problems related to three different vegetation types: grasslands, forests and peatlands. Grasslands are generally characterized by their small-sized plant species, thus only few studies have classified some of their species at the level of individuals. UAV-based small-sized pixels may present the opportunity to study sensor–community characteristics supporting or hampering their individual detection. Forests, however, usually depict large areas of shaded canopies due to sun angle and complex canopy overlaps at varying levels. Whilst shadows often impairs the proper classification of woody species, a systematic study comparing the effect of shadows on the performance of classifiers using varying predictor types has not been done yet. However, efficient methods are needed to optimize the quantity and quality of reference data to efficiently perform any species classification. Peatlands, finally, are the terrestrial ecosystems with largest carbon pools on Earth. Developing cost-efficient monitoring methods is thus important, specially if destructive and laboratory samples are reduced.

Therefore, this thesis approached the following three research gaps:

- How structural and community plant attributes impair the success of woody and herbaceous species mapping with UAVs?
- How very-high resolution data can be used to obtain reference data for subsequent species classifications?
- How aboveground vegetation structure and composition estimated from UAV relate to peatland belowground carbon stocks?

These research gaps were addressed within three papers published in international research journals. Their content is included in full length in the subsequent chapters:

1. **Lopatin, J.**, Fassnacht, F. E., Kattenborn, T., Schmidtlein, S. (2017). Mapping plant species in mixed grassland communities using close range imaging spectroscopy. *Remote Sensing of Environment* 201, 12-23.

2. **Lopatin, J.**, Dolos, K., Kattenborn, T., Fassnacht, F. E. (2019). How canopy shadow affects invasive plant species classification in high spatial resolution remote sensing. *Remote Sensing in Ecology and Conservation*.

3. **Lopatin, J.**, Kattenborn, T., Galleguillos, M., Perez-Quezada, J., Schmidtlein, S. (2019). Using aboveground vegetation attributes as proxies for mapping peatland belowground carbon stocks. *Remote Sensing of Environment* 231, 111217.

2 Mapping plant species in mixed grassland communities using close range imaging spectroscopy

This paper has been published as: Lopatin, J., Fassnacht, F. E., Kattenborn, T., Schmidlein, S. (2017). Mapping plant species in mixed grassland communities using close range imaging spectroscopy. *Remote Sensing of Environment* 201, 12-23.

2.1 Abstract

Grasslands are one of the ecosystems that have been strongly affected by anthropogenic impacts. The state-of-the-art in monitoring changes in grassland species composition is to conduct repeated plot-based vegetation surveys that assess the occurrence and cover of plants. These plot-based surveys are typically limited to comparably small areas and the quality of the cover estimates depends strongly on the experience and performance of the surveyors. Here, we investigate the possibility of a semi-automated, image-based method for cover estimates, by analyzing the applicability of very high spatial resolution hyperspectral data to classify grassland species at the level of individuals. This individual-oriented approach is seen as an alternative to community-oriented remote sensing depicting canopy reflectance as the total of mixed species reflectance. An AISA+ imaging spectrometer mounted on a scaffold was used to scan $1m^2$ grassland plots and assess the impact of four sources of variation on the predicted species cover: (1) the spatial resolution of the scans, (2) complexity, i.e. species number and structural diversity, (3) the species cover and (4) the share of functional types (graminoids and forbs).

Classifications were conducted using a support vector machine classification with a linear kernel, obtaining a median Kappa of ~ 0.8 . Species cover estimations reached median r^2 and root mean square errors (RMSE) of ~ 0.6 and ~ 6.2 respectively. We found that the spatial resolution and diversity level (mainly structural diversity) were the most important sources of variation affecting the performance of the proposed approach. A spatial resolution below 1 cm produced relatively good models for estimating species-specific coverages ($r^2 = \sim 0.6$; $RMSE = \sim 7.5\%$) while predictions using pixel sizes over that threshold failed in this individual-oriented approach ($r^2 = \sim 0.17$; $RMSE = \sim 20.7\%$). Areas with low inter-species overlap were better suited than areas with frequent inter-species overlap. We conclude that the application of very high resolution hyperspectral remote sensing in environments with low structural heterogeneity is suited for individual-oriented mapping of grassland plant species.

2.2 Introduction

During the last century, ecosystems have undergone an accelerated rate of environmental change due to anthropogenic impact (Smart et al., 2006). Among other impacts, these changes have affected the structure and functional composition of grasslands (Dallimer et al., 2009). Recent investigations assert that agricultural intensification – caused mainly by nutrient inputs – is one of the principal drivers of pronounced changes in grassland communities, often with associated losses in taxonomical and functional diversity (Wesche et al., 2012). Therefore, an accurate assessment of recent vegetation changes is crucial to understand current and future ecosystem dynamics. To assess these changes, two main approaches have been used in vegetation science: the establishment of permanent plots (where several measurements are repeated over time in the same plots), and the use of distribution data (where different plots are used over time, and the changes are assessed by modeling), with the first being the more reliable approach (Jandt et al., 2011).

One drawback of plot surveys is that they are expensive and time consuming when applied either to large areas or repetitively (Olsen et al., 1999). The effort and cost associated with plot surveys depend on the applied sampling approach. Most sampling approaches consider the

presence and the abundance or cover of the species (Vittoz and Guisan, 2007). The cover of species can be estimated visually, by exhaustive methods or by a mixture of both. Choosing an appropriate method for cover estimation is often a trade-off between monitoring small plots with accurate methods (e.g. the pin-point method of Levy and Madden (1933) and monitoring larger plots with lower accuracy (e.g. visual interpretation; Vittoz and Guisan (2007)). Exhaustive methods are usually very time consuming and only allow the monitoring of small vegetation plots, while visual interpretation is less time-consuming but may introduce an unknown level of observation bias into the measurements (Klimeš et al., 2001; Vittoz and Guisan, 2007).

Further problems of current vegetation survey approaches relate to the completeness of surveys and the consistency between surveyors. Vittoz and Guisan (2007) found that during vegetation surveys only about 45-63% of the species were seen by all observers (with the majority of overlooked species occurring with covers < 0.1 %). The study also reported that a pair of observers overlook about 10–20% less species than a single observer. The consistency between surveys also relates to the plot size as reported by Klimeš et al. (2001), who found that in larger plots the discrepancy between observers varies less ($\sim 10 - 20\%$) than in smaller plots ($\sim 33\%$). As species cover is more similarly estimated in small plots than in larger ones (Sykes et al., 1983), the use of frames that include a known number of grid squares can also increase the similarity of estimates among observers. This may even result in accuracies more similar than the pin-point method with trained observers, as well as requiring only half the field time (Sykes et al., 1983). In summary, the results of current vegetation surveys are likely to vary with the experience of the surveyor and contain a notable degree of uncertainty due to potentially missed species. The development of new, user-independent and objective methods that combine the high level of detail of exhaustive methods with high accuracies and time-efficiency (and eventually also with an option to cover larger areas), would be a great advance for vegetation monitoring.

Automated remote sensing (RS) techniques have been applied to classify individual trees since the 1980s (see Fassnacht et al. (2016) for a comprehensive review), while for grassland species few efforts can be found in the literature. In grasslands, we differentiate between community-oriented approaches and individual-oriented remote sensing approaches. Community-oriented approaches treat canopy reflectance as an expression of mixed species reflectance. In gradient-

based analyses, individual grassland species occurrences can be retrieved in a top-down approach relying on the occurrence of species along mapped gradients (Neumann et al., 2016, 2015). While this is suited for situations where species are hiding in sub-pixel information, individual-oriented methods are addressing species separately. Following the latter strategy, Gebhardt et al. (2006) used very high spatial resolution data (0.6 mm) from an RGB camera in an experimental setup to classify *Rumex obtusifolius* with an object-oriented approach. Similarly, Silva et al. (2014) used RGB imagery (1 cm pixel size) collected from a balloon-mounted camera to classify two species (*Setaria sphacelata* and *Pteridium arachnoideum*) using texture and object-based information. Booth and Cox (2008) used RGB imagery to estimate cow manure, green-grass and shrub covers under different grazing intensities in Colorado, USA. Further examples include the studies of Kumar and Sinha (2014), who successfully classified four species of salt-marsh vegetation in Australia using Quickbird data, and the studies of Andrew and Ustin (2008) and Lu et al. (2009), who used aerial hyperspectral data to identify *Lepidium latifolium* in riversides in California.

Nevertheless, no attempt has been made so far to classify all grassland species in a given area using hyperspectral imagery with very high spatial resolution (< 1 cm). In case of success, such an approach could be a turning point towards RS-based semi-automatic grassland surveys, covering reasonably large areas while limiting field-work to few calibration and validation plots. Unmanned aerial vehicles (UAV) arise as a suitable option for such a monitoring approach, due to e.g. their high spatial resolution and relatively low acquisition costs. Unfortunately, UAV-based sensors have not yet reached the ideal geometric or radiometric quality (e.g. close to the radiometric resolution of airborne spectrometers) for this task. Nevertheless, we believe that in the future small sensors with appropriate spatial and radiometric resolution will become available for UAV RS.

In this study, we classified grassland species using an AISA+ Eagle imaging spectrometer mounted on a scaffold at a height of 2.5 m above ground, in order to simulate future UAV-based image qualities. We collected hyperspectral images of one square meter field plots and subsequently classified all plants to obtain cover estimates of each species. The aims of the study were to assess the feasibility of this approach for classifying grassland species, and to determine

under which conditions this method could be useful in practice. To address these questions, we analyzed the influence of four sources of variation on the obtained results: the spatial resolution of the images (leading to an increased proportion of mixed pixels), the complexity of the grassland (along a gradient in species numbers and structural diversity), the species-specific cover values and the functional type of the species. We hypothesized that:

1. As the spatial resolution decreases, the agreement between field-estimated and remotely-sensed covers will decrease due to an increased proportion of mixed pixels;
2. While the complexity gradient increases, the correlation between field-estimated and remotely-sensed cover values will decrease due to an increased number of species occurring in the understorey;
3. Species with higher cover will have a higher chance to be classified accurately; and
4. Forbs will be classified with greater accuracy than grasses due to their broader leaves (higher chances of clearly assignable leaf spectra).

In addition, we examined the role of the classifier and the method for defining training areas in the hyperspectral scans as potentially influential

2.3 Methods

2.3.1 Study area

The study areas were grassland patches located in the Botanical Garden and other sites belonging to the Karlsruhe Institute of Technology, Karlsruhe, Germany. We selected four areas with different management treatments, including parks and an abandoned construction site. The treatments, including annual mowing and water irrigation, led to a species and structural diversity gradient which was suitable to test our hypotheses. Field plots were randomly placed inside those areas, keeping a minimum distance of 10 m between plots (Figure 2.1E).

In August 2016 a one square meter sampling frame was used to sample the grassland species (Figure 2.1B i) within 11 plots. The frame contained 16 sub-plots of $0.25m \times 0.25m$, where

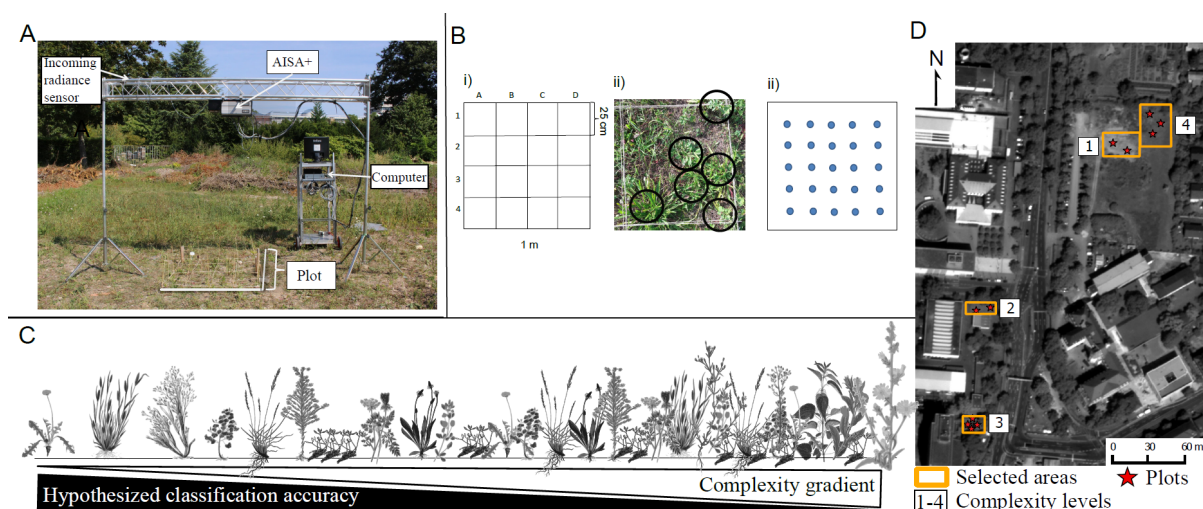


Figure 2.1: Experimental setup. A: image of the AISA+ sensor scanning a plot; B: plot structure (i), species occurrence and location recording at sub-plot level (ii) and the pin-point density grid to estimate species covers at the sub-plot level (iii); C: complexity gradient hypothesis, and D: location of the examined plots on the KIT Campus.

the species' positions (Figure 2.1B ii) and covers were recorded using the exhaustive pin-point (or point intercept) method with a systematic grid of 5 cm, and a total of 25 points per sub-plot (Figure 2.1B iii). The survey resulted in a total of 176 sub-plots.

We sampled a total of 41 species (forbs = 35, graminoids = 5 and bryophyte = 1; see Appendix A), with a maximum of 15 species per sub-plot (Table 2.1).

2.3.2 Complexity gradient

Diversity levels were defined for each selected study areas according to their species and structural diversity. Species diversity was determined by species richness and evenness - defined by Camargo (1992): $Evenness = richness \sum_{i=1}^n |P_i - P_j|$, where P_j is the relative abundance of a species i in a biological community h - while structural diversity was defined using the inter-species canopy mixture level (see Table 2.1, Figure 2.1D). We will refer to this interaction between species and structural diversity as the complexity gradient. The four defined complexity levels are:

- Complexity 1: This category is characterized by high species richness (20-21 spp) and evenness (0.37-0.4), but low cover values, where the sum of all individual species coverages does not reach 100%. This category represents vegetation on sandy-dry soils, where

Table 2.1: Summary of plot characteristics.

Complexity levels	Species diversity			Structural diversity	
	Plot id	Count	Evenness	Sum of covers (%)	Min/Mean/Max single species covers (%)
1	1	20	0.37	70	4/12.22/48
	2	21	0.4	48	4/3.38/36
2	3	13	0.25	222	4/32.23/92
	4	10	0.19	203	4/33.3/96
	5	14	0.39	256	4/9.31/36
3	6	14	0.28	230	2.77/24.17/88
	7	17	0.34	208	2.77/27.39/91
	8	14	0.28	203	2.77/32.23/92
4	9	23	0.41	324	4/25.92/92
	10	26	0.47	332	4/21.64/84
	11	24	0.42	284	4/29.42/96

mostly stress-adapted species occur. No management is applied, and the canopies have no or very limited inter-species overlap. In this class it is common to find bare soil areas. The most abundant species are *Elymus repens*, *Erigeron annuus* and *Setaria pumila*.

- Complexity 2: Here, the sum of individual species coverages is over 100 % but canopies show inter-species overlap in only few structural levels. The species richness (10-13 spp) and evenness (0.19-0.25) are rather low, with a sum of inter-species covers of up to 200 %. This category contains plots that are characterized by annual mowing and high water availability. Common species are *Nardus stricta*, *Medicago lupulina*, *Plantago lanceolata*, *Potentilla reptans* and *Achillea millefolium*.
- Complexity 3: Similar to Complexity 2, but with a larger number of species (14-17 spp).
- Complexity 4: This category has higher richness (23-26 spp) and evenness (0.41-0.47) than the other categories due to a reduced dominance of individual species, and the sum of all individual species covers reaches up to 300 %. Inter-species overlap occurs on several levels. These plots are unmanaged and located on soils with sufficient water availability.

The most abundant species of this category are *Trifolium repens*, *Setaria pumila*, *Plantago lanceolata*, *Daucus carota* and *Crepis capillaris*.

2.3.3 Spectral data

2.3.3.1 Sensor description and plot measurements

Hyperspectral data were acquired using an AISA+ Eagle spectrometer (Specim Limited, Oulu, Finland), a pushbroom scanner with an instantaneous field of view (IFOV) of 0.648 mRad and a field of view (FOV) of 36.04°. The scanner was mounted on a scaffold at 2.5 m height above the ground, obtaining pixel sizes of $\sim 3\text{mm}$ (≤ 0.2 mm of difference between nadir pixels and pixels at the edge of the plot). As the scanner needs motion to record frames, we applied it with a mirror scanner (Specim Limited, Oulu, Finland). All measurements were performed close to solar zenith (i.e. between 11:00 and 15:00 local time) on clear sky days in August 2016, which corresponds to late summer.

The sensor was used in four times spectral binning mode, which produced data with 61 spectral bands with a full width at half maximum (FWHM) of 8–10.5 nm in the spectral range between 398 nm and 957 nm. Using 61 bands was considered optimal in terms of the expected signal-to-noise ratio (Silván-Cárdenas and Wang, 2010). Fewer spectral bands would reduce computational demands but also lead to the loss of spectral information, while having a FWHM ≤ 8 nm would add more spectral bands but increase the data redundancy due to the increased band-to-band co-variation. We therefore decided to use a configuration with a FWHM of 10 nm which also conforms to the current specifications of most Unmanned Aerial Systems (UAV) hyperspectral cameras (Colomina and Molina, 2014).

During the image acquisitions, we recorded the internal dark current before each scan and incoming radiance during the scans, and performed a radiometric calibration using the CaliGeo-Pro plugin for ENVI (Specim Limited, Oulu, Finland). For further calibration, a 99 % Spectralon™ (Labsphere Inc., North Sutton, NH) was placed inside the FOV to align the scans radiometrically by linear interpolation (using the provided white reference reflectance).

2.3.3.2 Images for model calibration

Due to the small size and mixture of several species within the canopy the number of pure pixel samples for each species is limited. Therefore, we used a method for collecting independent species spectra outside the plots. Individuals of each species were first identified in the areas neighboring the plots. Then surrounding canopies of other species that may interfere in the reflectance were removed prior to the AISA+ scans to isolate the target species.

Image scans were taken on the same day as their corresponding plot to minimize the effects of changing radiation conditions. If more than one plot was scanned on the same day, validation samples were shared for co-occurring species within plots of the same complexity gradient with corresponding similar soil-water conditions. In total 41 calibration reference image scans were taken.

We further tested a second alternative to obtain the training areas, in which complete individuals were dug out and transplanted into small pots to maintain the structure of the individual plants prior the scans. Nevertheless, this approach depicted slightly lower accuracies and hence their results are not presented here. For the complete method description and a comparison of the results obtained with the two sampling methods we refer to Supplementary data 1.

2.3.4 Species classification and cover estimation

The whole work-flow of the species classification and cover estimation is summarized in Figure 2.2.

2.3.4.1 Training data collection

For the training spectra collection in the scanned hyperspectral reference images, we followed a polygon-based approach instead of collecting single pixels. Manually delineating training areas for 41 images would have been very time intensive. Therefore, we used a segmentation approach to delineate relatively homogeneous spectral regions. The applied algorithm is based on *K-means* clustering, which generates seeds for the segmentation. The segmentation approach has two key parameters: (1) the number of clusters (k), which are used to seed the *K-means*

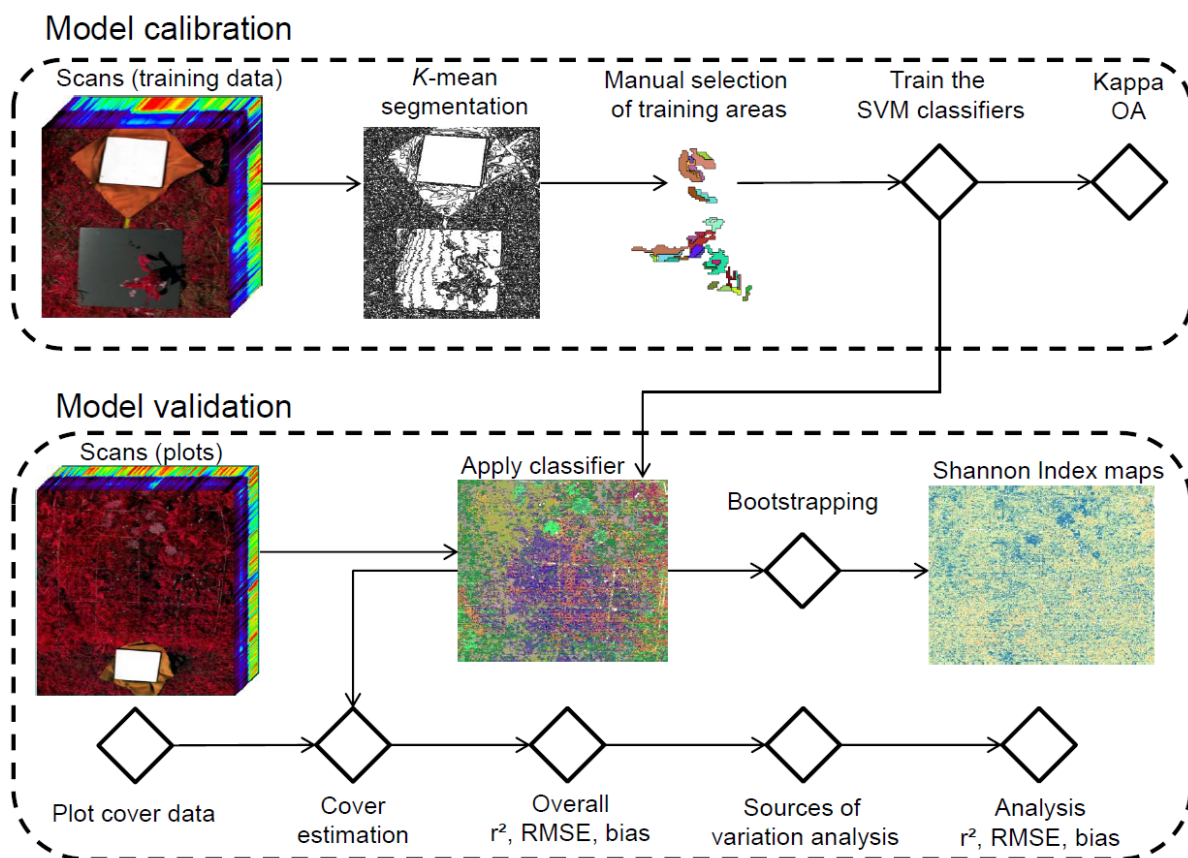


Figure 2.2: Schematic work flow of the analysis.

algorithm; and (2) the minimum object size. We set the minimum object size to one (pixel), considering that grass species with oblong leafs may have only one pixel width, while k was set to 100 so that the objects' sizes remained smaller than the average leaf sizes. The segmentation algorithm is available in the Remote Sensing and GIS library (RSGISLib) of Python (Clewley et al., 2014). After the segmentation, we manually selected polygons with relatively homogeneous areas of target species (visual interpretation supported by field recording).

We obtained a minimum of 30 samples per species for each plot (except for a few cases where some species were too scarce to reach this number). With the 30 samples we tried to cover the full spectral variability of each target species by for example equally sampling sunlit and shaded areas as well as areas rather at the center of leaves and areas closer to the edges of leaves. In total we collected 1412 samples for training and validation.

2.3.4.2 Image classification

When high spatial resolution imagery is used, the intra-species spectral heterogeneity is usually pronounced (Zhang et al., 2006). Even within the same individual, the reflectance can change drastically between one leaf and the other due to differing leaf angles and shadows. For these reasons, we used a Support Vector Machines (SVM) classifier, which is known for its capability in dealing with complex shapes in the feature space (Vapnik, 2000). SVM is a non-parametric classifier that works by constructing an optimal hyperplane separating two classes within a multidimensional feature space. When the linear separability of the two classes is not possible, SVM successively maps the data into a higher dimensional feature space via a kernel function until it finds a linear separation. More information on the concept of SVMs can be found in (Burges, 1998).

SVM was applied to all plots separately using a linear kernel. A radial basis kernel was also tested, but achieved slightly lower accuracies. To avoid overfitting, a bootstrap procedure with 500 iterations were applied to the models. In each bootstrap iteration, we used the samples that were not drawn in the bootstrap (on average, 36.8 % of the total number of samples) as holdout sample for an independent validation (Lopatin et al., 2015). Furthermore, as some species were rarer than others, we applied a stratified random sampling strategy – in which random samples of each species were drawn independently - to ensure that all existing species were always included. Model parameters cost and gamma were tuned (using a five-fold cross-validation with 5 repetitions) to find the best settings for each plot.

Subclasses were created for plants with spectrally clearly differing parts (e.g. leaf, flower and stem). The subclasses were merged after the classification. Furthermore, an NDVI mask was applied to remove areas without vegetation cover ($NDVI < 0.3$).

We furthermore analyzed the relative importance of each band when discriminating between all species and between graminoids and forbs using the Multiple Response Permutation Procedure (MRPP) algorithm (full description of the methods presented in Supplementary data 2).

All statistical analyses were performed in R, while the image processing was accomplished using Python 3 (The respective scripts are available in Appendix B).

2.3.4.3 Cover estimation

From the prediction maps of each bootstrapped SVM classification, the cover (%) of each species was estimated at the sub-plot level by counting the number of pixels of each class. Before this step, species with more than two classes (e.g. leaf and flower) were combined into single classes. The predicted coverages obtained by the classification were compared against the measured covers obtained by the pin-point method. The agreement of the predicted and measured cover values were estimated based on the coefficients of determination (r^2 – calculated as the squared Pearson’s correlation coefficient), the root mean square error (RMSE), where $RMSE = \sqrt{\frac{1}{n} \sum (y_j - \hat{y}_j)^2}$, and the bias, measured as one minus the slope of a regression without intercept of the predicted versus observed cover values of each species.

Finally, we obtained the Shannon Index of Entropy to quantify the variability in the class predictions per pixel during the bootstrapping. The Shannon Index is defined as $H = -\sum p_i \log_2 p_i$, where in this case S is the proportion of times that the pixel to-be-classified was assign to the class i during the bootstrapped classification. This is a measure of the prediction consistency, where the higher the index the more variable are the class predictions, and hence less accurate the predictions.

2.3.4.4 Impact of spatial resolution, canopy complexity, species cover and functional types on cover estimates

The applicability of the proposed method for proximal sensing in the field and UAV surveys was examined by investigating four factors likely to affect the performance of the approach:

1. Spatial resolution: the spatial resolution of the hyperspectral images was resampled (bilinearly) with factors of 2, 4, 6, 8, 10 and 12 times the original size (~ 3 mm – 36 mm). The procedure was used to identify the minimum resolution required to obtain reliable results for the classification of grassland species.
2. Complexity gradient: plots were divided and analyzed independently in the four complexity categories explained in section 2.2. These categories are related to the architectural complexity of vegetation.

3. Species cover: the species predictions were separated by their measured cover at the sub-plot level in five categories between 0 % and 100 %, with steps of 20 %. These values are related to the inter-species canopy mixtures of the ecosystem.
4. Species growth form analysis: the species cover estimation accuracies were divided into two growth forms of functional relevance: graminoids and forbs. Even though the number of forbs is greater than graminoids (35 and 5 respectively), their coverages were found to be similar along the complexity gradients. Graminoids usually have vertical leafs while forbs are more diverse, depicting small structures with planar big leafs (e.g. *Plantago major*) or complex structures with small vertical leafs (e.g. *Cichorium intybus*). Due to their sparsity (in both number of species and cover), we did not include bryophytes as an additional growth form class. This analysis indicates the importance of the growth forms being present in the target ecosystem.

2.4 Results

2.4.1 Model performances

Model performances are summarized in Figure 2.3. The median value of the classification accuracies (Kappa; Figure 2.3A) reached 0.8, while cover estimation reached median r^2 values of 0.59 (Figure 2.3B), RMSE of 6.23 % (Figure 2.3C) and a bias of -0.002 (Figure 2.3D), indicating relatively high performances. However, the range of r^2 values indicating the correlation between predicted and field-estimated cover values was large and reached from almost no correlation to almost perfect correlation (Figure 2.3B).

2.4.2 What causes the differences in model quality?

Figure 2.4A shows a high variance of predicted values for low coverages and a general underestimation in the predicted cover values. Also, the presence of false negatives (species observed in a plot that were not detected) and false positive (species not observed in a plot that were detected) in the species classifications are shown in Figure 2.4A. In Figure 2.4B, the frequencies of false negatives, false positives and correctly classified species per sub-plot are presented. The

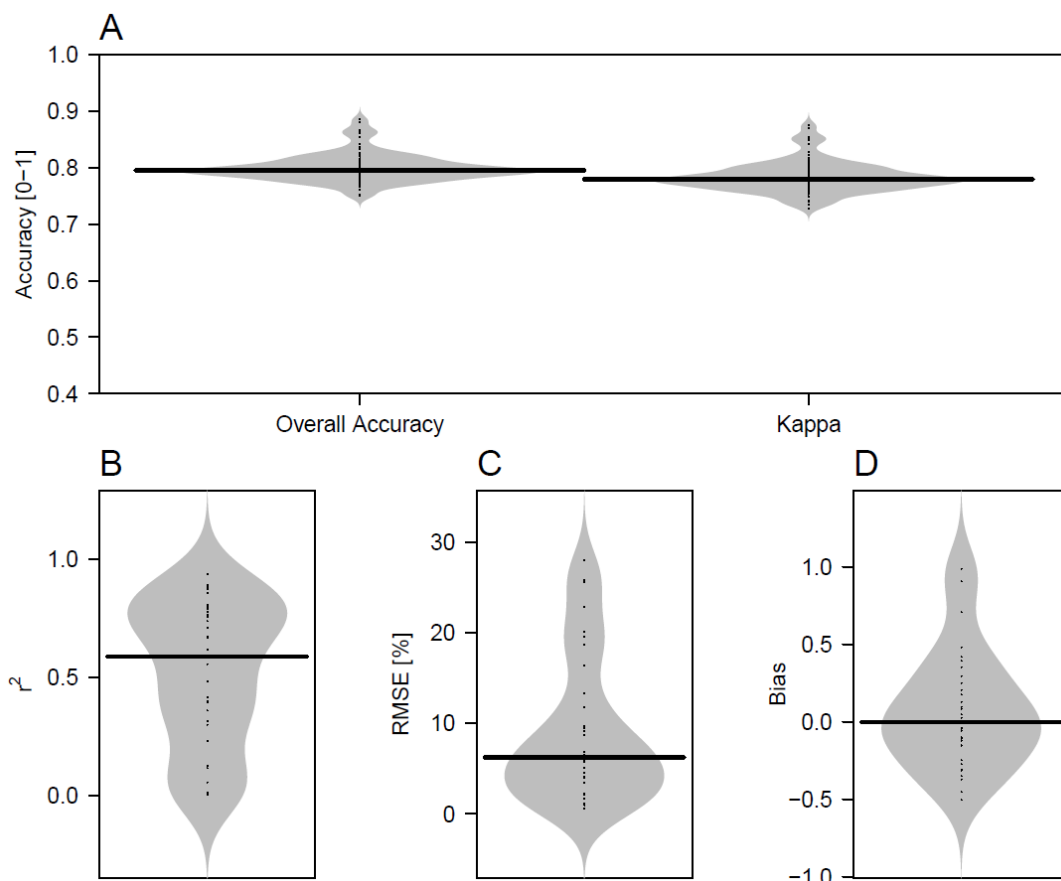


Figure 2.3: Bootstrap distribution of classification results using all sub-plots. In (A), the overall accuracy and Kappa of the SVM classification are presented, while in (B-D) the prediction accuracies (r^2 , RMSE and bias) of the measured against the predicted species covers are displayed. Beanplots show the relative distribution of the bootstrap results with the width indicating the frequency of a given value, while black horizontal lines indicate the median values of the distribution.

model correctly classified most of the species occurrences, while within sets of misclassifications, false positives were more frequent than false negatives.

Figure 2.5 shows RGB visualizations of AISA+ scans, the corresponding classified images and maps of the Shannon Index of Entropy indicating the diversity of the classes to which the pixels were allocated to during the bootstrapped classifications for one exemplified sub-plot for each complexity gradient class. It can be seen that high uncertainty areas (Shannon > 1.5) occur in similar proportions across the whole complexity gradient. Figure 2.6 depicts detailed examples of the two main sources that led to high diversity values: shadows and leaf edges. On the contrary, planar leaves, unique spectra (e.g. flowers) and homogeneous illumination areas show lower diversity values.

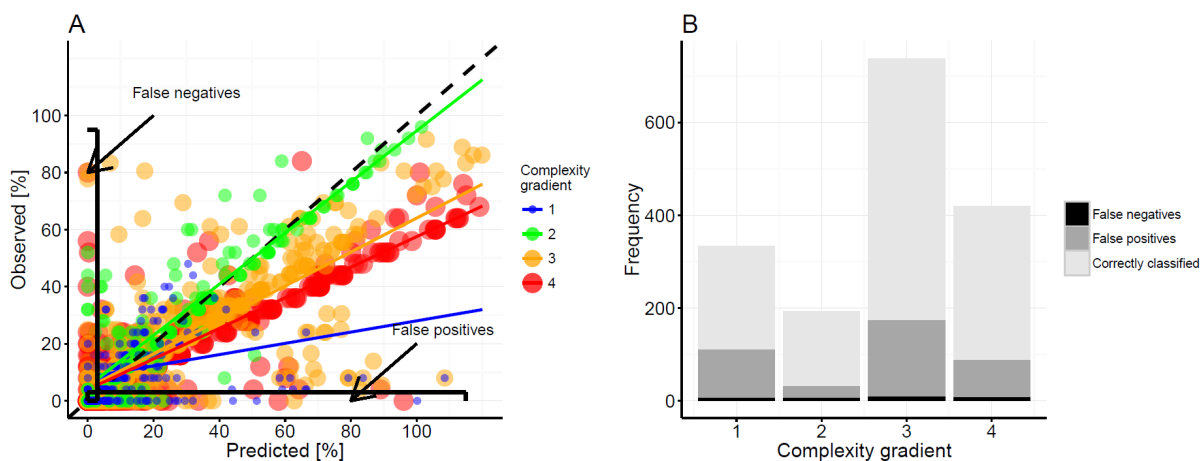


Figure 2.4: Model covers predictions. A: scatter plot of observed versus predicted species cover values; B: frequency distribution of false negative, false positive and correctly classified species (presence detected) at the sub-plot level are displayed.

Table 2.2: Summary of accuracies per functional types. The percentiles (P) 5 %, 25 %, 50 %, 75 % and 95 % are depicted.

	P05	P25	P50	P75	P95
Graminoids					
r^2	0.42	0.45	0.46	0.74	0.83
RMSE	6.98	12.03	14.29	29.77	37.28
Bias	-0.45	-0.18	0.06	0.12	0.27
Forbs					
r^2	0.38	0.43	0.56	0.7	0.91
RMSE	1.33	4.14	9.35	20.78	32.14
Bias	-0.35	-0.18	-0.04	0.35	0.93

Classification accuracies (producer's and user's accuracies) and r^2 , RMSE and bias of the cover estimation per species can be found in Appendix A, while a summary of accuracies according to functional types is presented in Table 2.2. Concerning cover estimates, the classification based results for forb species showed higher agreement with field-estimated covers than graminoid species as indicated by higher median r^2 values, lower median RMSE values and median bias value closer to zero. The single bryophyte species obtained an r^2 of 0.8 and a RMSE of 6.5 % (result not presented in Table 2.2).

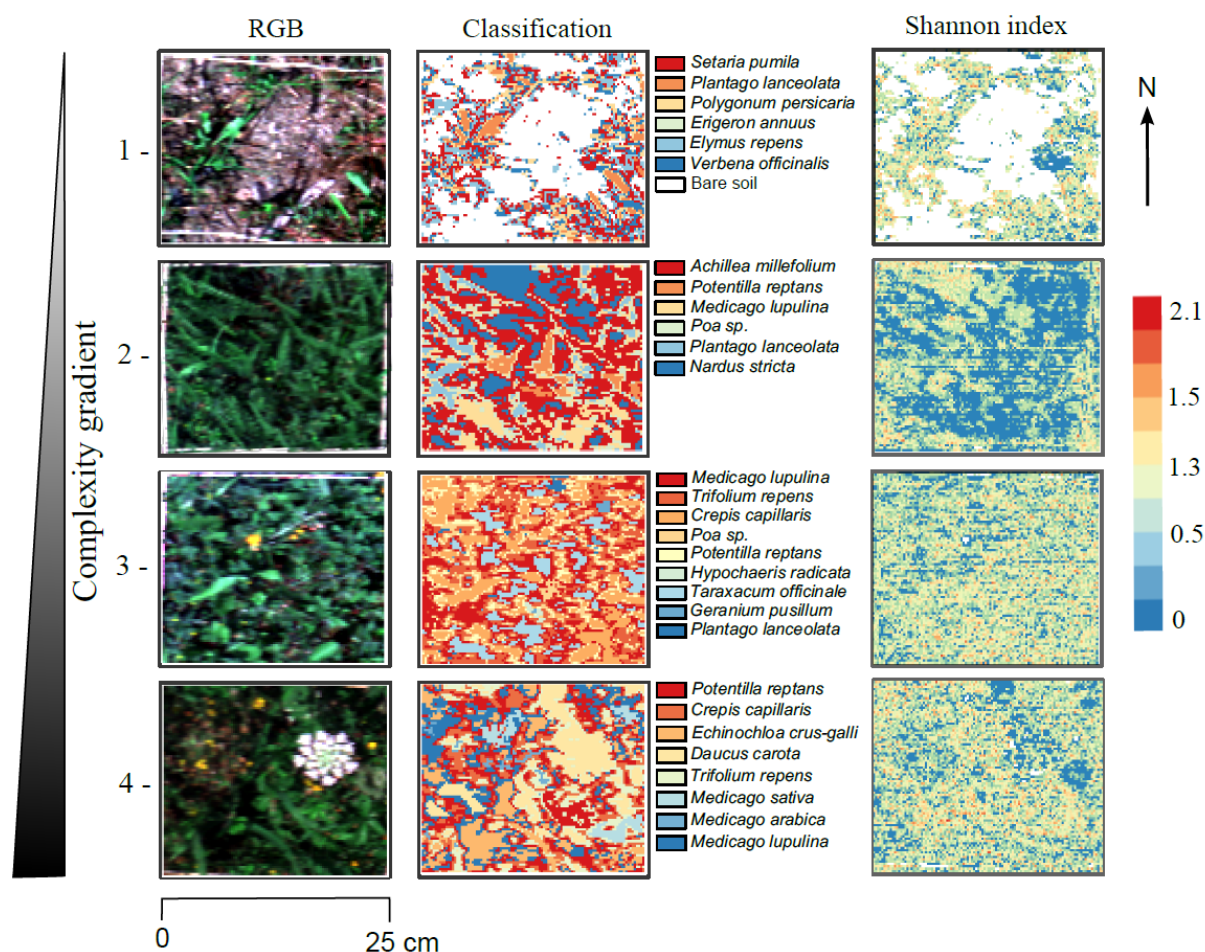


Figure 2.5: Examples of prediction maps at the sub-plot level for the four complexity categories. Images obtained with a RGB color composition of the AISA+ scan, the classification results and the coefficient of variation map of the bootstrap procedure are presented. For the classification, the mode class of the bootstrapping procedure is drawn in each pixel.

2.4.3 Impact of spatial resolution, canopy complexity, species cover and functional types on cover estimates

Figure 2.7 summarizes how the examined technical and ecological variables affected the agreement between classification-based and field-estimated cover values. The spatial resolution analysis (Figure 2.7A) shows that the pixel size is key to classify grassland species accurately. In the considered range of pixel sizes, the agreement between classified and field-estimated covers constantly decreases with increasing pixel size. For the species composition and complexity analysis (Figure 2.7B), our hypothesis was confirmed: the complexity of grassland species composition was negatively related to the agreement between classified and field-estimated covers. Sub-plots of the first complexity class obtained ~ 4.5 times better agreements than plots located

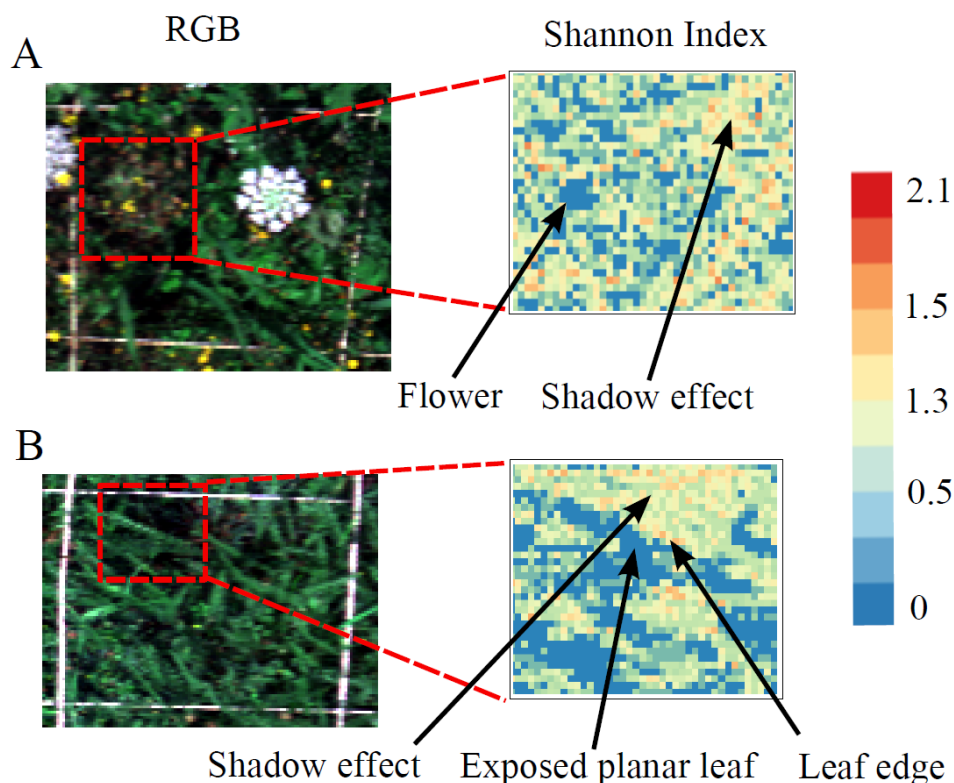


Figure 2.6: Per pixel variability in the classification results. Zoom-ins within two sub-plots (A and B) are presented with the RGB compositions (left) and the Shannon Index maps (right). Main sources for high variabilities are shadows and structural edges (mixed pixels).

in the complexity 4 category, while complexity 2 and 3 categories showed similar results. The results also agree with our hypothesis that with increasing cover of a species, the agreement of its classification-based cover value and the field estimates also increases (Figure 2.7C). Moreover, errors (RMSE) were smaller in the 20 % - 40 % species cover range than in the cover range of 0 % - 20 %. Finally, forbs obtained slightly higher agreements than graminoids, but not clear tendency was found (Figure 2.7D).

2.5 Discussion

2.5.1 Model performances

The species classification performances and the agreement between classification-based and field estimated covers indicated a good potential of the suggested approach. Nevertheless, cover estimation agreements showed high variances in the bootstrapped results (Figure 3B-D; r^2 fluctuating between 0 and 1) indicating less stable results as compared to the classification

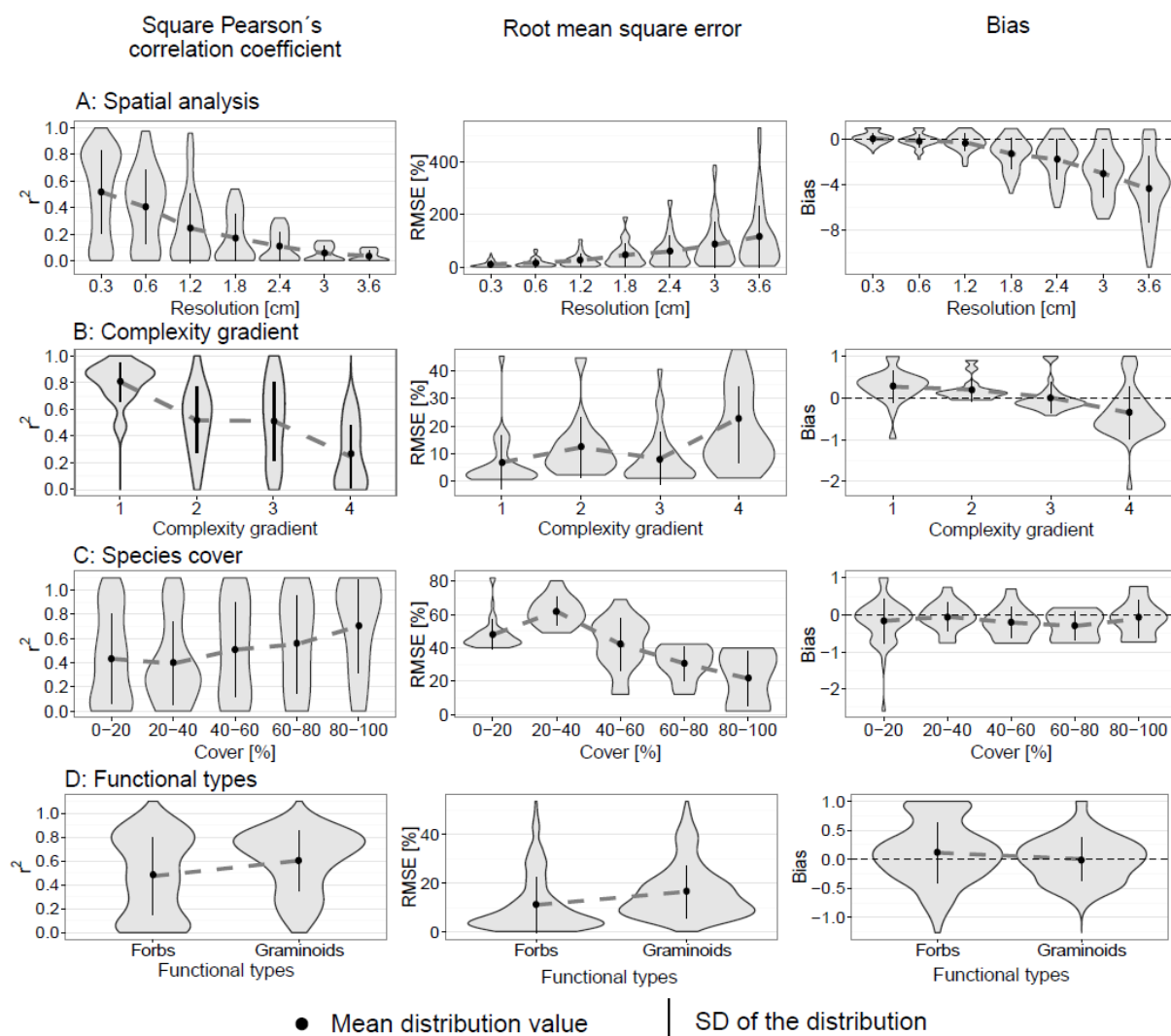


Figure 2.7: Impact of different sources of variation on the predicted cover. The sources of variation are: (A) the spatial resolution of the scans, (B) the complexity gradient of the plots, (C) the species cover within the sub-plots, and (D) the species functional types. All analyses (except for the spatial resolution) were performed with ~ 3 mm pixel size. The beanplots show the distribution of model performances for all sub-plots, where wider areas represent a higher frequency. Black dots show the mean distribution value and horizontal lines the standard deviation.

accuracies (Figure 3A; overall accuracy and Kappa fluctuating between approximately 0.75 and 0.9). The classification results are likely to be more stable than the cover predictions due to two reasons: First, they are based on training data collected from pure pixels of each species, which supports a better separation of the considered classes in the classification process, and second, the training and validation of the classification algorithm bases on samples that were collected with the same work-flow.

On the contrary, when applying the classifier on the full image to subsequently obtain the cover predictions, a notable portion of the to-be-classified pixels for each species were mixed pixels.

This particularly applies to species with cover values of below 5%. These effects are likely to get stronger along the increasing complexity gradient, as in more complex canopies, more species will tend to grow in the understorey of dominant species and thereby further increase the number of mixed pixels. This assumption is backed up with the results of Figure 2.7, where the cover predictions are notably more stable for the complexity class 1 as compared to all other classes. Furthermore, the cover predictions are validated with a completely independent dataset collected with a field-method (pin-point method) that quantifies cover values in a very distinct way which further reduces the chances of reaching high performances for cover predictions (see also section 2.4.3).

We also tested several other classification and pre-processing approaches including a Partial Least Squares Discriminant analysis and Random Forest algorithms, along with a minimum noise fraction transformation (MNF) of the spectral bands, and the brightness normalization proposed by Feilhauer et al. (2010) to reduce the effect of shadowing in the scans. Nevertheless, judging from a bootstrap significance test (Lopatin et al., 2016) these models did not significantly differ from the model described above. The results of all examined approaches are available in Supplementary data 3.

The Shannon Index of Entropy maps (Figure 2.5) showed that certain areas in the images presented higher diversity in the allocated classes than others. Especially image parts with higher fractions of shadows and leaf borders were found to have a low stability of the classes to which they were assigned to (Figure 2.6). Shadows are known to alter the magnitude of the spectral signal and hence contribute to misclassifications. This is likely to be especially pronounced in the classification of vegetation where most of the inter-species differences in reflectance are related to the amplitude rather than the shape of the spectrum (Fassnacht et al., 2016). On the other hand, leaf borders provoke mixed pixels effects that increase the spectral differences between training and target data and hence complicate the allocation of the corresponding pixel to one of the defined training classes. It can be seen that the Shannon Index maps presented some level of stripping noise in some of the plots. This problem is probably related to the mirror scanner that was applied during the AISA+ scans, however, we could not identify a sound explanation for the exact problem.

The classification accuracies and cover prediction agreements per species (Appendix A) depicted that forbs tend to obtain better results (Table 2.2), but not clear tendency was found. Species with noticeable low performances could be mostly allocated to three classes: (1) species with high intra-species heterogeneity (e.g. *Conyza canadensis*); (2) species occurring in the understorey (e.g. *Medicago lupulina*) and finally (3) spectrally very similar species such as *Echinochloa crus-galli* and *Elymus repens*.

These findings are only partly comparable to earlier studies attempting to classify grassland species due to notable differences in the methodical approach. Earlier studies typically either applied multi- or hyperspectral data with coarser spatial resolution (e.g. Andrew and Ustin, 2008; Kumar and Sinha, 2014) or used similarly high resolution but RGB imagery (e.g. Gebhardt et al., 2006; Silva et al., 2014). Furthermore, most of these studies focused on the detection of a single or few species, while a full classification of all species has not yet been attempted. Studies applying data with pixel sizes over 1 m have been tested in environments where the target species or vegetation type occur in sufficiently large, homogeneous patches (Andrew and Ustin, 2008) or when the spectral characteristics of such species is sufficiently distinct from the background species (Kumar and Sinha, 2014). The studies focusing on RGB imagery with pixel sizes below 1 cm focused more on differences in texture and shape between the target and background species. Correspondingly, the authors used object-based approaches including segmentation algorithms, RGB enhancements and transformations to intensity (to maximize RGB band differences) and textural variables from the gray-level co-occurrence matrix to classify the species of interest. The studies obtained good accuracies and judging from these results, object-based approaches to obtain variables related to species' shapes and textures could further improve our proposed method.

2.5.2 Impact of spatial resolution, canopy complexity, species cover and functional types on cover estimates

Based on the results of Figure 2.7 we assume that starting at a 1 cm pixels size, the cover agreements between classification-based and field-estimated covers decrease notably due to an increase of fraction of pixels containing mixed information from several species. Likewise, the

degree of mixture increases along the canopy complexity gradient. The results of the complexity gradient analysis support our hypothesis that the agreement between classification-based and field-estimated covers decreases with increasing complexity. For areas where the species occur without, or with only moderately overlapping canopies, the agreements in cover estimates were high with a median value of 0.86 r^2 , RMSE of 2.62 % and a slight tendency to overestimate cover values (bias of 0.3). When plants started to overlap the agreements decreased rapidly. In future works, we cannot expect any improvement of the agreements through better detection models when the understorey species do not appear at least partially in the image.

The species cover analysis showed that when the species abundance within one sub-plot increases, the agreement of the classification-based cover of that species with the field-estimated cover also increases. Along with this result, the scatterplot of observed against predicted species covers (Figure 2.4A) shows a general tendency towards higher variation with lower covers. Exceptions were species coverages ranging from 0 % to 20 %, which obtained lower agreements than species coverages of 20 % - 40 %. One potential explanation of this could be a larger effect of the background on small plants. The size of species' individuals may also influence the classification accuracies, since acquiring pure spectra is more likely for species with larger organs.

The comparison of the results between functional types presented a tendency towards higher classification accuracies and cover agreements in the discrimination of forbs. This may be due to the fact that graminoids usually have thinner leaves, which may induce a higher presence of mixed pixels. According to the MRPP analysis, the discrimination between graminoid species relied more on the NIR wavelengths - possibly related to structural information, such as leaf area index and leaf angle Ollinger (2011) – while forbs were better discriminated in the VIS spectral region – typically related to photosynthetic pigments, but also containing structural information Ganapol et al. (1999); Jacquemoud et al. (2009); Posada et al. (2009). For a comprehensive description of these results we refer to Supplementary data 2.

The effects of structural complexity on cover estimations can be seen in the prediction maps (Figure 2.5), where predicted classes of the low complexity category visually agree better with the real patterns (RGB image) than the other maps. Nevertheless, the Shannon Index maps

feature approximately the same relative amounts of high diversity (index over 1.5) pixels along the complexity gradient, indicating that the structural diversity may not have an influence on the predicted spatial patterns. Instead, the structural diversity does have a clear influence on the model accuracies (Figure 2.7).

Finally, other factors not considered in our analysis could contribute to the variability in classification accuracies and the corresponding estimates of species' covers, including for example leaf size, species height and phenology. Fung et al. (1998) found the classification success to be dependent upon leaf size when they applied hyperspectral data (400 nm – 900 nm) to discriminate subtropical tree species using a linear discriminant classifier. Moreover, the vegetation structure (e.g. height) and phenology have been found to be useful to separate between functional traits (e.g. between graminoids and forbs; McIntyre et al. (1999)).

2.5.3 Semi-automatic field survey: strength, limitations and future considerations

The main drawback of the study is that the presented approach requires a large number of scans which is associated to (1) to a notable amount of post processing and model preparation time and (2) the need for an appropriate calibration of each scan as otherwise differences in day light conditions may induce spectral variability affecting spectral signatures in the training data.

Furthermore, we assessed the quality of the classification-based species cover predictions by comparing them to cover estimates obtained in the field using the pin-point method. This is rather a comparison between two different estimation approaches than a real validation. The pin-point method records the presence of all species occurring at fixed locations defined in a grid within a plot. The species' covers are then estimated based on these samples. The pin-point method is explicitly able to quantify cover values in plots with overlapping canopies. On the contrary, the classification-based estimation of cover values can only allocate a single class to a single pixel and hence is inherently unable to accurately depict multi-layered canopies. Furthermore, with the examined approach we were only able to assess the agreement between the absolute species cover estimates of the two approaches and could not validate the spatial agreement of the species' covers. This would have been only possible by comparing the species located at the top of the canopy at each sampling location within the pin-point grid with the cor-

responding classified pixel. However, this would require mayor sampling efforts as the location of each pin-point must either be precisely known or directly visible in the images. Within the given time-restrictions of this study, we were not able to develop an appropriate approach for this issue.

2.5.4 Transferring the present approach to UAVs

Some of the shortcomings discussed above might be resolved using data from a UAV system. For example, issues related to differing sun-sensor geometries during the individual scans are minimized if all plots are covered by an individual flight which typically does not last longer than 20-30 min.

Training data could then be collected from the same overflight. For instance, one option could be to add visible signs on the ground outlining individuals positions (as in this investigation, around 5 individuals per species may be reasonable) for the training data collection. Of course, this requires knowing in advance which species are present in the study area. For some purposes, this might be challenging, however, in the context of permanent monitoring plots with repeated measurements it might be feasible as species lists might already exist.

Also related to long-term monitoring, achieving a sub-centimeter positioning accuracy in an absolute geographic coordinate-system to allow for comparisons between multiple UAV-acquisition will be challenging. However, using species coverages as target measure within permanent plots could be an approach to reduce positioning accuracy requirements for repeated monitoring. For example small plots (e.g. 50 cm × 50 cm) could be permanently marked in the study area. During the UAV flights, sufficiently thick frames (visible in the UAV images) can be accurately positioned at the plots and serve as easily identifiable objects to co-register imagery from repeated UAV-flights. These plots can at the same time serve as reference area to collect species presence and cover data for validation purposes.

We believe that a UAV-based semi-automatic approach for grasslands surveys may have a particularity interesting potential for long term monitoring, where relative large areas can be mapped at the field scale with high temporal flexibility and resolution. This approach may allow us to achieve robust seasonal data collection without the errors and biases of visual interpretation

methods, but also with the discussed limitations of the remote sensing approach. In this investigation the analysis was carried out during late summer (August 2016), which corresponds to a theoretically reliable time in the year to perform the analysis. For example, Feilhauer and Schmidtlein (2011) found that June, July and August were suitable to link hyperspectral data with floristic gradients in a nutrient-poor grassland, a wet heath and a floodplain meadow. However, more investigation (for example also related to flowering events) is needed to fully understand how seasonality affects grassland species classification.

Furthermore, even without the use of a UAV, plot-based monitoring using a fixed sensor – such as the AISA+ sensor applied in this investigation – could already represent a step forward towards an objective and robust (seasonal) monitoring of grasslands. With the continued miniaturization of the sensor-systems, such an approach could become notably more flexible in the near future.

2.5.5 Suitable environments and applications of the model

Based on our analyses, the application of future field-based hyperspectral proximal sensing or UAV-based remote sensing for classifying individual grassland species is feasible under the following considerations:

First, the spatial resolution has to be appropriately high to avoid or minimize mixed pixels of all classes. The recommended resolution for obtaining reasonably high accuracies will vary greatly between grassland ecosystems, but we assume that the resolution requirements will increase with the structural complexity of the plant community and with a decreasing size of the plant individuals or leaves. In our study, pixel sizes below 1 cm are recommended due to the structural diversity of the plant communities.

Second, probably the most restrictive feature in classifying grassland species is their diversity level, or complexity gradient. We found that increasing complexity of the examined ecosystem – especially the structural component – leads to decreased classification accuracies and corresponding decreases in agreement between classification-based and field estimated cover values.

Taking into account these two major factors, we assume that in ecosystems where the structural heterogeneity is high and the canopy overlap occurs in several layers, the presented classification techniques will not be possible. Nevertheless, for target ecosystems where the plant community grows in separate species patches or the average species size is comparably large and species tend to have hardly overlapping canopies, the approach is feasible. Examples of such plant communities could be stress-prone grassland such as dune communities, where above-ground competition is reduced. This means that species tend to grow in patches, decreasing the chance of inter-species canopy overlap. The importance of environmental context for classifying grassland species has also been discussed in Andrew and Ustin (2008).

Alternative applications for UAV-based approaches in grassland ecosystems include applications such as weed detection in precision agriculture (Booth and Cox, 2008; Gebhardt et al., 2006) and invasive or key species mapping (Andrew and Ustin, 2008). In these cases the use of one-class classifiers may be an option as only the target species is needed, decreasing considerably the time required for field work (Stenzel et al., 2017).

2.6 Conclusions

We assessed the possibility of future applications of UAV hyperspectral data for semi-automatic field surveys. We classified grassland species and estimated their cover within a gradient of diversity levels (species and structural diversity). We found that classifications of grassland species at the level of individuals have strong limitations when inter-species signal mixtures are present due to either high structural complexity or insufficient spatial resolution of the applied imagery. Nevertheless, it was found that under favorable conditions - that is a comparably low structural complexity with low canopy overlaps - an accurate classification of all co-occurring species and the subsequent accurate estimation of the species' cover is possible. This approach could be combined with earlier presented community-based approaches which cannot provide accurate species' cover estimates but are at the same time less affected by the structural complexity and the spatial resolution and hence can give estimates about the probabilities of a species' presence in a given area even if it is located in the understory. Further

investigations are needed to assess structural and spatial resolution thresholds from which one alternative turn to be advantageous over the other.

In conclusion, this pioneer study showed that close range imaging spectroscopy has potential to support the monitoring of grassland ecosystems at individual species level, but more research concerning validation techniques, efficient collection of training data as well as integration with community-based approaches in areas of high structural complexity is needed to progress towards an operational approach.

3 How canopy shadow affects invasive plant species classification in high spatial resolution remote sensing

This paper has been published as: *Lopatin, J., Dolos, K., Kattenborn, T., Fassnacht, F. E. (2019). How canopy shadow affects invasive plant species classification in high spatial resolution remote sensing. Remote Sensing in Ecology and Conservation.*

3.1 Abstract

Plant invasions can result in serious threats for biodiversity and ecosystem functioning. Reliable maps at very-high spatial resolution are needed to assess invasions dynamics. Field sampling approaches could be replaced by unmanned aerial vehicles (UAVs) to derive such maps. However, pixel-based species classification at high spatial resolution is highly affected by within-canopy variation caused by shadows. Here, we studied the effect of shadows on mapping the occurrence of invasive species using UAV-based data. MaxEnt one-class classifications were applied to map *Acacia dealbata*, *Ulex europaeus* and *Pinus radiata* in central-south Chile using combinations of UAV-based spectral (RGB and hyperspectral), 2D textural and 3D structural variables including and excluding shaded canopy pixels during model calibration. The model accuracies in terms of area under the curve (AUC), Cohen's Kappa, sensitivity (true positive rate) and specificity (true negative rate) were examined in sunlit and shaded canopies separately. Bootstrapping was used for validation and to assess statistical differences between models. Our results show that shadows significantly affect the accuracies obtained with all types of vari-

ables. The predictions in shaded areas were generally inaccurate, leading to mis-classification rates between 65 % - 100 % even when shadows were included during model calibration. The exclusion of shaded areas from model calibrations increased the predictive accuracies (especially in terms of sensitivity), decreasing false positives. Spectral and 2D textural information showed generally higher performances and improvements when excluding shadows from the analysis. Shadows significantly affected the model results obtained with any of the variables used, hence the exclusion of shadows is recommended prior to model calibration. This relatively easy pre-processing step enhances models for classifying species occurrences using high resolution spectral imagery and derived products. Finally, a shadow simulation showed differences in the ideal acquisition window for each species, which is important to plan revisit campaigns.

3.2 Introduction

Invasive plant species can alter ecosystem functioning and services, causing loss of biodiversity (Binggeli, 1996) and water availability (Little et al., 2015), alterations in primary production and shifts in the N- and C-cycle (Vilà et al., 2011). Worldwide annual economic losses caused by biotic invasions are estimated to be one order of magnitude higher than those caused by all natural disasters together (Ricciardi et al., 2011). Mapping the arrival and spread of invasive species is hence crucial for risk assessments and to enable their control and eradication Rocchini et al. (2015).

Remote sensing has been used to map invasive species occurrences in space and time, usually by combining field measurements with satellite or airborne data (e.g. see review of Huang and Asner, 2009). Recently, Unmanned Aerial Vehicles (UAVs) have been used to map the occurrence of invasive plant species. One advantage of UAVs is that they allow for flexible acquisitions of very-high resolution imagery. This is important for early and accurate prediction of invasive species occurrences (e.g. Cao et al., 2018; Baena et al., 2017). Such UAV approaches are especially suitable to: 1) understand the invasion dynamics and processes at local scale through repetitive acquisitions, and 2) to derive reference data for large-scale satellite-based

mapping of the invasions (Kattenborn et al. submitted). General benefits of UAV-based sensing include the possibility of optical data acquisition under cloudy conditions (e.g. de Sá et al., 2018) and the generation of orthomosaics that allows the comparison of temporal images comprising similar view angles (contrary to satellite-based high-resolution imageries where temporal data often differ in view angles; Anderson and Gaston (2013)). Meanwhile, disadvantages of UAV-based sensing include their relatively small area cover and the relatively low radiometrical quality of the sensors (Hruska et al., 2012). UAV-based invasive species mapping has yielded high accuracies using different data types, like RGB or VNIR information (Michez et al., 2016; Alvarez-Taboada et al., 2017; Baena et al., 2017; Mafanya et al., 2017; Cao et al., 2018; de Sá et al., 2018), hyperspectral data (Cao et al., 2018) or 2D textural (Michez et al., 2016; Cao et al., 2018) and 3D structural Kattenborn et al. (2014); Franklin et al. (2017) information derived from photogrammetric algorithms.

The development of user-friendly photogrammetric software with Structure-from-Motion (SfM) capabilities makes the processing of UAV data attractive for natural management practitioners with basic knowledge in geomatics. These SfM algorithms resolve the alignment of camera positions, which allows to generate orthorectified aerial imagery and 3D models without the allocation of ground control points (Westoby et al., 2012). Most studies that used such UAV products focused on mapping a single species using one or a few of the abovementioned data types. However, a detailed comparison of data types for more than a single species is still missing. Such a study is relevant to assess the consistency of UAV-based invasive mapping requirements.

The extremely high spatial resolution and acquisition flexibility of UAV data offers new opportunities but also challenges. One drawback of very-high spatial resolution imagery is the increase of spectral within-class variability caused by canopy structure and shadows, which often hamper the separability of classes in pixel-based studies (Lopatin et al., 2017). Shadows result from the obstruction of light, causing a decrease of reflectance. In vegetation areas, cast shadows receive diffuse radiation (mostly Rayleigh scattering) from light scattered within the atmosphere or surrounding objects (Gu and Robles-Kelly, 2014). In practice, shadows can lead to either a reduction or a total loss of the spectral signal of a canopy (Zhang et al., 2015), affect-

ing the success of classification tasks (Saha et al., 2005; Liu and Yamazaki, 2012). Therefore, careful consideration regarding acquisition time of the day is particularly important, as during some parts of the day shadows can cover a large part of the area of interest (Milas et al., 2017). Many approaches have been developed to reduce the effects of shadows and improve classification performances. For instance, increasing pixel size has been found to be helpful to decrease within-class variability, usually improving classification performances when an ideal relation between pixel and crown size is obtained (Nagendra, 2001). This ideal relation obviously depends upon the crown size and the canopy closure of the investigated species or ecosystems and can vary widely. Likewise, object-based analysis have been used to decrease the spectral variance at individual level (e.g. one spectral value per individual crown), obtaining in some cases higher classification performances than pixel-based approaches (Yu et al., 2006). However, obtaining a meaningful delineation of tree crowns is often challenging, especially for closed and overlapping canopies and in the presences of shadows (Nevalainen et al., 2017). Deep learning may also cope with shadows by using the shadows as additional species-specific structure information. Nevertheless, deep neural networks usually need a large amount of training data which could hamper their use for practical applications with limited field data (Dyrmann et al., 2016). Other alternatives to address shadow effects are shadow correction methods, which consist in the radiometric enhancement of shaded pixels usually based on information extracted from neighbouring non-shadowed regions (empirical models; Singh et al., 2012) or on incident light sensor information (physical methods; Sismanidis et al., 2014). Yet, these methods may introduce noise and aberrations to the radiometrically corrected areas (Sismanidis et al., 2014) that could hamper class separability of spectrally similar classes, such as different plant species. This may be one reason why these methods have so far been mostly applied in urban contexts, where the class interfaces are often comparably clear.

In summary, averaging or smoothing the spectral information of adjacent pixels may improve classification performances, but at the risk of excluding meaningful variance of the target species' spectral signal due to canopy architecture. For these reasons, the use of only sunlit canopies for pixel-based species classification may be a suitable alternative to decrease within-class variability by excluding the undesirable information given by shadows, while keeping

important variations related to canopy architecture. Whilst earlier UAV-based studies have reported negative influences of shadows in invasive species mapping (Franklin et al., 2017; Müllerová et al., 2017; de Sá et al., 2018), it is still uncertain whether or not the exclusion of shadows from the training data improves the UAV-based mapping results.

Hence, the main aim of this investigation was to assess the effects of shadows on the occurrence predictions of the woody species *Acacia dealbata*, *Ulex europaeus* and *Pinus radiata* using different combinations of spectral, 2D textural and 3D structural UAV-based data in central-south Chile. This aim is embedded in the overarching effort to develop a UAV-based work-flow to map individual target species with a minimum amount of training data and with possibly high accuracies for subsequent ecological analysis. We further investigated by means of simulations the role of the species-specific canopy structure in the production of daily shadows. This is important to assess ideal UAV acquisition periods and revisits.

3.3 Materials and methods

The applied workflow consisted of six steps: 1) first, remote sensing data were acquired using unmanned aerial vehicles (UAV) in three different areas. Each area hosted one of the invasive species along with native woody species; 2) then, canopies of the invasive species were manually delineated by visual interpretation of the UAV data to create training and validation data; 3) shadows occurring inside the canopies were identified using an automatic approach; 4) independent variables were created from the UAV data, to create the datasets needed for modeling (MaxEnt); 5) MaxEnt models were trained to estimate relative likelihoods of occurrences of each invasive species. Results in sunlit and shaded canopy areas were compared to assess the relative effects of shadows in the classification performances; 6) finally, simulations were carried out to assess the effect of day-time and species-specific canopy shape on the quantity of shadows occurring in the corresponding canopies.

3.3.1 Study sites and target species

Central-south Chile is considered a world's biodiversity hotspots (Myers et al., 2000), harboring a high level of endemism because of its geographical isolation. Furthermore, in central-south

Chile, species from the sclerophyll forest ecosystems of the North and the deciduous *Nothofagus* forests in the souths are co-occurring which leads to a particularly high biodiversity. This biodiversity is threatened by diverse biotic and abiotic factors, including pronounced land-use changes occurring over the last decades but also invasive species which are global drivers of extinctions; they compete with native species for resources, and can alter the community dynamics (Binggeli, 1996). With the arrival of the colonists, areas formerly cover by native forests and/or shrublands were cleared for agriculture and silviculture purposes, causing the introduction of several European and Oceanic invasive plants (Holmgren and Persson, 2004). We studied the presence of three woody invasive species, *Pinus radiata*, *Ulex europaeus* and *Acacia dealbata*, in three study areas including the ‘Maule’, the ‘Biobio’ and the ‘Los Lagos’ regions (Figure 3.1). *P. radiata* was introduced in the Maule region for timber production (Clapp, 1995), while *U. europaeus* was introduced as a hedge plant to contain livestock (Norambuena et al., 2000). Finally, *A. dealbata* was introduced for ornamental purposes (Fuentes-Ramírez et al., 2011). These species have been found to be very noxious worldwide, but particularly in South American countries (Chile, Argentina and Brazil; Richardson et al., 2014), causing serious losses in biodiversity and affecting water supply (Little et al., 2015). Here, the three invasive species dominantly occurred in different parts of central-south Chile. We decided to use more than a single target species to develop an understanding of the reliability and stability of the proposed methods (Figure 3.1). All of the targeted species are suspected to endanger both native flora and fauna.

3.3.2 UAV data acquisition and derivation of presence data for the target species

We performed one UAV flight for each study site using an octocopter (Okto-XL, HiSystems GmbH, Germany). Flights were carried out in March, November and December 2016 for *P. radiata*, *U. europaeus* and *A. dealbata*, respectively, partly overlapping the flowering season for *A. dealbata* and *U. europaeus*. The octocopter was equipped with two optical sensors: an RGB standard consumer-grade camera (Canon 100D, 28 mm focal length, 5196 × 3464 pixels) and a snapshot hyperspectral camera (OXI-II, Gamaya, Switzerland) with 41 spectral bands ranging

from 450 to 950 nm and a 10 nm bandwidth. The flight plans aimed for an average of 90 % of forward and 70 % of sideward overlap for both sensors at 150 m above ground.

Photogrammetric point clouds, digital surface models (DSM) and orthomosaics were obtained for both sensors using a standard Structure-from-Motion (SfM) pipeline (Agisoft Photoscan, Agisoft, Russia; Kattenborn et al., 2018b). The point cloud densities was at average $\sim 1,000$ *points/m*² while the selected pixel size for the final digital surface models (DSM) and RGB and hyperspectral orthomosaics were ~ 0.1 m. The point cloud was filtered using TreesVis (Weinacker et al., 2004) to ensure uniform spaces between points of ~ 0.03 m. The corresponding Agisoft photoscan parameters can be found in Table S1. The UAV GPS trajectory logged during the flights were used to automatically georeference the tiles during the SfM workflow. Finally, hyperspectral reflectance data were obtained by calibrating the raw data with a reference panel with known reflectance, placed in the field during the flights. The final coverage of the acquired scenes were ~ 7 , 18 and 37 hectares for *U. europaeus*, *A. dealbata* and *P. radiata* respectively.

Costs for assessing the invasion status of a species via field sampling are usually high and may lead to biased results (Cacho et al., 2006; Kaplan et al., 2014). Instead of field sampling, we hence used the UAV orthomosaics to manually delineate all occurring canopies of the target invasive species (presences) in each flight (Figure 3.1). The canopy characteristics of the examined target species differed clearly in terms of their structural and spectral (e.g. flowering) properties to the native vegetation which enabled reliable delineations.

3.3.3 Shadow detection

All shadows occurring inside the manually delineated invasive species canopies (section 2.2.) were determined using an RGB-based histogram thresholding, which gives relative high accuracies while being straightforward to implement (Adeline et al., 2013). The thresholds were derived by visual interpretation (e.g. Adeline et al., 2013); where values below 80 digital number (DN; from a range of 0-255 DN; ~ 30 % reflectance) of the red band showed a reliable separation between sunlit and shaded canopies for the three species. Shaded areas accounted

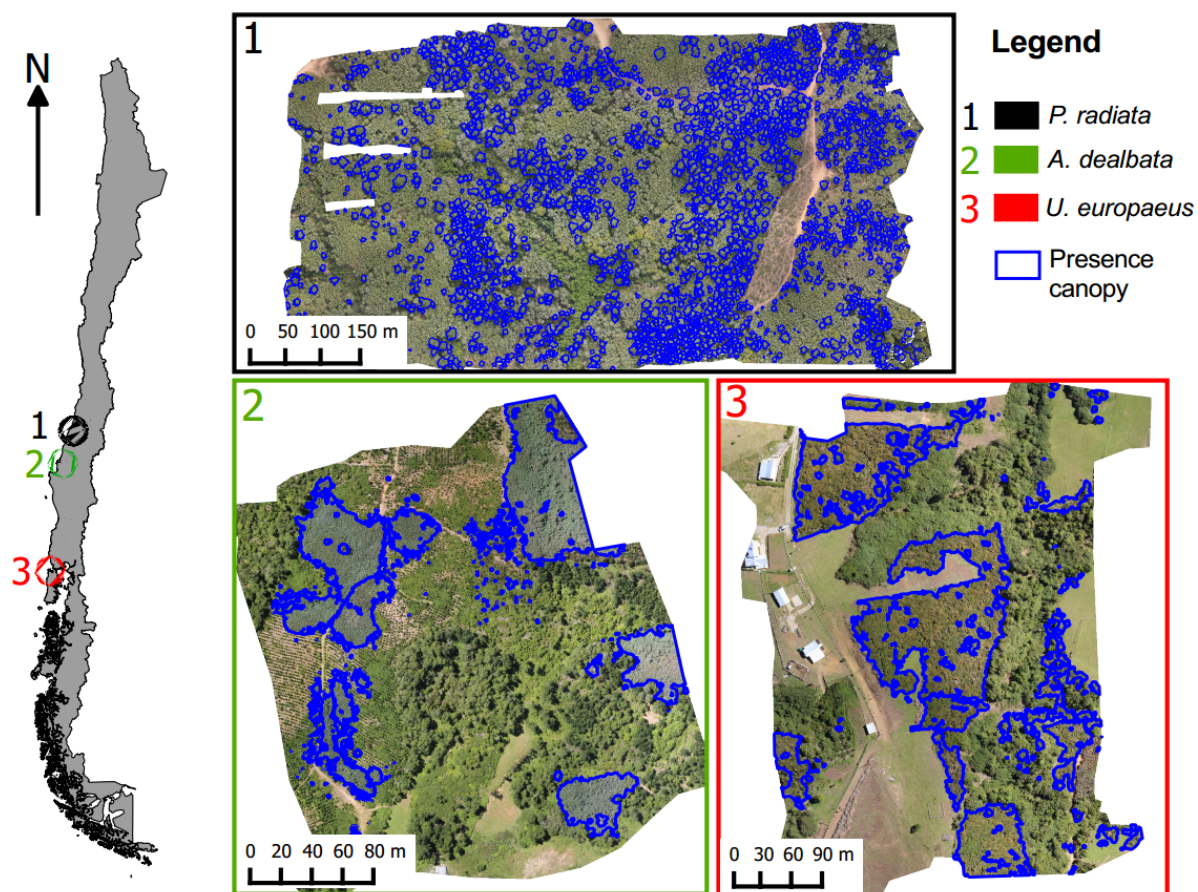


Figure 3.1: (A) Study areas in central-south Chile. (B–D) show the UAV-based RGB imageries. Blue polygons indicate the presence of the invasive species.

for $\sim 20\%$ of the invasive species canopies in all cases. Sunlit canopies were obtained by excluding the shaded areas from the delineated target species canopies.

3.3.4 Derivation of independent variables from the UAV data

Two types of spatial textural metrics were obtained from the RGB products: 1) a set of 2D texture layers based on the gray-level covariance matrix (GLCM; mean, variance, homogeneity, and entropy), and 2) a set of 3D structure layers derived from a multi-scale analysis of the photogrammetric point cloud (Brodu and Lague, 2012). Each metric type was calculated in 10 different spatial scales ranging from 0.25 to 4 m window size (using a 0.25 m and 0.5 m step between 0.25 m - 1 m and 1 m - 4 m, respectively). The different scales were chosen to derive information from both branch- and canopy-level. The GLCM indices were obtained by applying a moving window approach where each pixel was assigned with the above-mentioned

Table 3.1: Datasets for each invasive species. Texture corresponds to the GLCM variables while Structure corresponds to the CANUPO 3D variables. All datasets were tested at ~ 0.1 m pixel size.

# Model	Datasets included (number of variables)	Model abbreviation
1	RGB (3)	rgb
2	Hyperspectral (41)	hyper
3	Texture (40)	text
4	Structure (10)	struct
5	Structure + Texture (50)	structtext
6	Structure + RGB (13)	structrgb
7	Structure + Hyperspectral (51)	structhyper
8	Texture + RGB (43)	textrgb
9	Texture + Hyperspectral (81)	texthyper
10	Structure + Texture + RGB (53)	structtextrgb
11	Structure + Texture + Hyperspectral (91)	structtexthyper

metrics of the neighbouring pixels using the original RGB images at a spatial resolution of 0.1 m. The 3D structure algorithm processed principal component attributes at different spatial scales (3D neighborhood) for each point in the photogrammetric point cloud, representing the local dimensionality characteristics (shape and density) of the canopy (CANUPO algorithm; Brodu and Lague, 2012). Metrics calculated from the point clouds were rasterized (0.1 m pixel size) to facilitate the analysis. The R-package ‘gldm’ was used to create the GLCM, while the CANUPO toolbox along with LAStools and Python 3.6 were used to create the 3D structure raster components.

In total, we created eleven datasets by combining layers of spectral (i.e. RGB and hyperspectral), 2D textural and 3D structural information (Table 3.1). RGB and hyperspectral data were not combined as they contain redundant information.

3.3.5 Modeling and validation

We used the maximum-entropy (MaxEnt) classifier (Phillips et al., 2006) to model the occurrence of the invasive species for each UAV dataset. MaxEnt is a one-class classifier that uses presence (labeled) and background (unlabeled) data to create a relative likelihood distribution

(between 0 and 1) of the invasive species. MaxEnt has shown reliable results with remote sensing data (Mack et al., 2016; Skowronek et al., 2017a; Stenzel et al., 2017). From an operational point of view, the application of MaxEnt is very promising, as the delineation of training data of unwanted classes (e.g. other tree species, bare ground and water bodies) are not required during modeling, which notably decreases pre-processing or sampling efforts. In each study area, 500 presence samples were selected by randomly sampling pixels inside the delineated polygons of the invasive species crowns, while 2,000 background pixels were randomly sampled from the whole area. We used the R-package 'dismo' with default setting for the MaxEnt modeling.

To test how the 11 UAV-based independent variables (Table 3.1) were influenced by the presence of shadows, two types of models were tested: 1) MaxEnt models calibrated using all available presence data, including pixels of sunlit and shaded canopies, and 2) MaxEnt models calibrated using only presence data of sunlit canopies.

A variable selection was applied to each model. Variable selection minimizes the chances of overfitting (Merow et al., 2013) and enhances model transferability (Duque-Lazo et al., 2016). First, MaxEnt classifications using all available variables were performed using a 10-fold cross-validation. Then, the variables that obtained a permutation importance $< 5\%$ were dropped. Finally, from the remaining variables only the variables with shared correlations $r < 0.8$ were kept, while in case of correlation $r > 0.8$ the variable with higher permutation importance was considered. The particular method applied here was selected due to its lower CPU processing time compared to iterative methods (Jueterbock et al., 2016).

An iterative validation based on stratified bootstrapping (Kohavi, 1995) was used to obtain the distribution of model accuracies and rel. likelihood predictions that enable the estimation of significant differences among models. The model performances were evaluated for sunlit and shaded canopies separately. We used a stratified bootstrapping procedure with 100 repetitions. In each repetition, we randomly selected samples with replacement for the presence and background datasets, while we used the samples that were not selected in both cases ($\sim 36\%$) as holdout samples for validation. We evaluated the model performances in terms of area under the curve (AUC), Cohen's Kappa, sensitivity (true positive rate) and specificity (false positive

rate). We selected the thresholds for Kappa, sensitivity and specificity according to the values of maximum Kappa and (sensitivity + specificity), respectively.

We used a one-sided bootstrap pair test to check for significant differences ($\alpha = 0.05$) in the obtained accuracy (AUC, Kappa, sensitivity and specificity) between models. We specifically tested if: 1) models performed significantly better in sunlit canopies than in shaded canopies; 2) models excluding shaded canopies in calibration performed significantly better in sunlit areas than models including shadows in calibration; 3) models including shadows in calibration performed significantly better in shaded areas than models excluding shadows in calibration; 4) models including spectral, 2D textural and 3D structural information performed significantly better than one variable type alone. This bootstrap test has been applied in earlier studies following similar approaches (Lopatin et al., 2016; Castillo-Riffart et al., 2017; Araya-López et al., 2018).

3.3.6 Species occurrence maps

Relative likelihood prediction maps of the invasive species occurrences were obtained by estimating the median value of the 100 bootstrap iterations per pixel. We further estimated the coefficient of variation (CV) of each pixel as a measure of model stability during bootstrapping, where pixels with low CV denote higher predictive stability. Finally, binary maps of the invasive species presence were produced by using the median predicted likelihood maps and applying the median threshold value according to Kappa.

3.3.7 Shadow fraction simulation analysis

Species-specific canopy architecture influences the way species interact with light and hence their reflectance (Kattenborn et al., 2018a). The fraction of shadows is highly dependent on the sun-angle during the acquisition of optical remote sensing data. Understanding the dynamics of shadow fractions in the acquired images as a function of the sun angle is hence important to assess the potential effects on classification accuracies and to plan optimal data acquisition windows accordingly. This is particularly interesting for UAV applications which allow for a comparably flexible selection of the acquisition times.

To model how the 3-dimensional canopy architecture of the three examined species influence the production of shadow fractions throughout the course of a day, we simulated the shadows using the ~ 0.1 m DSMs of the study areas. Here, we varied the solar elevation and azimuth of beginning, middle and end of the 2017-2018 summer season along a daily period between 09:00 hrs - 18:00 hrs. We masked out all the canopies that did not correspond to the studied invasive species to exclude the effects of the neighbouring canopies. We used the R-packages 'insol' and 'suncalc' for the analysis.

3.4 Results

3.4.1 Model performances and independent variable selection

The accuracies of the models based on all presence samples (sunlit + shadows) and only sunlit canopies are summarized in Figure 3.2, while Table 3.2 shows the occasions where each model performed significantly better in sunlit areas than in shaded areas. Overall, model accuracies in terms of Kappa were significantly higher in sunlit canopies compared to shaded areas in almost all cases. Moreover, the accuracies in sunlit canopies improved when excluding shaded samples from the calibration data. Inaccurate classifications were found in shaded canopies even when shadows were included in calibration; presenting median Kappa values < 0.3 , uneven performances of sensitivity and specificity, and coefficient of variation (CV) values near 100% for Kappa and specificity (Figure S1). Concurrently, AUC values remained high in the shadow areas, showing less sensitivity to the effects caused by shadows than Kappa. Classification accuracies were higher for *A. dealbata* than for *P. radiata* and *U. europaeus*.

Models including RGB information improved significantly ($\alpha = 0.05$) when excluding shadows from the calibration data, while hyperspectral, 2D textural and 3D structural data alone did not vary significantly among model types (Figure 3.2). Sensitivity and specificity were found to vary more than AUC and Kappa, presenting few stable significant differences among model types. When using one type of independent variable, spectral information outperformed 2D textural and 3D structural information in most cases in terms of Kappa: RGB was found to be the best single option for *A. dealbata* while hyperspectral information was the best variable for

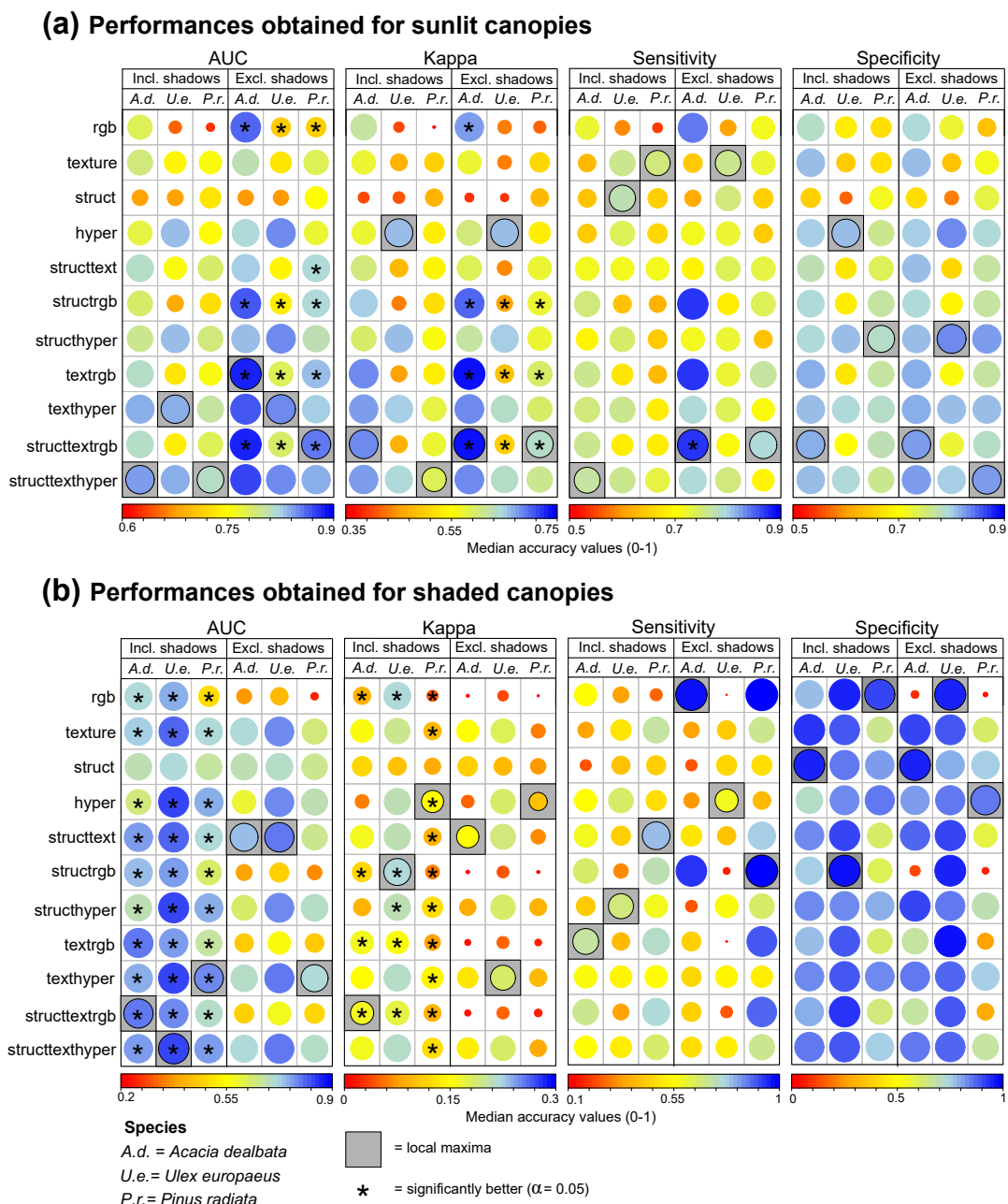


Figure 3.2: Model performances for sunlit (a) and shaded (b) canopies using models that include (incl.) and exclude (excl.) shadows in the calibration data. The median iterative values are presented, with dot size scaled to the values. *A.d.* = *Acacia dealbata*; *U.e.* = *Ulex europaeus*; *P.r.* = *Pinus radiata*. * depicts significant ($\alpha = 0.05$) improvements of the models: (a) shows significant improvements of models excluding shaded canopies. Contrary, (b) shows significant improvements of models including shaded canopies.

Table 3.2: Significant differences in terms of model performance between evaluations in sunlit and shaded canopies. Model including (incl.) and excluding (excl.) shadows during calibration are shown. Marks depict for which variable combinations and calibration data the performance was significantly better for sunlit than in shaded areas. A.d. = *Acacia dealbata*; U.e. = *Ulex europaeus*; Pr. = *Pinus radiata*.

	AUC														
	Kappa			Sensitivity			Specificity								
	Incl.	Shadows	Excl.	Incl.	Shadows	Excl.	Incl.	Shadows	Excl.	Incl.	Shadows	Excl.	Shadows		
rgb	A.d.	U.e.	Pr.	A.d.	U.e.	Pr.	A.d.	U.e.	Pr.	A.d.	U.e.	Pr.	A.d.	U.e.	Pr.
texture	***	**	**	***	***	***	***	**	***	***	***	*	**		
struct	**	***	**	***	**	***	***	***	*	***	**	**	**	*	**
hyper	***		**	**	*	***	*	**	***	*	**	**	**		
structtext	***	***	***	***	***	***	***	***	***	***	***	***	***	*	***
structrgb	***	*	***	***	***	***	***	***	***	***	***	*	**		
structhyper	***	**	***	**	***	***	***	***	***	***	***	*	*		
textrgb	***	***	***	***	***	***	***	***	***	***	***	**	*		
texthyper	***	*	***	***	***	***	***	***	***	***	***	*	**	*	
structtextrgb	***	***	***	***	***	***	***	***	***	***	***	***	**	**	*
structtexthyper	***	***	***	***	***	***	***	***	***	***	***	**	**	*	*

*Significance levels (α): *** 0.001, ** 0.05, * 0.1.

U. europaeus and *P. radiata*. The worst type of independent variable for *A. dealbata* and *U. europaeus* was the structural information while for *P. radiata* it was RGB. When combining multiple types of independent variables, the best data combination for *A. dealbata* and *P. radiata* was RGB + texture + structure. For *U. europaeus* the best combination of independent variables was hyperspectral + texture + structure. Only for *U. europaeus* the use of a single variable type (i.e. hyperspectral) resulted in higher performances compared to the combination of independent variable types. Significant differences between the use of the best single independent variables and the best combination of variables were obtained for *U. europaeus* and *P. radiata* in terms of Kappa. Only *A. dealbata* and *U. europaeus* showed significant differences among variable types in terms of sensitivity and specificity, respectively (Figure S2).

When combining hyperspectral, 2D textural and 3D structural information the variable importance (assessed by permutations of MaxEnt) was higher for spectral and 2D textural information than for 3D structural information (Figure 3.3). Nonetheless, for *P. radiata* the importance of 3D structural information was higher than for the other species. In most cases, 2D textural information obtained at canopy-level (1 m - 4 m window size) were more important than information obtained at branch-level (0.25 m - 1 m window size), except for *U. europaeus* which also selected branch-level variables. In all cases 3D structural information was only relevant at canopy scales.

3.4.2 Model predictions

The predicted rel. likelihood values using different independent variables (Figure 3.4) indicate good performances of the spectral information for identifying *A. dealbata* and *U. europaeus*. Predicted patterns improved for *P. radiata* when combining spectral, 2D textural and 3D structural information. All models had a general tendency towards overpredictions.

In Figure 3.5, examples of the predicted rel. likelihood based on the best models according to Kappa are displayed. Models where shadows were excluded during calibration obtained higher contrasts between the target species (higher median and lower CV rel. likelihood values) and the rest of the scene (lower median and higher CV rel. likelihood values). However, models calibrated using only sunlit canopies resulted in occurrence maps with a higher amount of canopy

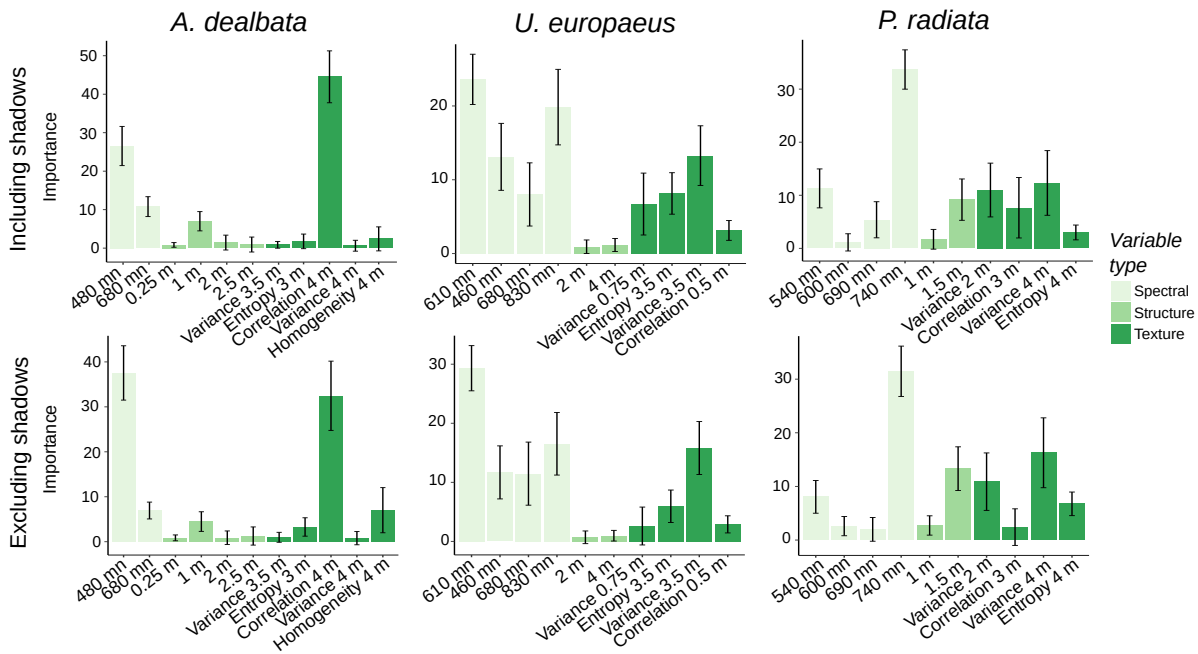


Figure 3.3: Variable importance based on MaxEnt permutation for the models including and excluding shaded canopies in the calibration data. Median and standard deviation values of the iterative validation are represented by barplots and error bars, respectively.

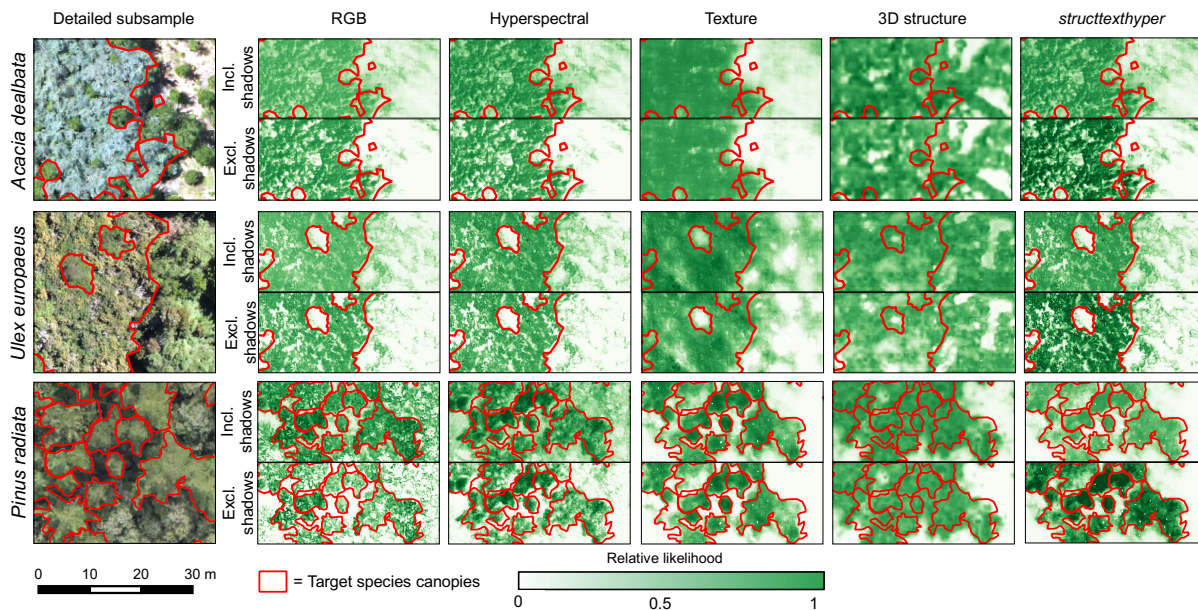


Figure 3.4: Relative likelihood predictions using different independent variables. Models including and excluding shadows during calibration are presented.

gaps (pixels with low rel. likelihood), corresponding to areas with shadows. Hence, models excluding shadows from the calibration data also yielded high false negative rates (lower specificity). The exceptions were models based on 2D textural information, which due to their multi-level window sizes were able to fill the canopy gaps (Figure 3.4).

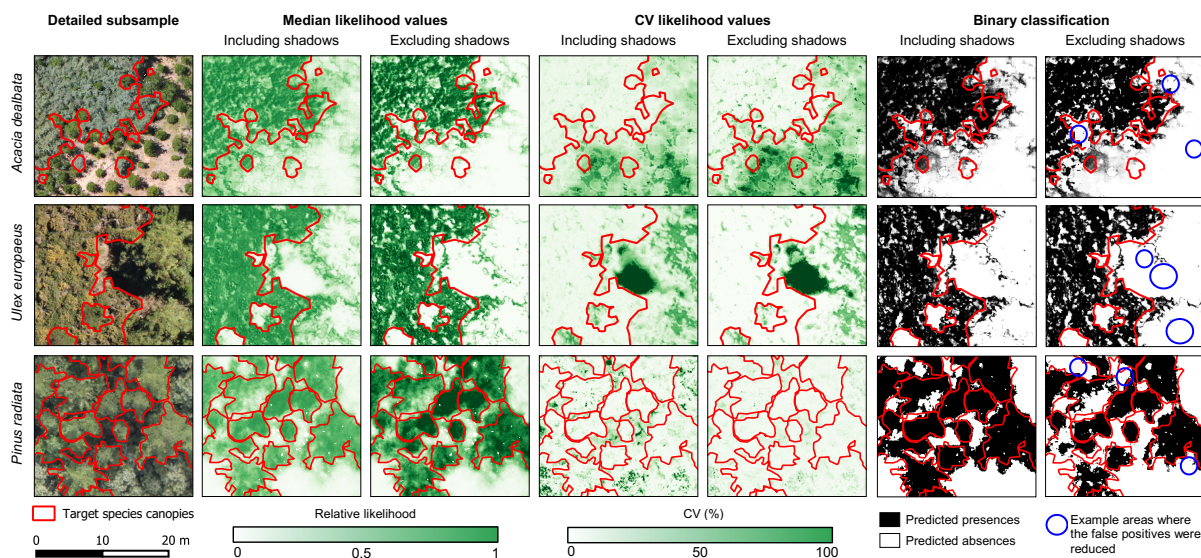


Figure 3.5: Comparison of species occurrence maps between models including and excluding shaded canopies in the calibration data. Models presented: *A. dealbata* and *P. radiata* = strcttexprgb, *U. europaeus* = hyper.

The relative likelihood, obtained in the shadowed areas by models including shaded canopies in the calibration data, was predominately lower than the Kappa threshold. Hence, binary presence/absence maps also presented large amounts of false negatives. The amount of false negatives (i.e. presences falsely predicted as absence) inside the invasive species crowns ranged between $\sim 20\%$ and $\sim 13\%$, which corresponded to $\sim 100\%$ and $\sim 65\%$ of the shadow areas for the models excluding and including shadow during calibration, respectively. Likewise, false positives outside the target crowns decreased by $\sim 17\%$ when excluding shadows during calibration (e.g. Figure 3.5 blue circles). This can be seen in the increase of sensibility of almost all models when excluding shadows from the calibration data (Figure 3.2a). Finally, the total amount of area covered by the invasive species canopies according to the binary maps of the models excluding shadows were $\sim 27\%$, 29% and 30% for *A. dealbata*, *U. europaeus* and *P. radiata* respectively. Models including shadows during calibration tended to overestimate the invasive species presence's with $\sim 5\%$ in all three species.

3.4.3 Shadow fraction simulation analysis

The simulations using the digital surface models (DSM; Figure 3.6) showed that the optimal acquisition window (here defined as less than 20% shadows) varied among the considered

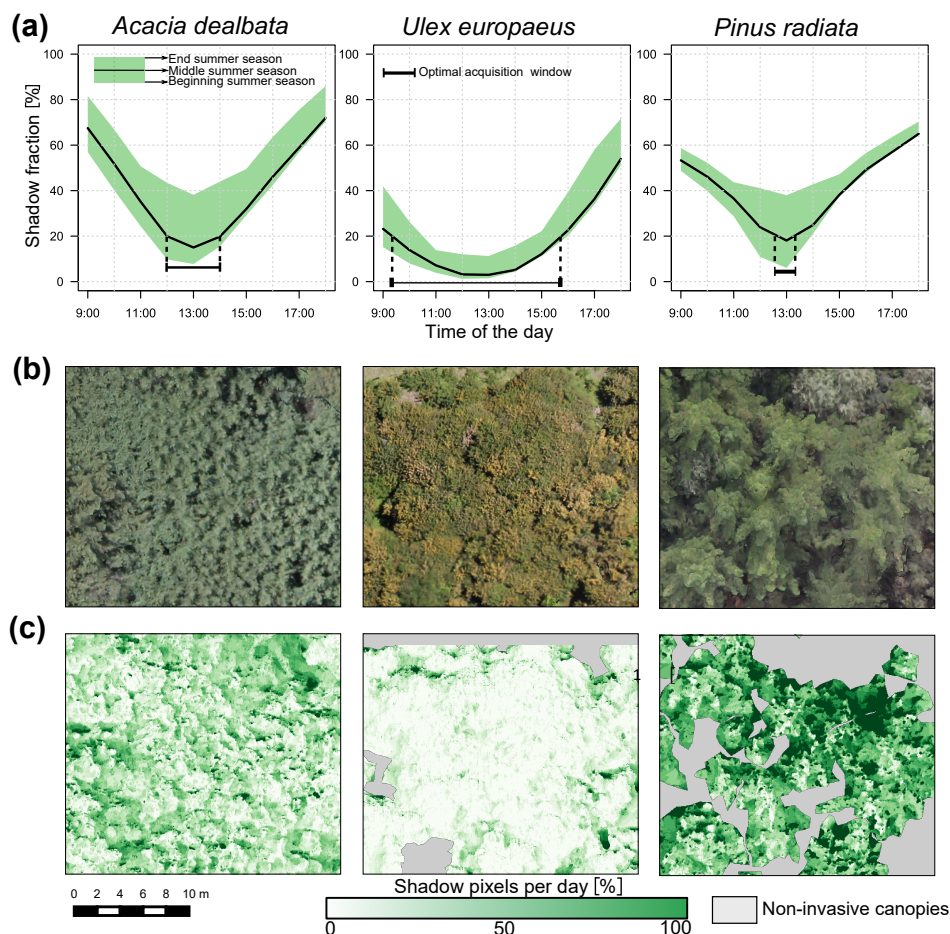


Figure 3.6: Shadow simulation using the digital surface models (DSM) and the sun elevation and zenith angles corresponding to beginning, middle and end of the summer season (i.e. 21-12-2017, 04-02-2018 and 20-03-2018) of each study site: (a) shows the simulated shadow fractions between 9:00 hrs - 18:00 hrs; (b) shows an RGB subsample of the target species canopies; and (c) shows the number of times (in percentage) that the pixels of the target canopies were under shadow for the daily period of the middle summer day (04-02-2018).

species: *U. europaeus* and *P. radiata* obtained the longest and the shortest optimal acquisition period, respectively. The simulated proportion of shaded crowns during the course of the day (Figure 6c) confirms that *P. radiata*'s canopies are shaded during a large portion of the day, while *U. europaeus* canopies are mostly sunlit.

3.5 Discussion

3.5.1 Shadows effects in MaxEnt models

Our analyses show that MaxEnt predicted likelihood values for shaded areas are inaccurate even when including shaded canopies during calibration (Figure 3.2b). This leads to a general

decrease of contrast in rel. likelihood between the actual target species canopies and the rest of the landscape which increases the false positive rate (Figure 3.5). Generally, between 65 % - 100 % of shaded parts of the target species were wrongly classified as absences. This ~13 % - 20 % wrongly classified canopy area could hamper the use of the predicted occurrences for subsequent ecological analyses, such as the analysis of detailed invasion dynamics or to upscale the mapping of the invasive species to larger scales via satellite imagery (e.g. Kattenborn et al. submitted). These errors were comparable to other UAV-based invasive species mapping studies which obtained user accuracies between 60 % - 95 % (Alvarez-Taboada et al., 2017; Mafanya et al., 2017; Müllerová et al., 2017; Cao et al., 2018).

Few UAV-based studies discussed the effects caused by shadows on their classification results: de Sá et al. (2018) found that shadows significantly decreased model accuracies in the detection of species of the genus *Acacia* under sunny conditions, while acquisitions under diffuse light conditions caused by clouds significantly increased classification accuracies due to a reduction of cast shadows. Nevertheless, cloudy conditions would also decrease the separability of spectrally similar classes (Zhang et al., 2015). In contrast, other studies showed that the inclusion of shadows into the training samples improved classification performances (Milas et al., 2017; Ishida et al., 2018). However, these classifications involved the separation of classes with less overlapping spectral signatures compared to the classes considered here. When the separation of a species from other species with similar spectral characteristics is pursued, the high amount of intraspecific variance can hamper pixel-based classification performances (Lopatin et al., 2017).

According to Milas et al. (2017), the amount of detected shadows vary depending on the spatial resolution, which we did not consider in this investigation. We also did not account for gradients of shadows in our analyses (e.g. Milas et al., 2017), but used a binary classification. Nevertheless, from our results (i.e. between 65 % - 100 % of misclassification rate inside shaded areas) we assume that shadows in general negatively affect the performance of pixel-based classification algorithms and that should be avoided whenever possible. However, we do not dismiss the possibility that shadows could at some point enhance classifications when algorithms that efficiently exploit complex neighborhood information are used (e.g. convolutional

neural networks). This assumption could be supported by the fact that all three species showed differences in their daily shadow fractions and temporal distributions (Figure 3.6)

The amount of cast shadows could be reduced (and hence the false negative rate) by acquiring the UAV data at an ideal time. In our simulation exercise, this ideal time was consistently identified to be around $\sim 13:00$ hrs local time. The shadow simulation performed in our study sites showed that the width of the optimal temporal acquisition window varied greatly according to the species-specific canopy characteristics (Figure 3.6). At the spatial scales considered in this study, *U. europaeus* usually builds more homogeneous canopies, yielding generally less shadow fractions in comparison to *P. radiata*, which depicted the highest amount of shaded areas during the day (Figure 3.6c). These differences are explained by the canopy architecture of the species, as the spherical crown shapes from *U. europaeus* and *A. dealbata* results in relatively homogeneous canopy structures when canopies are closed. This leads to generally low shadow fractions. Contrary, the vertical conical shapes and the star-shape branching pattern of *P. radiata* lead to high shadow fractions. Even in high density stands there are relative distinct height differences between the higher and the lower parts of the neighboring crowns. Because we were mostly interested in the species-specific shape characteristics of the invasive species canopies, we did not include the canopies of the native species in the analysis. In highly heterogeneous interspecific stands such as the one presented in the *P. radiata* flight, neighboring species with different canopy shapes and sizes may also influence the shadow fraction of the general canopy.

In order to minimize shadows and their effects on classification tasks in UAV-based species mapping applications, species-specific considerations regarding data acquisition are recommended. The approach proposed here to simulate shadows using digital surface models can be a useful tool to assess the shadow fractions during the course of a day and to plan revisit acquisitions accordingly. The canopy structure of the invasive species also differ from the structure of the native forests and shrublands. Chilean native forests of the area tend to growth in highly heterogeneous stands of broadleaf species (e.g. tree species richness between 4 and 30 species in 225 m^2 plots; Lopatin et al., 2016) with many understorey species. On the contrary, woody individuals in shrublands tend to growth in a scatter manner (Luebert and Pliscoff, 1999). Both

vegetation types contrast with the clustered growth and relatively uniform canopies of *A. dealbata* and *U. europaeus* (e.g. Fuentes-Ramírez et al., 2011) and the conical canopy shape of *P. radiata*. These characteristics make the selected invasive species suitable for experimentation with remotely sensed data, as they clearly differ from the native stands in terms of structure and growth strategy and hence should be comparably easy to detect.

3.5.2 Variable importance

We found that AUC responses were not sensible to the observed negative effects of shadows in the model predictions, hence we will refer only to Kappa for general tendencies. Our results show that the best combination of independent variables depends on the target species, and that shadows significantly affected models using all types of independent variables. Models including RGB depicted largest improvements when excluding shadows from calibration, while 3D structure varied the least (Figure 3.2a and 5). The models combining RGB, 2D textural and 3D structural information yielded high performances for *A. dealbata* and *P. radiata*, maybe due to the eye-catching silver and dark color of the species leaves respectively (see detailed subsample of Figure 3.4). This could be advantageous from an operational point of view as the cost and processing efforts of RGB data are generally lower than for hyperspectral data. This corroborates the findings of de Sá et al. (2018), which also classified a species of the genus *Acacia* (i.e. *A. longifolia*) with high accuracies using RGB imagery.

Contrary, *U. europaeus* was mapped with highest accuracies when applying hyperspectral data alone, which could be due to its rather homogeneous canopy with few structural and hence textural differences (Figure 3.6c). On the other hand, the 3D structure was particularly relevant for mapping *P. radiata* (Figure 3.3). This is because *P. radiata* have a conical crown shape that clearly differs from the native broadleaved species (Ishii and Asano, 2010). Contrarily *A. dealbata* and *U. europaeus* have relatively similar crown shapes and structure as the native flora. The structural specifics of conifer species were found to be well captured in UAV-based 3D structural metrics also in other studies (Franklin et al., 2017).

Generally, the canopy-level information (1 m - 4 m window size) outperformed the branch-level information (0.25 m - 1 m window size) for both 2D texture and 3D structure variables. This

indicates that branch characteristics – e.g. branch form, branch orientation and leaf clumping - are less important than canopy differences. The importance of 2D textural metrics was found also in other studies (Michez et al., 2016; Lu and He, 2017; Cao et al., 2018). It can be assumed that, in contrast to information of single pixels (e.g. as for RGB or hyperspectral predictors), the textural metrics are less affected by small scale variations, since these metrics are based on larger spatial scales (0.25 m – 4 m). Moreover, it can be assumed that the texture metrics can even bundle this spatial variation (e.g. small scale variation of sunlit and shaded crowns) in information that facilitates the classification task.

We found significant performance differences based on the validations in sunlit and shaded canopies in almost all cases (Table 3.2). This also applied for models trained with only structural information, indicating that shadows also hampered the creation of the photogrammetric point clouds (performed in Agisoft Photoscan, Agisoft, Russia). Nevertheless, for spectral variables (especially RGB) the predicted rel. likelihood differed stronger between models including and excluding shadows from the calibration than for 2D textural and 3D structural variables (Figure 3.4). This was more pronounced in *P. radiata* than for the other two species. We assume that spectral predictors were more affected by shadows in *P. radiata*, because of its more complex canopy structure and higher shadow fraction (Figure 3.6c).

For all species we observed false negatives, that were spread in a rather scattered manner (Figure 3.4). One option to address this issue could be to apply pre- and post-processing techniques, such as local filters (e.g. clump and sieve operators) and object-based analysis. Object-based analysis is known to decrease the so called salt-and-pepper effect caused by pixel-based classifications (Yu et al., 2006). This is one reason why many previous UAV-based invasive species mapping studies have used it. These studies did not consider the elimination of shadows prior to the allocation of spectral values to the segmented clumps (Alvarez-Taboada et al., 2017; Baena et al., 2017; Cao et al., 2018). Integrating both sunlit and shaded canopy reflectance into the segments could hamper the success of classification tasks if shadows are considered as noise.

3.5.3 Classification approach

One-class classifiers (OCC) are promising for invasive species mapping as only presence data of the target species are needed, decreasing field and laboratory work (hence being appealing for management agencies). MaxEnt is considered to be a robust and transferable OCC (Duque-Lazo et al., 2016) that yield high performances compared to other OCC algorithms in remote sensing applications (Stenzel et al., 2017). Because MaxEnt is very CPU demanding (Mack et al., 2016), especially combined with bootstrapping validation, we reduced CPU processing time by using a comparable small set of presence/background samples. We used 500/2,000 instead of the sometimes recommended $\sim 5,000/10,000$ presences/background samples (Stenzel et al., 2017). We compared MaxEnt performances for the *structtexthyper* independent variables (median accuracies and predictions) using 500/2,000 and 5,000/10,000 presence/background samples with a 10-fold cross validation for the three species and found no marked differences. Hence, we assume that the lower number of samples did not affect our result notably in this study.

3.6 Conclusions

Here, we investigated the effects of shadows on the predicted occurrences of three woody invasive species of central-south Chile using spectral (RGB and hyperspectral data), 2D textural and 3D structural variables derived from photogrammetry.

We found that shadows significantly affect the results of models trained with all types of variables. Areas with shadows obtained misclassification rates between 65 % - 100 %, even when shadows were included during model calibration. Particularly spectral and 2D textural variables were affected by shadows, leading to inaccurate model predictions in shaded areas and resulting in an increase of false negative predictions. Accordingly, the use of UAVs for mapping invasive plant species benefits from ad hoc pre-processing. The exclusion of shadows prior to model calibrations improved model predictions in all cases, especially in terms of false positives. Most accurate and robust results were usually obtained when combining spectral, 2D textural and 3D structural information. The use of hyperspectral instead of RGB data im-

proved accuracies only for one of the three species (i.e. *U. europaeus*). Finally, the performed shadow simulations based on the photogrammetric digital surface models demonstrated that each species-specific canopy structure result in different shadow fractions during the course of a day. *P. radiata* showed a comparably narrow time period with a small shadow fraction. The rather smooth canopies of *A. dealbata* and *U. europaeus* resulted in a longer time span during the day with smaller shadow fractions. Hence, UAV data acquisitions need careful planning to minimize shadows and their related problems in species mapping applications. From the results of this investigation we hypothesize that shadows should not be used during calibration when pixel-based classifiers are used. Nevertheless, we do not discard the possibility that the negative effects of shadows on classification results could be reduced by using approaches that include complex neighborhood information as information (e.g. deep learning). More investigation is needed to decrease the large amount of false negatives produced by shadows.

4 Using aboveground vegetation attributes as proxies for mapping peatland belowground carbon stocks

This paper has been submitted as: *Lopatin, J., Kattenborn, T., Galleguillos, M., Perez-Quezada, J., Schmidlein, S. (2019). Using aboveground vegetation attributes as proxies for mapping peatland belowground carbon stocks. Remote Sensing of Environment 231, 111217.*

4.1 Abstract

Peatlands are key reservoirs of belowground carbon (C) and their monitoring is important to assess the rapid changes in the C cycle caused by climate change and direct anthropogenic impacts. Frequently, information of peatland area and vegetation type estimated by remote sensing has been used along with soil measurements and allometric functions to estimate belowground C stock. Despite the accuracy of such approaches, there is still the need to find mappable proxies that enhance predictions with remote sensing data while reducing field and laboratory efforts. Therefore, we assessed the use of aboveground vegetation attributes as proxies to predict peatland belowground C stock. First, the ecological relations between remotely detectable vegetation attributes (i.e. vegetation height, aboveground biomass, species richness and floristic composition of vascular plants) and belowground C stock were obtained using structural equation modeling (SEM). SEM was formulated using expert knowledge and trained and validated using *in-situ* information. Second, the SEM latent vectors were spatially mapped using random forests regressions with UAV-based hyperspectral and structural information. Finally, this en-

abled us to map belowground *C* stock using the SEM functions parameterized with the random forests derived maps.

This SEM approach resulted in higher accuracies than a direct application of a purely data-driven random forests approach with UAV data, with improvements of r^2 from 0.39 to 0.54, normalized RMSE from 31.33 % to 20.24 % and bias from -0.73 to 0.05. Our case study showed that: (1) vegetation height, species richness and aboveground biomass are good proxies to map peatland belowground *C* stock, as they can be estimated using remote sensing data and hold strong relationships with the belowground *C* gradient; and (2) SEM facilitates to incorporate theoretical knowledge in empirical modeling approaches.

4.2 Introduction

Peatlands are important for the regulation of carbon (*C*) cycling and store one third of the world soil *C* stock (Parish et al., 2008), from which belowground *C* accounts for ~95% of the total peatland *C* pool (Smith et al., 2004). These are fragile ecosystems and if the conservation of their peat properties is degraded either due to anthropogenic impact or climate change, they release accumulated soil *C* to the atmosphere (in the forms of CH_4 and CO_2) faster than it is being sequestered (Fenner and Freeman, 2011). This accelerates the greenhouse effect and global warming (Phillips and Beerli, 2008; Schaepman-Strub et al., 2008). Although concerns about the consequences of human-induced changes to the *C* cycle have generated many international initiatives to quantify peatland *C* stocks (Hribljan et al., 2017), the contribution of *C* stock in small isolated peatlands in comparison to larger systems is still uncertain (McClellan et al., 2017).

Remote sensing provides a rapid and economical approach to supplement traditional direct methods such as coring and probing (Rudiyanto et al., 2018). Frequently, in-situ measurements include peat thickness, dry bulk density and carbon concentration, which has to be obtained by laboratory analysis (Dargie et al., 2017), while remote sensing products include the peatland area and vegetation types. These variables are then used to predict belowground *C* stock by applying allometric functions to the obtained vegetation classes. For example, Dargie et al.

(2017) have used a maximum likelihood classification with radar, optical and DEM-derived data to classify different land covers including *terra firme* and peatland classes. Afterwards, they have used *in-situ* data to create allometric functions with peat and soil properties as input to estimate the total *C* pools of the central Congo basin. Other studies have used remote sensing to map peatland attributes, such as peat thickness, and derived continuous estimations of belowground *C* stock by allometric functions using these spatially explicit estimations (Rudiyanto et al., 2018). Despite the accuracy of such approaches, their application is hampered by high field and laboratory costs. Hence, linkages between belowground *C* stock and aboveground peatland attributes derived by remote sensing, such as vegetation attributes, could be used to decrease monitoring efforts.

Ecological studies have already established empirical knowledge about linkages between aboveground vegetation attributes and belowground *C* stock. For example, vegetation properties such as aboveground biomass, species richness and plant functional type cover are related to the decrease of water-logging and peat mineralization processes in peatlands (Dorrepaal et al., 2005; Jonsson and Wardle, 2009). The abundance and biomass of certain vascular species have proven to be good proxies of belowground *C* stock, while species richness has been shown to be positively related to soil microbial activity (Chen et al., 2017, 2018; Cong et al., 2014; Lange et al., 2015) and hence to organic matter decomposition rate (Fenner and Freeman, 2011). Previous studies have retrieved these proxies in peatlands using remote sensing data directly. For example, Castillo-Riffart et al. (2017) and Cabezas et al. (2016) estimated species richness in anthropogenic peatlands using a combination of satellite optical and textural data, while Turetsky et al. (2011) successfully estimated aboveground biomass. Likewise, species composition, plant functioning and growth forms have been mapped successfully by hyperspectral data with reasonable accuracies (Harris et al., 2015; Schmidtlein et al., 2012; Schmidtlein and Sassin, 2004).

To assess the relationship between vegetation attributes and belowground *C* stocks, we propose to use structure equation models (SEM). SEMs are a family of multivariate methods that allows the definition of preexisting relationships between variables (expert knowledge). Accordingly, SEMs are well-suited for hypothesis testing and understanding underlying processes. Further-

more, SEMs can be constrained using prior knowledge (e.g. causal relationships) of the system at hand and they thus feature a higher transferability than pure data driven modeling approaches (Grace et al., 2010).

The main objective of this study was to assess the potential of vegetation attributes as proxies to predict and map belowground *C* stock in a small isolated peatland in Chiloé Island, Chile. First, linkages among vegetation attributes and belowground *C* stock were investigated using SEM. Second, we combined hyperspectral and photogrammetric information derived from an Unmanned Aerial Vehicle (UAV) to spatially extrapolate the previously selected vegetation attributes with random forests regressions. Finally, we fed the SEM with the random forests extrapolations to obtain the belowground *C* stocks maps.

Using this general setup, we addressed the following research questions:

- Does the structural equation model outperform a purely data-driven random forests approach?
- Which mappable aboveground vegetation attributes are reliable indicators of belowground *C* stocks?

4.3 Materials and methods

4.3.1 Study site

The study site is an anthropogenic acidic peatland located at the FLUXNET site Senda Darwin Peatland (CL-SDP; 418520 S, 738400 W) in the north of Chiloé Island, in the Los Lagos region of Chile (Figure 1a,b). This peatland was formed due to the burning of a temperate rainforest, which produced a poorly drained soil that was later colonized by moss species of the genus *Sphagnum* (Díaz et al., 2007). The belowground *C* stock of this peatland were estimated as $\sim 11.56 \pm 1.57 \text{ kg m}^{-2}$ (Cabezas et al., 2016).

The study area is about 16 ha and covers two types of land use (Figure 1b): a conservation area (~ 5.5 ha; southern part of the area) which has been protected and used for scientific investigations for the last 20 years, and a managed area (~ 10.5 ha; northern part of the area) where

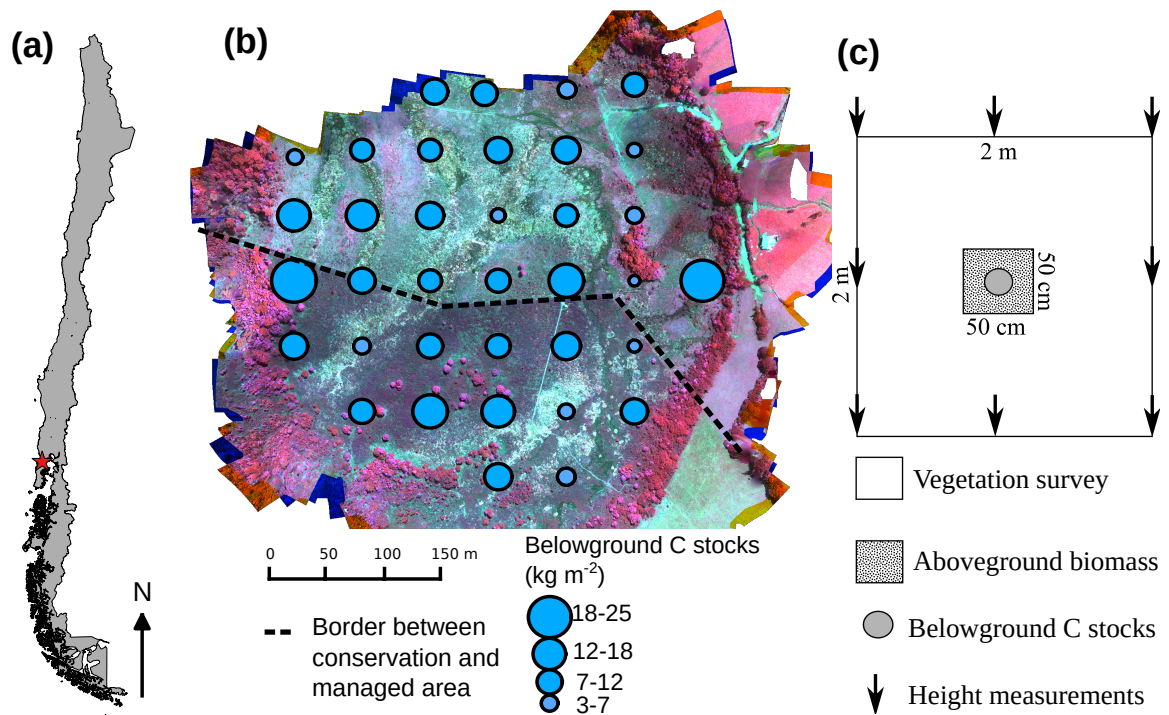


Figure 4.1: (a) Location of the study area in Chile; (b) UAV false color composite (R = 765 nm, G = 665 nm, B = 565 nm) of the study area with plot locations scaled with the measured belowground C stock (blue points). The dashed line shows the border between the conservation area (bottom) and the managed area (upper); (c) detailed sampling design.

Sphagnum mosses are artisanally harvested for commercial purposes (~10 kg of dry moss per month) and for grazing of four oxen (see Cabezas et al. (2016) for a full description of the area). The floristic composition of the area is dominated by *Sphagnum magellanicum*, but also by the bryophytes *Dicranoloma imponens* and *Campylopus introflexus*. These species can be found in sites affected by water logging. With less water availability, dominant graminoids species are *Danthonia chilensis*, *Schoenus rhynchosporoides* and *Uncinia tenuis*. On poorly-drained and water-saturated areas dominant species are *Juncus procerus*, *Juncus planifolius* and *Juncus stipulatus*. Common forb species are *Anagallis alternifolia*, *Centella asiatica* and *Lotus pedunculatus*, while common shrub species are *Baccharis patagonica*, *Gaultheria mucronata* and *Myrteola nummularia* (list of species in Appendix A of Cabezas et al., 2016).

4.3.2 In-situ / reference data

A vegetation assessment was conducted between January and April 2014, in which 36 plots were established in a systematic grid with 60 m × 60 m spacing. Each plot was a 2 m × 2 m

quadrat where the species presence, cover, biomass, vegetation height, soil depth and the C stocks were estimated.

Species coverages were obtained by averaging visual estimates of two observers. The biomass and C reservoirs were divided into two type of stocks: the aboveground stock included the vascular flora growing on the substrate, and the underground stock included the peat, live moss, debris (fine and coarse) and buried trunks (remnants from burning the forest). A detailed description of the sampling methods is presented in Cabezas et al. (2016); the aboveground biomass stock for each plot was estimated by harvesting the vascular flora in a 0.25 m^2 sub-plot located in the center of the plot. Belowground C stock, consisting of peat, living moss, woody debris (fine and coarse) and buried burnt trunks, were sampled using a peat profile sampler (Eijkelkamp, Giesbeek, Netherlands) at the central point of the plot (Figure 1c). Soil and aboveground C stocks were dried at $70\text{ }^\circ\text{C}$ for 72 h to obtain the weight and density of the material, and to estimate their values in kg m^{-2} . Five composite samples were generated from random sampling points to obtain the C fraction for each stocks (Cabezas et al., 2016). From these composite samples a sub-sample of 10 g was extracted, ground mixed and processed in an elemental analyzer (NA2500, Carlo Erba, Milan, Italy). Soil depth was measured by summing up all these composites.

4.3.3 UAV data acquisition

Hyperspectral data were collected in February 2016 using a UAV (octocopter) based on NAZAM V2 flight controller (DJI, Shenzhen, China). The UAV carried two small snapshot mosaic cameras (Gamaya, Lausanne, Switzerland), one covering the visible spectral region (VIS) with 16 bands and the other the near-infrared (NIR) spectral region with 25 bands. The flight plan aimed for an average of 80 % of forward and 70 % of sided overlap, and an altitude of 100 m above the ground. The image frames were processed in a Structure-from-Motion (SfM) pipeline (Agisoft Photoscan, Russia) to obtain a single hyperspectral brick of 41 bands (450 nm - 950 nm and 10 nm bandwidth) and a point cloud with elevation information (Kattenborn et al., 2018b; Lopatin et al., 2019). Reflectance data were obtained by calibrating the raw hyperspectral data with a reference panel with known reflectance placed in the field during the flight. The resulting

pixel size of the hyperspectral orthomosaic was ~ 0.1 m while the point cloud densities resulted in $\sim 1,000$ points/ m^2 (i.e. an average of 1 point every 0.003 m).

The height values of the point cloud were transformed from meters above sea level to meters above the ground using TreesVis (Weinacker et al., 2004). Retrieving absolute vegetation height information from SfM-based point clouds can be challenging in peatlands as there is a low chance that points representing the terrain will be reconstructed (Mercer and Westbrook, 2016). As we considered peat as part of the belowground stocks, only vascular vegetation height was measured. We used the measured *in-situ* vascular vegetation height to correct for possible shifts in the SfM-based elevations. A bilinear interpolation was applied to the average height values of the point cloud falling inside the plots using the average plot measurement as targets. The vegetation height accuracy resulted in root mean square errors (RMSE) of ~ 0.02 m.

Finally, both hyperspectral data and the point cloud were georectified with bilinear interpolation using a Pleiades panchromatic image ($0.5 \text{ m} \times 0.5 \text{ m}$) collected on January 28, 2014. We selected 23 steady features (e.g. tree crowns and corners of an elevated footbridge located in the conservation area) as ground control points. The positional accuracy resulted in RMSE of ~ 0.40 m. Moreover, we placed markers without georeference in the corners of all 36 plots to make the plots directly visible from the hyperspectral orthomosaic. From the 36 plots, only 31 were finally visible in the orthomosaic. Unseen markers were located mainly in the conservation area, where the visibility was hampered by the high shrub biomass. For plots where the markers were not visible in the orthomosaic, we retrieved the spectral and vascular vegetation height information from the GPS position, assuming the small level of errors added to the data.

4.3.4 Selected aboveground vegetation attributes

We reviewed the literature to determine the main vegetation characteristics related to peatland belowground *C* stocks. We used this information to develop a structural equation model that assimilates this knowledge into a network of multivariate interactions, which were trained with and tested against our data.

The key aboveground vegetation characteristics influencing belowground *C* stocks were related to the decrease of water-logging and peat mineralization, which are causing the decline

of *Sphagnum* cover and promoting the colonization by vascular plants. Hence, these characteristics relate to processes that alter belowground fluxes and gas-exchanges, resulting in a slow decrease in *C* stocks. Moss species (mainly *Sphagnum* spp) exude inhibitory polyphenol compounds by the rhizoids that increase the accumulation of belowground *C* due to a low decomposition rate of organic matter (i.e. the decomposition rate is lower than the accumulation rate; Fenner and Freeman, 2011). On the contrary, vascular plants tend to stimulate belowground microbial activity through increased labile carbon, accelerating the decomposition rate of the organic matter. This is followed by an expected alteration of soil nutrient content, pH conditions and a water table that further reinforce the vascular plant colonization. This will cause the decrease of peat abundance and eventually belowground *C* stocks (Fenner and Freeman, 2011). For this reason, the cover and biomass of growth forms (i.e. bryophytes, graminoids, forbs and shrubs) and certain vascular species have been shown to be proxies for the *C* stocks (Dorrepaal et al., 2005; Ma et al., 2017). Likewise, a higher plant diversity has been demonstrated to increase rhizosphere *C* inputs and belowground microbial activity (Chen et al., 2017, 2018; Cong et al., 2014; Lange et al., 2015), hence increasing the organic matter decomposition rate on peatlands (Fenner and Freeman, 2011).

Following these relations, we selected four aboveground vegetation characteristics from the literature related to belowground *C* stocks that can be estimated from remote sensing data with moderate accuracies: vegetation height (Rudiyanto et al., 2018), species richness (Castillo-Riffart et al., 2017), aboveground biomass (Turetsky et al., 2011) and the assemblages of vascular species communities or floristic gradients estimated by an ordination algorithm (Non-metric Multidimensional Scaling, NMDS, see Supplementary data; e.g. Schmidlein and Sassin (2004). The range observed for these variables and their indicators are presented in Table 1. Furthermore, we included soil depth as a key intermediate mediator (Akumu and McLaughlin, 2014).

Table 4.1: Plot-based variables included in the modeling.

Variables	Indicators (unit)	Min	Mean	Max
Vascular vegetation height	Vegetation height (cm)	2.83	30.3	130.55
Floristic composition	NMDS 1	-0.78	0	1.18
	NMDS 2	-1.13	0	0.71
	NMDS 3	-0.66	0	1.13
Vascular aboveground biomass	Shrub biomass ($kg m^{-2}$)	0	0.38	5.36
	The sum of graminoid, forb and fern biomass ($kg m^{-2}$)	0.03	0.13	1.86
Vascular species richness	Shrub richness (N)	0	4	7
	Graminoid richness (N)	0	1.81	4
	Forb richness (N)	0	1.43	5
	Ferns richness (N)	0	2.01	5
	The sum soil depth of peat, live moss, debris (fine and coarse) and buried trunks (remnants from burned forest) (cm)	18.5	38.47	91
Belowground C stocks	The sum carbon stocks of peat, live moss, debris (fine and coarse) and buried trunks (remnants from burned forest) ($kg m^{-2}$)	3.07	11.4	24.91

4.3.5 Algorithms used

4.3.5.1 Random forests

The ensemble regression tree method random forests (RF; Breiman, 2001) has been reported to be an efficient regression algorithm when the numbers of observations is comparably low in relation to the number of predictors (Svetnik et al., 2003). RF requires two parameters to be set: 1) *mtry*, the number of predictor variables used for the data partitioning at each split and 2) *ntree*, the total number of trees to be grown in the model run. We set *ntree* to 500 based on literature recommendations, whereas *mtry* was tuned using leave-one-out cross-validation. The importance of predictor variables was measured by the Gini decrease in node impurity measure, which is computed by permuting the predictor variables with the out-of-bag data in the RF validation approach (compare Liaw and Wiener, 2002).

4.3.5.2 Structural equation modeling

Structural equation modeling (SEM) is a multivariate family of methods that can model a large number of interactions simultaneously, providing a framework for inferring cause-effect relationships and estimating direct and indirect relations among variables (Grace et al., 2010).

We used partial least squares path modeling (PLS-PM or PLS-SEM; Tenenhaus et al., 2005), a non-parametric composite-based SEM, which is mainly used in social science, but has already shown potential in ecological (Ferner et al., 2018) and remote sensing applications (Lopatin et al., 2015). PLS-PM is validated at different levels (i.e. loading, weights, R^2), and has an overall model goodness-of-fit (GoF; ranging from 0 to 1, where 1 is a perfect representation) proposed by Tenenhaus et al. (2005). The significance ($\alpha = 0.05$) of each interaction and model outputs were obtained by means of bootstrapping (1,000 iterations).

PLS-PM can create latent variables (LVs) comprised of one or several variables in a supervised manner. Thus, PLS-PM can create components to separate predictors according to their correlations and reduce overfitting. We used all LVs in reflective mode or type 'A' (see Tenenhaus et al. (2005) for information on the LVs types). The interactions among LVs are explained by Linear Ordinary Least Squares (OLS). We standardized variables to normalize path coefficients and intercepts (i.e. turn variables with different raw units into standard deviation units; Grace and Bollen, 2005). The PLS-PM was tuned using the Cronbach's alpha index (check for unidimensionality among indicators) and the loading values (correlation within the indicators of a LV; variables with loadings below 0.5 were dropped).

The theoretical construct of the model is presented in Figure 2 and the indicators used in Table 1. We used Moran's I index and spatial correlograms to check for spatial autocorrelation on the residuals of the bootstrapped LVs.

4.3.6 Modeling and validation

Three types of belowground C stocks predictive models were tested (summarized in Figure 3):

1. using random forests and PLS-PM independently with plot-based predictors (Figure 3a);
2. using random forests and PLS-PM independently with UAV-based predictors (Figure 3b);

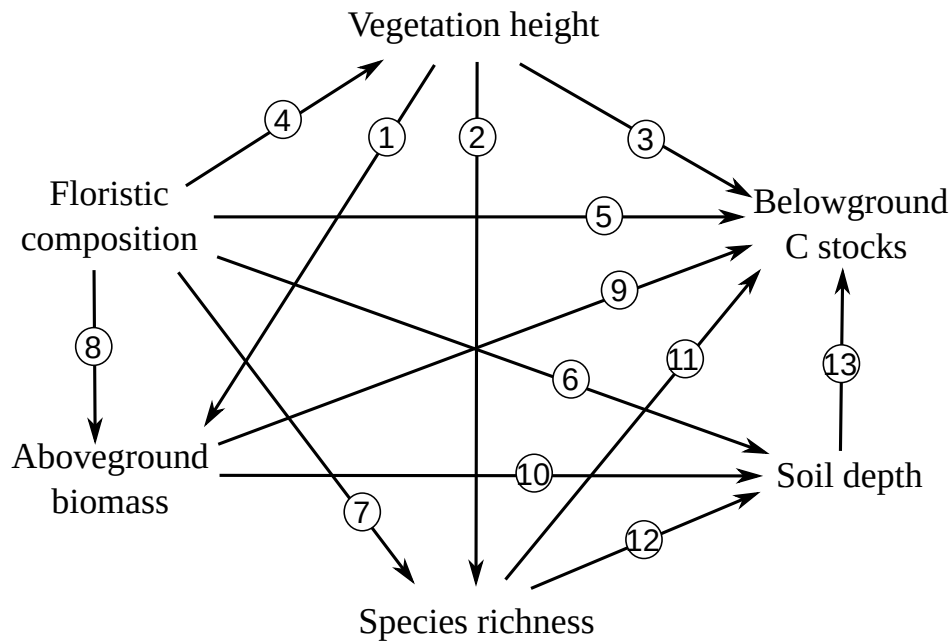


Figure 4.2: The hypothesized model for the plot-based PLS-PM. Solid black lines represent expected effects obtained from literature. Examples are (1), (2), (3), (4), (5) and (6) Lawson et al. (2014); (7) Rocchini et al. (2018); (8) Dorrepaal et al. (2007); (9) and (10) Dorrepaal et al. (2005); (11) and (12) Lange et al. (2015) and (13) Lawson et al. (2014), Akumu and McLaughlin (2014) and Draper et al. (2014).

3. using a hybrid model combining PLS-PM plot-based information with random forests UAV estimations (Figure 3c).

In the models depicted in Figure 3 a) and b), PLS-PM and RF were used independently to compare their performances. For the plot-based models we used the variables presented in Table 1, while the remote sensing models (Figure 3b) were parameterized with UAV-based spectral and height information. We applied a brightness normalization (Feilhauer et al., 2010) to the hyperspectral data to compensate for high heterogeneity in illumination owed due to the high spatial resolution and a minimum noise fraction transformation (MNF; Green et al., 1988) algorithm to reduce noise. We selected the first three MNF components ($\sim 99\%$ of the original information) for the analysis. The canopy height information was obtained from the point cloud using FUSION (McGaughey, 2018). The point cloud variables included common vegetation height metrics, such as the minimum, maximum, mean, median, mode and standard deviation of the vegetation height (compare Supplementary data for the full list of variables).

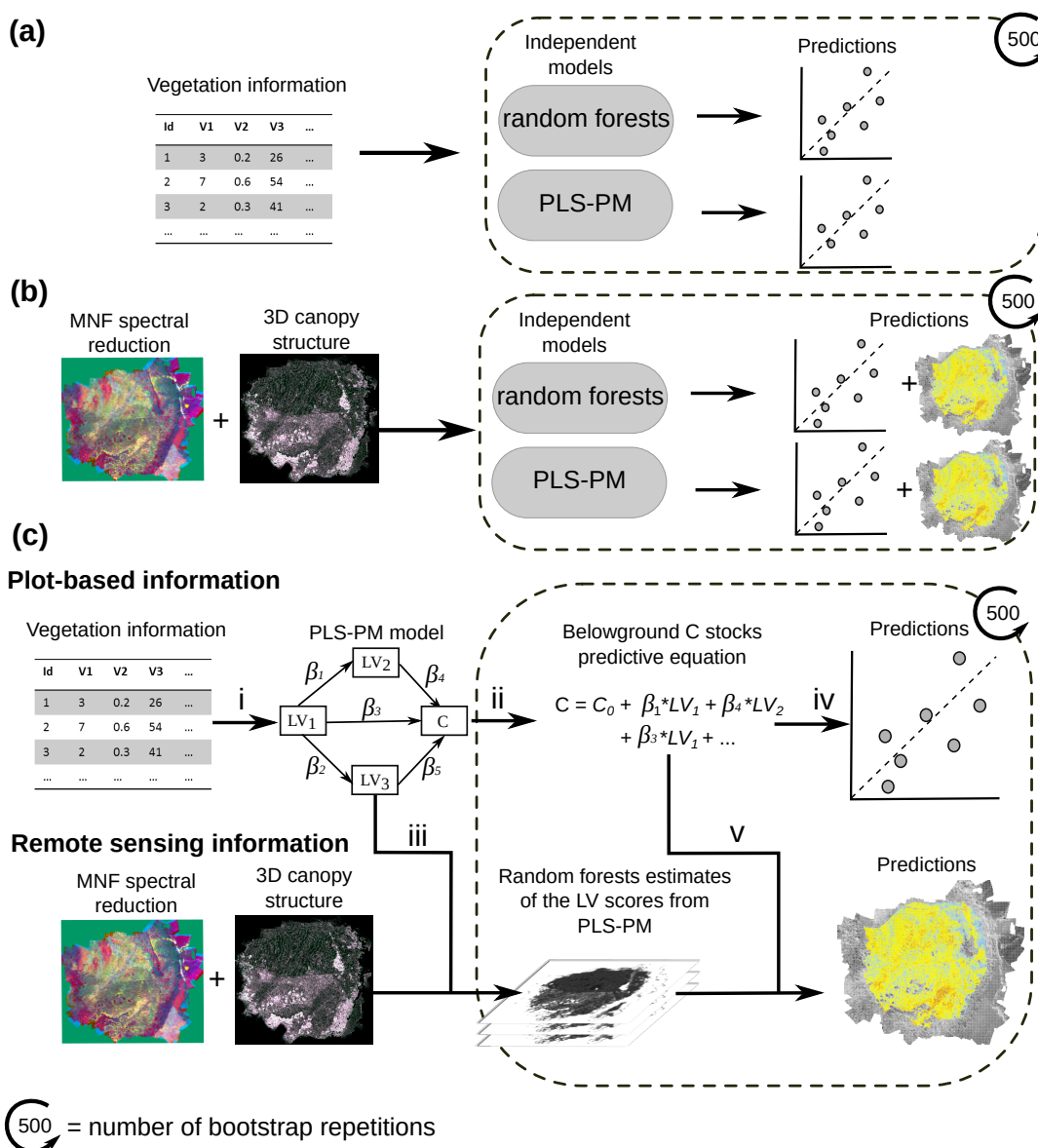


Figure 4.3: Methodological workflow of the predictive models. In (a) and (b) belowground C stocks independent predictive models using RF and PLS-PM were applied using the plot-based and UAV-based predictors, respectively; and (c) the hybrid models combining the SEM plot-based information with the RF UAV estimations.

The 3D metrics were rasterized to pixel size of $2\text{ m} \times 2\text{ m}$ to match the field plots size. The PLS-PM structural model for the remote sensing estimation is presented in Figure A1.

For the hybrid model c), we trained and validated PLS-PM with plot-based information (Figure 3c i) to find significant vegetation characteristics influencing belowground C stocks and to use their path coefficients (β) to build a predictive function (Figure 3c ii) as:

$$C = \sum_{i=1}^n \beta_i * LV_i + \varepsilon_i \quad (4.1)$$

where C is the estimated belowground C stocks, LV_i is a significant vegetation LV , β_i is the path coefficient of the LV_i , ε_i is the error and n is the number of significant vegetation characteristics detected by PLS-PM. We then used RF to extrapolate the selected PLS-PM LV scores using the UAV-based predictors (Figure 3c iii). Finally, we used equation (1) to predict and map belowground C stocks using the RF map extrapolations (Figure 3c iv and 3c v respectively). To avoid overfitting and to assess model accuracy and the map extrapolation stability, all three types of models (Figure 3a, b and c) were embedded in a bootstrapping procedure with 500 repetitions. In each iteration, 36 observations were randomly selected with replacement from the 36 available samples, from which on average 36.8 % (~13 samples) were not selected. We used this observations as holdout samples for the validation (Kohavi, 1995). Model performances were compared based on differences in the coefficients of determination (r^2 ; calculated as the squared Pearson's correlation coefficient), the normalized root mean square error (%RMSE) and the bias between predicted and observed variables of the holdout samples in the bootstrap. The normalized root mean square error was calculated as:

$$\%RMSE = \left(\frac{\sqrt{\frac{1}{n} \sum_{j=1}^n (y_j - \hat{y}_j)^2}}{\max(C) - \min(C)} \right) * 100 \quad (4.2)$$

where C is the measured belowground C stocks, while the bias of prediction was measured as one minus the slope of a regression without intercept of the predicted versus observed values (Lopatin et al., 2016, 2017).

We applied a one-sided bootstrapping test to check for significant differences (in terms of r^2 , %RMSE and bias) among models (Araya-López et al., 2018; Lopatin et al., 2016). We tested for differences between PLS-PM and RF in the three type of models presented in Figure 3.

Finally, it is worth-mentioning that still *in-situ* values of belowground C stocks are needed to calibrate and validate the relationships obtained by the vegetation characteristics. Hence, we did not obviate soil sampling completely for the analysis. We used the R-packages '*plsmpm*'

(Sanchez et al., 2017) and ‘*randomForest*’ (Liaw and Wiener, 2002) for the analyses, while the image processing was accomplished using Python 3.6 with the ‘*Scikit-learn*’ (Pedregosa et al., 2011) and ‘*Scikit-image*’ libraries (van der Walt et al., 2014, scripts available in Appendix C).

4.3.7 Maps

We calculated the median and the coefficient of variation (CV, in percentage, calculated as $CV_p = (SD_p / \text{mean}(C)_o) * 100$, where CV_p is the pixel’s coefficient of variation, SD_p is the pixel’s standard deviation and $\text{mean}(C)_o$ is the mean belowground *C* stocks value of all reference measurements of the 500 predicted belowground *C* stocks maps produced by the models in Figure 3b and c during the iterative validation (Araya-López et al., 2018). Pixels with high CV indicate higher uncertainties of the predictive model, while low values depict areas with stable predictions.

We masked out areas that were not represented in the plot-based information to avoid predictions outside the training range (non-vegetation: NDVI < 0.3; and areas with presence of trees: vegetation height > 2 m).

Finally, we used RGB maps of the PLS-PM LV scores extrapolated by RF (Figure 3c iii) to see the spatial distribution of the plot-based information and support the analysis of the predicted belowground *C* stocks gradients. The components were normalized between 0-255 and plotted with a 20–80 % percentiles linear stretching for visual interpretation of variable interactions.

4.4 Results

4.4.1 Model performances

The PLS-PM plot-based model yielded an overall goodness-of-fit of 0.65. Moran’s I test showed that LVs (inner models) and their residuals were not significantly affected by spatial autocorrelation (aboveground biomass: I = -0.02 and P = 0.72; species richness: I = -0.02 and P = 0.71; soil depth: I = -0.04 and P = 0.42; and belowground *C* stocks: I = -0.04 and P = 0.41). Details on the construction of the LVs (outer model) are presented in Table A1. The model path diagram with significant path feedbacks and total variable importance on belowground *C*

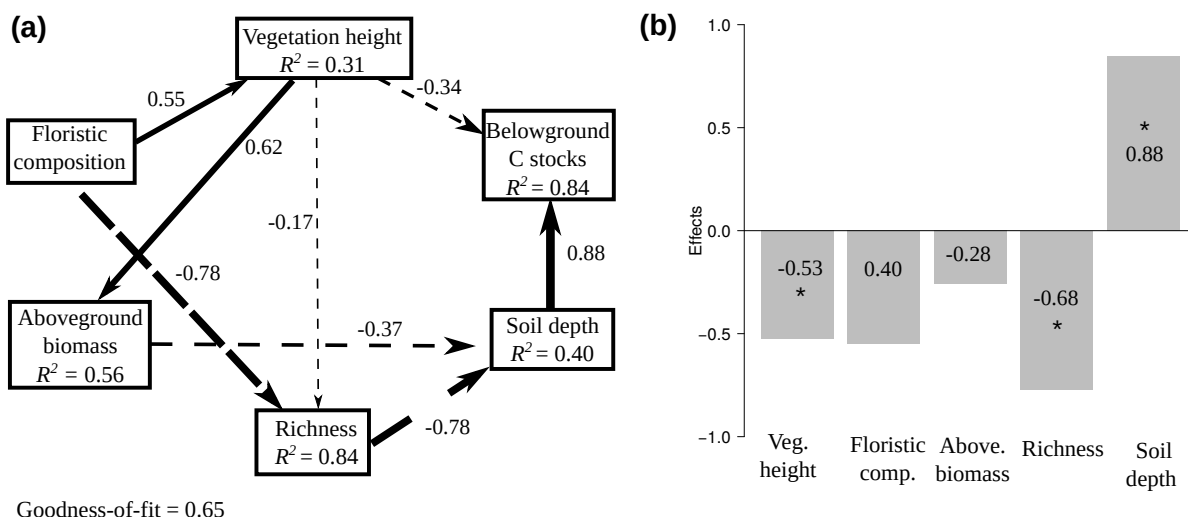


Figure 4.4: (a) Resulting PLS-PM model using plot-based information. Arrows represent unidirectional relationships among LVs. Solid and dashed arrows denote positive and negative relationships, respectively. Arrows with non-significant coefficients ($\alpha = 0.05$) were not drawn. The thickness of the paths is scaled based on the magnitude of path coefficient (β). Path coefficients and internal R^2 correspond to mean bootstrap values of the internal PLS-PM validation. (b) Bar plot showing the variable importance (direct + indirect effects) of the vegetation attributes to predict belowground C stocks. Asterisks (*) indicate a significant ($\alpha = 0.05$) influence over belowground C stocks.

stocks are presented in Figure 4. Only soil depth and vegetation height showed a significant direct relation to the belowground C stocks. The relation of species richness with belowground C stocks became significant when the indirect influences were included (mainly caused by the relation between vascular species richness and soil depth; Figure 4b).

Soil depth appeared to be negatively related to aboveground biomass and species richness. The latter fits well with the fact that species richness in water-logged, acidic bogs with peat accumulation tends to be low. Surprisingly, no direct link was observed to floristic composition. Hence, a linear equation was created using vegetation height and soil depth to predict belowground C stocks. To use only vegetation attributes in the equation, we used aboveground biomass and species richness path coefficients to predict soil depth, resulting in the following equation:

$$C = -(H * 0.34) + \underbrace{([-(BM * 0.37) - (SR * 0.78)] * 0.88)}_{\text{Soil depth}} \quad (4.3)$$

where C is the belowground C stocks estimation, H is the vegetation height [cm], BM is the aboveground biomass [$kg m^{-2}$] and SR is the species richness.

Table 2 shows the results of belowground C stocks accuracy prediction using RF and PLS-PM independently with plot-based predictors (models of Figure 3a). Both algorithms yielded high median accuracies with r^2 over 0.70 and %RMSE below 25 %. However, PLS-PM showed more parsimony as fewer predictors were used and presented significant improvements ($\alpha = 0.05$) in terms of %RMSE and bias. RF variable importance is presented in Table 3, showing that soil depth obtained the highest model scores, whereas all vegetation attributes appear were non-important. Table 4 presents the modeling results using UAV-based predictors (models of Figure 3b), where it is shown that RF outperformed PLS-PM significantly in all models. The canopy 3D variables derived from the point cloud showed higher importance than the spectral MNF components for all models except for the model of belowground C stocks (compare Supplementary data). Finally, Fig. 5 depicts the results of the hybrid model coupling the plot-based information (PLS-PM) and UAV data (RF). The hybrid model resulted in higher accuracies than the purely data-driven random forests approach, with improvements from of r^2 from 0.39 to 0.54, normalized RMSE of from 31.33% to 20.24%, and bias from -0.73 to 0.05.

Table 4.2: Prediction accuracies of belowground C stocks applying plot-based information with random forests (RF) and PLS path modeling (PLS-PM). The median values of the iterative validation are shown. Asterisks (*) indicate a significant difference ($\alpha = 0.05$) between PLS-PM and RF.

Algorithm	r^2	%RMSE	Bias	N° predictors
PLS-PM	0.79	14.48*	0.12*	3
RF	0.72	22.35	0.7	5

Table 4.3: Variable importance of the random forests plot-based model (Figure 3a).

Variables	Gini purity index
Soil depth	100
Vascular species richness	16.98
Floristic composition	10.41
Vascular vegetation height	1.01
Vascular aboveground biomass	0

Table 4.4: Prediction accuracies of peatland characteristics (latent variables) using PLS-PM and RF with solely remote sensing information. Vegetation height was obtained directly from the UAV photogrammetric point cloud. All values are the median of the bootstrapping validation.

Latent variables	PLS-PM			RF		
	r^2	%RMSE	bias	r^2	%RMSE	bias
Vascular vegetation height	-	-	-	-	-	-
Floristic composition	0.22	26.77	-0.78	0.57***	22.57**	-0.59**
Vascular aboveground biomass	0.3	38.13	-0.69	0.67**	20.18**	-0.27*
Vascular species richness	0.32	26.44	-0.69	0.59**	25.30***	-0.58***
Soil depth	0.4	30.93	-0.62	0.45*	28.83**	-0.79
Belowground C stocks	0.34	36.67	-0.62	0.39*	31.44**	-0.73**

Significant differences: * $\alpha = 0.1$, ** $\alpha = 0.05$, *** $\alpha = 0.001$.

4.4.2 Spatial extrapolation of belowground C stocks

The prediction maps (Figure 6) show that the use of RF with UAV-based predictors resulted in an underestimation of belowground C stocks (see also Figure 5). Furthermore, the hybrid model depicted lower model uncertainties in prediction, with coefficient of variation (CV) values $< \sim 30\%$.

The extrapolated PLS-PM plot-based LV scores by the RF models (Figure 3c iii) showed clear differences between land use types (Figure 7). The conservation area (to the south) featured more interactions (color combinations), with higher LV score values of aboveground biomass, species richness, floristic composition and soil depth, while the managed area (to the north) was characterized by simpler and smoother patterns of species richness and floristic composition scores. Areas where the bootstrap iteration procedure showed higher CV agree with areas of higher (LV) biomass and species richness.

4.5 Discussion

4.5.1 Linkages between vegetation attributes and belowground C stocks

The conservation area (to the south) presents higher cover of shrub species (more aboveground biomass) and abundance of native species related to a peatland in the original state (Figure 7), such as *Sphagnum magellanicum*, *Sticherus cryptocarpus* and *Blechnum cordatum* (low NMDS

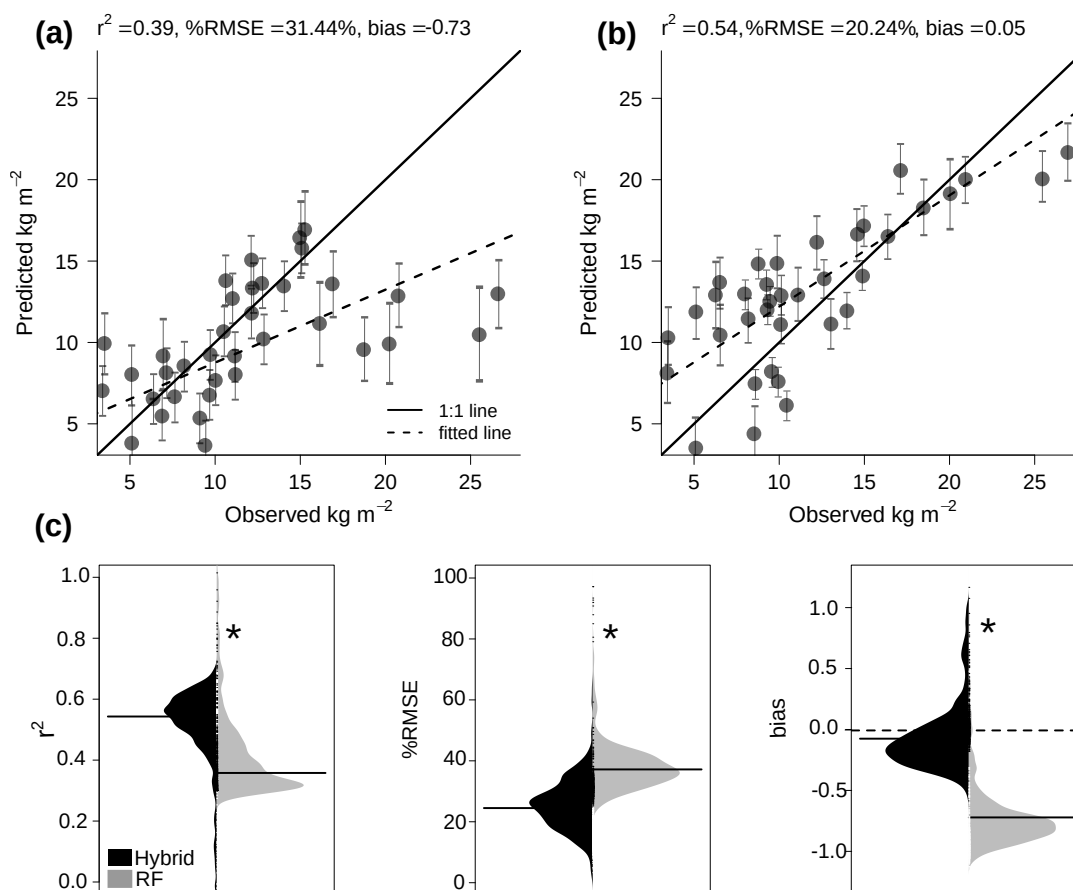


Figure 4.5: Scatterplots of observed versus predicted values of belowground C stocks for: (a) the direct use of random forests using UAV-based predictors, and (b) the hybrid model combining PLS-PM plot-based information and RF UAV predictions. The dots and the error bars represent the median and the standard deviation of the values generated in the iterative validation, respectively. (c) Bootstrapping distribution of accuracies. Asterisks (*) indicate a significant differences ($\alpha = 0.05$)

axis score; Figure A2). In contrast, the managed area (to the north) has higher species richness and presence of vascular invasive species such as *Plantago lanceolata*, *Agrostis capillaris* and *Trifolium repens* (higher NMDS axis score; Figure A2), which relates to a more degraded peatland (Dorrepaal et al., 2005; Jonsson and Wardle, 2009). The differences in species composition relate to the colonization of less water-logged areas by vascular plants. The colonization of vascular plants decrease the reservoirs of belowground C stocks in the long term by producing changes in soil nutrient content and pH will eventually hamper further growth of *Sphagnum* species (Fenner and Freeman, 2011). Vascular plants further increase the oxygenization of soils, the microbial activity and decomposition rate of the organic matter, which facilitates liberation of ancient carbon as CO_2 to the atmosphere (Walker et al., 2016) and inhibits further accumulation of C (Chen et al., 2017, 2018; Cong et al., 2014; Gorham, 1991; Lange et al., 2015). This

process is likely to be faster and occur more frequently under climate change scenarios, as an increasing temperature promotes drought and accelerates colonization by vascular plants and microbial activity (Fenner and Freeman, 2011).

The negative effects that the colonization of vascular plants exert over belowground *C* stocks is well represented in the PLS-PM model: vegetation height, aboveground biomass, floristic composition (higher scores showing an increase of invasive vascular species) and species richness depicted negative effects (Figure 4b). From all aboveground variables, only vegetation height showed a significant direct relation to the belowground *C* stocks. This is clearly an expression of the fact that bog vegetation is low when peat accumulation is high. When considering also indirect effects through the use of moderator variables (especially soil depth), all the above mentioned variables increased their relative importance. This shows the importance of studying variable inter-dependencies when modeling complex systems (see section 4.4.3 below).

4.5.2 Model performances

The predictions of random forests (RF) and PLS-PM using plot-based information (Figure 3a) showed high accuracies in both cases. Nevertheless, PLS-PM outperformed RF significantly using linear relations and fewer variables, indicating that SEM is indeed useful to constrain the models using ecological expert knowledge.

RF outperformed PLS-PM significantly when using remote sensing data to directly predict belowground *C* stocks (Figure 3b). This showed that PLS-PM could not handle the high colinearity of the remote sensing data. Although PLS is known to be able to address a certain degree of colinearity, machine learning algorithms like RF behave more flexible by applying complex relationships in higher dimensional feature spaces (Svetnik et al., 2003).

We also tested the use of PLS and support vector machines (SVM) regressions for the predictions. Their performances in terms of r^2 , %RMSE and bias were lower than those obtained by RF, hence their results were not presented here.

When using UAV-based independent variables, the aboveground vegetation variables were predicted with higher accuracies than the belowground variables (Table 4). Nevertheless, predictions of aboveground vegetation variables still showed high uncertainties (i.e. average r^2 of

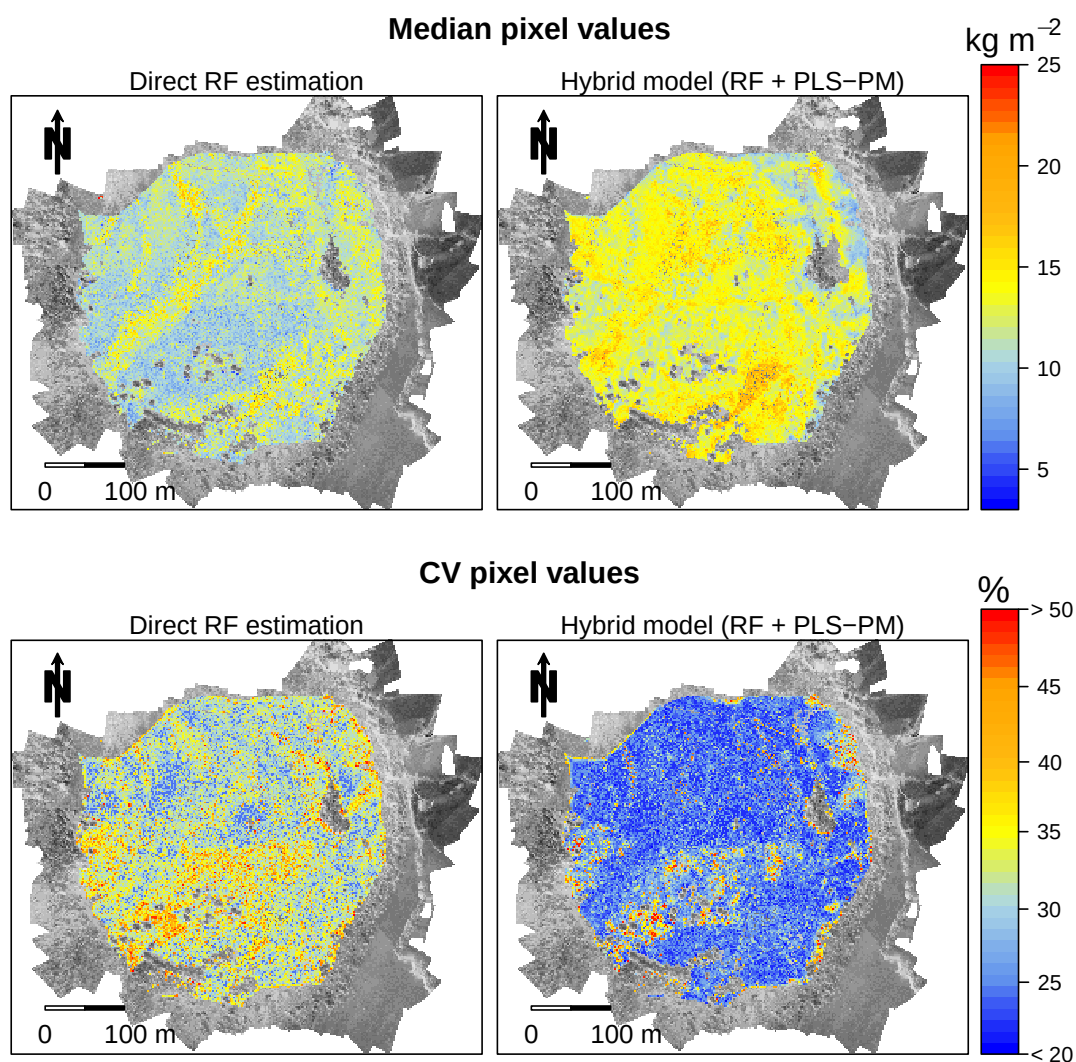


Figure 4.6: Belowground C stocks prediction maps using random forests (RF) with UAV-based predictors (left) and the hybrid model combining PLS-PM plot-based information and RF UAV estimations (right). The maps represent the median (top) and the coefficient of variation (CV; below) of the 500 bootstrapping iterations.

~ 0.61 and %RMSE of ~ 22.68). In this study, the accuracies for the vascular aboveground biomass, species richness and floristic composition are likely to be affected by three factors: 1) the destructive sampling performed in a $0.5 \text{ m} \times 0.5 \text{ m}$ area located at the center of the 4 m^2 plots (Figure 1) prior to UAV acquisition; 2) the time lag of two years between the field (2014) and the UAV (2016) campaigns. In this time period, Sphagnum and shrub biomass and abundance were expected to remain stable due to their slow growth but herbaceous properties may have experienced shifts; 3) the inaccuracies during UAV data georectification of may have added errors in the five field plots where markers were not visible from the hyperspectral ortho-

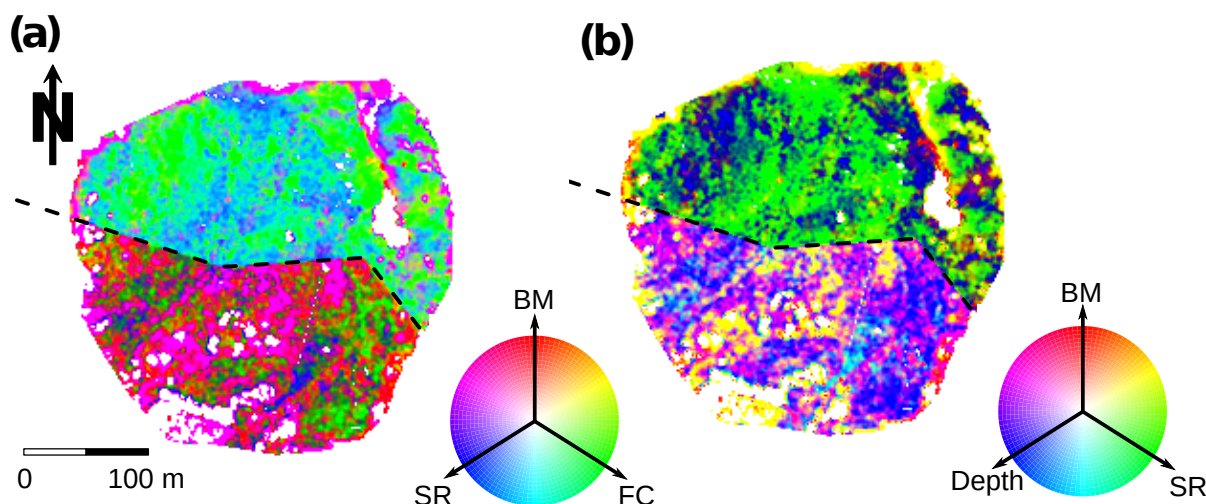


Figure 4.7: Spatial distribution of the PLS-PM LV scores produced by RF regressions (Figure 3 iii). RGB map representations using only aboveground peatland characteristics (a), and a mix of above with below-ground variables (b). The variables were normalized (0-255) and plotted with a 20–80 % percentiles linear stretching. BM = vascular aboveground biomass, FC = floristic composition, SR = vascular species richness and Depth = soil depth. The dashed line is the border between the conservation (southern) and the managed (northern) areas.

mosaic. These observations could have been skipped during the analysis, but we decided to use them anyway as the number of observations was already low.

The prediction of the aboveground variables showed relatively similar results as other studies: Castillo-Riffart et al. (2017) estimated species richness in the same study are using satellite-based sensors, yielding model r^2 between 0.54 and 0.6 and %RMSE between 18 % and 20 %. Moreover, Harris et al. (2015) mapped the floristic composition of a temperate peatland in the west coast of Wales using a full-range airborne-based hyperspectral data and PLS regressions. They obtained a r^2 in validation of 0.72 and RMSE 0.18 (in feature space units). Estimations of aboveground biomass in acidic peatlands have been obtained mainly by allometric equations and land cover maps obtained by high resolution imageries (e.g. Beilman et al., 2008).

Compared to the RF models based on UAV-based predictors alone (Fig. 3b), the hybrid model coupling PLS-PM plot-based information and RF UAV predictions (Figure 3c) resulted in significant improvements. This suggests that the use of vegetation attributes as predictors improved the estimation of belowground C stocks by incorporating known ecological relations constraining the model. SEM theoretical constructs are generalizable, allowing their comparison across sites (Grace et al., 2007) and scales Grace and Keeley (2006), while empirical models based on

remote sensing data alone, despite precision and ease of implementation, lack portability as they are largely affected by sensor and site-specific conditions (Kattenborn et al., 2017; Schmidlein et al., 2012; Vuolo et al., 2013). The proposed approach showed similar accuracies as other studies using a more complex set of predictors (such as peat thickness, dry bulk density and carbon concentration) and/or allometric functions (Akumu and McLaughlin, 2014; Beilman et al., 2008; Dargie et al., 2017; Draper et al., 2014; Gumbrecht et al., 2017; Jaenicke et al., 2008). The advantage of using aboveground vegetation characteristics as proxies are: 1) field efforts and costs are reduced by allowing non-destructive sampling. This may decrease soil sampling and laboratory analyses, and 2) variables can be mapped by remote sensing with higher accuracies than belowground variables (Castillo-Riffart et al., 2017; Harris et al., 2015). The aboveground vegetation variables used in the present study relate to changes in *C* fluxes (e.g. gas-exchange to the atmosphere) that slowly alter the *C* stocks (Fenner and Freeman, 2011). Therefore, the use of such proxies will always require validation as relations between vegetation proxies and belowground *C* stocks may depend on site specific conditions, such as floristic composition, management treatments and successional stages. Nevertheless, improving the understanding of interactions between below and aboveground plant and community properties could advance the operationalization of such mapping approaches by decreasing the amount of data required for training and validation.

The accuracies obtained in this investigation are still not sufficient for an operational monitoring of peatland belowground *C* stocks. To achieve this goal, higher accuracies are needed (e.g. > 80 % of variance explained) to decrease the amount of field data without compromising model performances. Likewise, the approach portability needs to be assessed, as site specific approaches are not ideal for management tasks. To improve the estimation of belowground *C* stocks with the proposed approach, an increase of the prediction accuracy of the indirect proxies is needed (i.e. vascular species richness and aboveground biomass). For example, the development of an accurate allometric equation to assess aboveground biomass in a non-destructive manner would facilitate the proposed procedure. The vascular species richness estimation could be enhanced e.g. by using detailed multi-scale canopy 3D and textural information based on the point cloud and the orthomosaic Lopatin et al. (2019).

4.5.3 Variable importance

The plot-based PLS-PM model showed significant links (direct + indirect) between soil depth, species richness, vegetation height and belowground C stocks (Figure 4). The model showed that for every centimeter increase of soil depth, centimeter decrease of vegetation height and reduction of species numbers by one species, there is a belowground C stocks increase of $\sim 0.88 \text{ kg m}^{-2}$, $\sim 0.53 \text{ kg m}^{-2}$ and $\sim 0.68 \text{ kg m}^{-2}$, respectively. In comparison to these results, the RF model was rather uninformative: the RF Gini purity index (Table 3) showed that soil depth was the only meaningful predictor of belowground C stocks in the RF model. This suggests that considering only direct relations (i.e. regression coefficients or model variable importance) may lead to an underestimation of the ecological importance of several variables in the model. For example, in the PLS-PM plot-based model the influences of species richness and floristic composition on determining the belowground C stocks using the direct links (path coefficients) yielded non-significant results ($\beta < 0.1$ each), whereas presenting strong importance if indirect links were considered (species richness = -0.68; floristic gradient = -0.40); the assessment of only direct influences may lead to an erroneous evaluation of the ecosystem dependencies (Irwin, 2006).

Although ecological interdependencies and indirect linkages can be estimated as well by applying several separate linear or multiple regressions (e.g. Gough et al., 1994) or analyses of variance (e.g. Dorrepaal et al., 2005), SEM tracks these relationships while allowing the prediction of its variables within a composite model (e.g. Grace and Keeley, 2006).

The variable importance of the random forests models using the UAV-based predictors showed that the canopy 3D information outperformed the spectral information in all cases except in the prediction of belowground C stocks (see Supplementary data), where the first MNF component yielded the highest importance. In addition, variables such as the mode and the coefficient of variation of the point cloud also depicted a high importance. This indicates that for the prediction of belowground C stocks, the combination of spectral and canopy 3D information has a high potential.

4.5.4 Belowground C stocks extrapolations

The prediction maps (Figure 6) agreed with our knowledge about the study site, where the belowground C stocks has a smoother transition between the conservation and managed areas than the aboveground vegetation variables (Cabezas et al., 2015).

The total amount of C stocks estimated with the hybrid model was $\sim 233,790 \text{ kg m}^{-2}$. This is a rather low C stocks value compared to other natural peatlands in Chilean Patagonia (Cabezas et al., 2015), which is attributed to its young stage (Díaz et al., 2008). Chiloé Island presents many similar isolated small peatlands, which despite their relatively low individual C pools, sum up to considerable amounts of total C stocks (McClellan et al., 2017). Given the fact that these wetlands are numerous and isolated, the measurement bias and field sampling costs could be high (Jobe and White, 2009). The lower field operational costs of assessing aboveground vegetation attributes compared to soil samples makes the presented mapping approach suitable to estimate the overall C contribution of the landscape.

Lower CV pixel values were obtained in areas where the vegetation variables presented larger variability, whereas higher CV were caused mainly by extremes in aboveground biomass and species richness (Figure 7). The models resulted in higher uncertainties for the conservation area due to a higher abundance of shrubs, while the managed area presented high uncertainties in eroded grasses with presence of exotic species. This difference is an expression of the low representativeness of pure aboveground biomass and exotic rich plots compared to plots with intermedium gradient values (i.e. only one pure shrub plot in the conservation area and two plots with high number of invasive species in the managed area were included in the analysis). Maps of the vegetation attributes evaluated in this study can be obtained at different spatial scales. For example, vegetation height can be obtained by airborne LiDAR, photogrammetry based on UAV, airborne or high resolution optical satellites (e.g. WorldView or Pleiades stereo-imagery; Maack et al. (2015)) or SAR interferometry (e.g. TanDEM-X; Kattenborn et al. (2015)). More research is needed to link such products with ecological studies to assess if the hypothesis developed from local ecological studies hold across spatial scales (Pettorelli et al., 2014). Further work is needed to find stable and mechanistic links between belowground

C stocks and vegetation characteristics, which would facilitate a continuous monitoring of soil pools while reducing the amount of destructive soil samples. We believe that SEM is suitable to find ecological meaningful interactions and to link ecosystem properties with remote sensing. Nonetheless, the relationships presented in this investigation needs to be tested against new data to see if their assumptions hold across landscapes.

4.6 Conclusions

This study evaluated the use of remotely sensed vegetation attributes as proxies to predict peatland belowground *C* stocks. By using a hybrid model that combines plot-based ecological knowledge of the ecosystem functioning (structural equation modeling) with remote sensing estimates (machine learning), we conclude the following:

1. The use of vegetation characteristics such as vascular vegetation height, aboveground biomass and species richness as proxies resulted in more accurate belowground *C* stocks estimations, compared to the use of raw remote sensing data. The use of vegetation characteristics is advantageous because of their easy and non-destructive assessment. However, more investigation is needed to check whether the relationships found here hold across landscapes.
2. The assessment of indirect relationships between the vegetation attributes and belowground *C* stocks improved the interpretation of variable importance. Considering only direct linkages (coefficients) resulted in underestimation of the vascular species richness and floristic composition contribution to the model.
3. Structural equation models are suitable to track indirect and bi-directional links among components in a defined model. Nonetheless, they cannot handle correctly the number and dimensionality of the remote sensing data, so their integration with machine learning algorithms is appropriate for mapping purposes.
4. The SEM model showed flexibility to fit the large gradients of peatland vegetation attributes caused by land use differences.

5. Peatland belowground *C* stocks is difficult to estimate directly using optical and structural remote sensing information. Algorithms that take into account more complexity in the predictors, such as random forests and support vector machines, are able to model the relations between canopy reflectance/structure and the *C* gradient, obtaining higher accuracies than linear models. Nevertheless, these accuracies were not sufficient for a reliable estimation of belowground *C* stocks.

The integration of ecological expertise into remote sensing applications has great potential to improve not only the final mapping accuracy, but to contribute to the knowledge of ecosystem functioning and processes. Nevertheless, more investigation is needed to find generalized aboveground proxies of belowground *C* stocks to effectively decrease the amount of soil samples needed for model calibration.

5 Synthesis

Very-high resolution remote sensing is a promising tool to track detailed Earth's processes. Within these, unmanned aerial vehicles (UAVs) have gained special interest for mapping plant attributes in small areas and for experimentation due to their operational flexibility (Anderson and Gaston, 2013). However, approaches dealing with the particular characteristics of submeter spatial resolution are still needed to harvest their full potential. Hence, the aim of this thesis was to assess the strengths and limitations of UAVs for vegetation mapping, specifically concerning two topics: plant species classifications, and detailed predictions of ecosystem attributes. The thesis addressed research gaps for grassland, forest and peatland vegetation types separately, which were summarized in three main research questions (Chapter 1 section 5). Finally, operational constraints and future considerations on UAV applications are discussed.

5.1 How structural and community plant attributes impair the success of woody and herbaceous species mapping with UAVs?

This thesis addressed the effects of plant community attributes in the success of species mapping with UAV data. Here, the first study focused on the classification of all occurring species in a semi-natural grassland with hyperspectral data (Chapter 2). The study found that the distribution patterns of species and plant functional types have high influence in the classification success. Here, plots with high species cover and low structural complexity resulted in high classification accuracies. The effect of growth form or plant functional types in the classification was however less clear.

Forb species were classified with higher accuracies than graminoids, likely because graminoids often have thinner leaves than forbs, which may have caused higher presence of mixed pixels,

even at 3 mm pixel size, and/or spectral variability due to varying leaf structure and angles. The analysis also showed that NIR and VIS accurately discriminate graminoids and forbs, respectively. This suggests that both photosynthetic pigments and structural properties are important features to classify forb species, while mostly structural attributes are for graminoids (Kattenborn et al., 2018a). Therefore, the use of UAV data to classify grassland species is of operational interest only in communities with low structural complexity and canopy overlaps, such as stress-prone dunes, and the ideal sensor technical requirements may differ between grassland communities.

The second study (Chapter 3) analyzed the effects of shadows in the classification of invasive woody species. The study found that shadows significantly affect the accuracy of pixel-based classification procedures using a range of spectral, textural and canopy 3D structure variables. The amount of daily shadows varied depending on the canopy architecture of each species. Species with uniform canopies, such as *Ulex europaeus*, produced less shaded areas over time than stepped canopies, like *Pinus radiata*, resulting in less classification errors and broader suitable daily-window for UAV acquisitions. Therefore, site-specific considerations on species canopy architecture should be used to constrain UAV campaigns and minimize shadow areas in the images.

5.2 How very-high resolution data can be used to obtain reference data for subsequent species classifications?

Both species classification studies (Chapter 2-3) innovated in the reference data collection methods aimed to enlarge the quantity of observations needed to obtain reliable results. In Chapter 2, data was collected by independent scans of isolated herbaceous individuals. This was combined with object-based analysis to semi-automatically obtain spectrally-homogeneous training and validation areas for each species. Unuseful objects were obviated by applying vegetation masks and visual interpretation. This approach obtained > 1,400 observations that otherwise would have been challenging to collect manually from the field. Yet, the study found mismatches between the accuracies depicted during model calibration (training-validation phase) and prediction (cover estimation in independent scans). This could have been provoked by

differing sun-sensor geometries, where references were usually collected near nadir from the sensor (\downarrow) while the predicted species had differing viewing angles ($\swarrow\downarrow\searrow$).

Likewise, reflectance-based models are often impaired by sensor and local site differences (Vuolo et al., 2013), hampering their general portability. Therefore, using different sets of images for training and validation may incur in additional model errors. Model portability could be improved by adding reflectance variability, for example by permutation–bootstrapping approaches (Verrelst et al., 2015). The thesis used bootstrapping as cross-validation procedure and to assess the accuracy and spatial variability of models, where the median and coefficient of variation was used as model confidence metrics. An assemblage of all bootstrapped models could be further used to increase model variability and thus enhance portability.

Meanwhile, Chapter 3 innovated in the use of UAVs to acquire presence-absence reference data of the three invasive species by using visual interpretation of the orthomosaics. This approach discarded the need of *in-situ* validations and thus decreased the amount of man labor. This allowed the collection of <1,500 samples covering the fully representative extension of the study areas. This could be of particular interest to e.g. acquire data on sites with restricted access, such as bird nesting areas. However, field labor is still needed when the species are complex to differentiate visually from the background.

5.3 How aboveground vegetation structure and composition estimated from UAV relate to peatland belowground carbon stocks?

Chapter 4 presents an approach to map peatland belowground carbon (C) stocks using aboveground vegetation attributes as proxies. Reflectance is a powerful type of data to describe vegetation attributes. It can be further used to depict soil properties that are linearly linked with vegetation traits (Angelini et al., 2017). However, some belowground properties, such as C stocks, presents non-linear or complex interdependencies with the aboveground vegetation attributes (Dorrepaal et al., 2007). Hence, their mapping using solely remote sensing data is often challenging (Cabezas et al., 2015).

Here, for the first time remotely sensed reflectance and canopy structure data were linked to peatland belowground C stocks by coupling an ecological-based empirical model of above-

ground–belowground feedbacks and UAV-based data. This innovated approach differ from previous studies, where C stocks are mapped using remotely sensed land covers and allometric equations, as it presents continuous C estimates. This is important as peatland-vegetation types present high variation within small distances (Cabezas et al., 2015). Therefore, continuous mapping of C gradients could further enhance scientific knowledge of feedback interactions.

The study used structural equation modeling (SEM) to find significant aboveground–belowground feedbacks, and describe how these are related with each other (direction and strength; Figure 4.4). SEM allowed to incorporate mediator variables, here soil depth, that cannot be directly estimated with UAV data, but added stability to the overall model as is considered a key ecological driver (Lawson et al., 2014; Akumu and McLaughlin, 2014; Draper et al., 2014). Irwin (2006) stated that the assessment of only direct influences may lead to erroneous evaluation of ecosystem dependencies. Mediator variables can be estimated indirectly during model prediction by applying a ‘cascade’ modeling approach. For example in $A \rightarrow B \rightarrow C$, B is the mediator variable of C , and both B and C can be predicted only by A . Nevertheless, as noise is added in each modeling step, such approach would be only recommended when the interdependencies among model variables are high.

The study found that vegetation heights, aboveground biomass and species richness were the three most important proxies to predict belowground C stocks. Biomass and richness were predicted by UAV-based differences in spectral and 3D canopy structural data related to varying environmental conditions. For biomass, both the plot and UAV-based models explained comparable amounts of variance (plot $\sim 56\%$ and UAV $\sim 67\%$), meaning that the UAV data was able to account for the full vegetation height gradient. Likely, the slightly higher accuracy of the UAV model was produced by the spectral data, which possibly accounted for extra information such as canopy closure and branch density.

The species richness prediction was more challenging using the UAV-based data. The study showed that even with ~ 10 cm pixel size, the heterogeneity of spectral values is not sufficient to fully predict plant diversity. This could be due to spectral similarities among peatland species, thus full-range hyperspectral sensors are expected to outperform by depicting more detailed spectral variability. Likewise, diversity indices including neighboring pixel information, such

as the Rao's quadratic diversity metric (Rocchini et al., 2018), and temporal data could enhance models predictions.

5.4 Potentials for future research

Unmanned aerial vehicles (UAVs) are highly dynamic platforms to obtain very-high resolution data. This thesis demonstrated that UAVs are useful tools to map a range of different species types, to obtain synoptic reference data, and to predict community and ecosystem attributes in highly heterogeneous environments. The pixel sizes used in the thesis varied between 0.3–10 cm. This level of detail is challenging from an operational perspective as more spectral variation is presented, hampering e.g. pixel-based species identification (*'The devil is in the detail'*; Nagendra and Rocchini, 2008). However, the common acknowledgment that submeter pixel sizes hamper classification performances should be addressed carefully, as technological advances and processing approaches are still under development to harness the full potential of very-high resolution data.

Here, Chapter 3 showed that ~ 10 cm spatial resolution data could present opportunities instead of a drawbacks, as this level of detail decreases the amount of shaded–sunlit canopy mixed pixels, thus allowing the complete removal of shadows (noise) from the images. Most studies did not treat UAV data to reduce variance accordingly, applying instead similar approaches as e.g. with satellite-based data (Zaman et al., 2011; Hill et al., 2017; Lu and He, 2017). Alternatively, common approaches use object-based analysis, which has been ascribed with high potential to reduce spectral variability (Alvarez-Taboada et al., 2017; Michez et al., 2016; Mafanya et al., 2017). However, none of these studies excluded shaded canopies prior allocating spectral values to the segmented clumps, hence still adding shadow noise to the models during calibration. The allocation of only sunlit canopies into the segmented clumps could thus be a straightforward alternative to decrease both spectral variability from the raw images and false negatives from the classified results, as shaded areas could at some extent be replaced by sunlit information inside the segmented clumps. But, what if canopy shadows could be used as co-variable to classify plant species? Even when shadows are considered as noise in pixel-based applications

(Zhang et al., 2015), they could add additional information in algorithms including neighboring context, such as in convolutional neural networks or deep learning. There, the training observations are not single values (pixels) but e.g. small frames of UAV orthomosaics, where the 3D context of the frames are used in classification and regression tasks (compare Li et al., 2018, for a review of possible models).

UAVs have been increasingly used to map plant species (Lu and He, 2017; Alvarez-Taboada et al., 2017; Michez et al., 2016), however these studies remain small compared to satellite and aerial-based approaches. This could be due to the relatively small area cover of small-sized UAVs, which impair their use for large-scale management. Yet, UAV-based models can be used as reference data for upscaling procedures because they are often as detailed as field measurements—e.g. field estimates of species abundance can presents up to 60 % errors using visual interpretation (Vittoz and Guisan, 2007).

For example, Kattenborn et al. (2019) used UAV-based predicted presence/absence as reference data to train and validate satellite-based models of species distributions. This approach has three major advantages: First, both platforms share the same perspective, top of the canopy, and thus both data can easily be matched. Second, UAV can acquire data in inaccessible terrains, widening the spatial distribution of samples. Third, larger quantities of observations can be obtained. These advantages are specially suitable for forested areas, where closed and dense canopies often hamper the measurement of sample locations due to GPS inaccuracies (Valbuena et al., 2010), or for areas with denied access, such as wetlands with nesting birds. Therefore, solving the technical challenges of UAV-based products may enhance both local and regional remotely sensed models in the near future. However, the solely use of UAV data as reference is constrained to situations where the target species-vegetation type are directly recognizable from the images.

Chapter 2, meanwhile, showed that there is only few practical uses of UAV-based data to map individual grassland species due to their high dynamism and canopy complexity. Instead, species may be aggregated into functional types to decrease the complexity of classes, which may further ease their relation with ecosystem processes. To accomplish this, the use of independent images to semi-automatically obtain large quantities of reference data showed promising results.

However, the study found mismatches between the obtained accuracies during calibration and prediction, possible caused by differing sun-sensor geometries and calibrations (Verrelst et al., 2015). This might be solved by using UAV acquisitions instead of sensor scans, as differing view geometries and image calibrations are minimized by using one (near) nadir orthomosaic covering both the isolated training–validation samples and the area where to predict the occurrences.

Traditionally, vegetation processes have been studied at coarse scales using satellite data (Ustin et al., 1991), which often include complex combinations of fine-scale properties and processes due to nonlinear responses and intricate feedbacks (Gamon et al., 2019). Likewise, it has been found that some processes are scale-dependent, meaning that their feedbacks may shift according to the scale (Chase and Knight, 2013; Svejcar et al., 2015; van Wesenbeeck et al., 2008). Therefore, understanding local processes may help disentangle feedbacks across scales. Here, the thesis showed that UAVs can be used to upscale complex plot-based processes to the field level (Chapter 4), as both field measurements and UAV-based predictions share the same spatial resolution. Consequently, UAVs hold great potential to spatially test ecosystem feedbacks and hypothesis based in years of field research. Structural equation modeling (SEM) has been ascribed high potential to describe such ecosystem feedbacks (Grace et al., 2016, 2010; de Vries and Bardgett, 2016), and is thus suitable to be coupled with UAV-based predictions. This coupling may help to spatially assess, for example, shifts of peatland belowground–aboveground feedbacks depending on scale or phenological stages.

UAVs are flexible in their deploy, thus allowing for high temporal resolution studies. This thesis did not include temporal data as a co-variable during modeling. However, phenological characteristics have proved to help species and vegetation types identification (Somers and Asner, 2014; Andrew and Ustin, 2008; Melaas et al., 2013) and for describing carbon sequestration processes (Keenan et al., 2014). Phenological data may, at some extent, help closing the gap for community-based attributes models, as it largely correlates with e.g. aboveground biomass (Filella et al., 2004) and plant diversity (Fairbanks and McGwire, 2004). Therefore, the inclusion of phenology data in future UAV approaches is highly encouraging.

Optical UAV sensors, such as hyperspectral sensors, are still constrained in either radiometric or spectral resolution compared to airborne and satellite sensors (Colomina and Molina, 2014). This implies that the efforts of UAV applications are often restricted to empirical instead of physical models, such as radiative transfer models (but see Zarco-Tejada et al., 2018). However, UAV can also indirectly increase the physical understanding of reflectance studies. For example, Zarco-Tejada et al. (2019) used airborne hyperspectral and Sentinel-2 images to estimate chlorophyll content in an open-canopy conifer forest. They used high resolution airborne data to estimate tree cover, sunlit and shaded areas. This information was then used to improve the radiative transfer model inversion in the forest. Therefore, UAV could be used to enhance radiative inversions of coarser grain remotely sensed data, such as Sentinel-2, by adding detailed spatial context.

Overall, this thesis demonstrated that unmanned aerial vehicles (UAVs) are useful for vegetation mapping and experimentation. From herbaceous to woody species, UAVs showed high potential to map species occurrences and community attributes in highly heterogeneous situations by depicting both spectral and 3D information that otherwise will be challenging to obtain from a single sensor. State-of-the-art software developments in image acquisition and processing make the use of UAVs suitable even for practitioners with few knowledge in geomatics, broadening their field of applications from science to management.

Bibliography

- Agarwal, S., Vailshery, L., Jaganmohan, M., and Nagendra, H. (2013). Mapping Urban Tree Species Using Very High Resolution Satellite Imagery: Comparing Pixel-Based and Object-Based Approaches. *ISPRS International Journal of Geo-Information*, 2(1):220–236.
- Akumu, C. E. and McLaughlin, J. W. (2014). Modeling peatland carbon stock in a delineated portion of the Nayshkootayaow river watershed in Far North, Ontario using an integrated GIS and remote sensing approach. *CATENA*, 121:297–306.
- Alvarez-Taboada, F., Paredes, C., and Julián-Pelaz, J. (2017). Mapping of the invasive species *Hakea sericea* using Unmanned Aerial Vehicle (UAV) and worldview-2 imagery and an object-oriented approach. *Remote Sensing*, 9(913).
- Anderson, C. B. (2018). Biodiversity monitoring, earth observations and the ecology of scale. *Ecology Letters*, pages 1572–1585.
- Anderson, K. and Gaston, K. J. (2013). Lightweight unmanned aerial vehicles will revolutionize spatial ecology. *Frontiers in Ecology and the Environment*, 11(3):138–146.
- Andrew, M. and Ustin, S. L. (2008). The role of environmental context in mapping invasive plants with hyperspectral image data. *Remote Sensing of Environment*, 112(12):4301–4317.
- Angelini, M. E., Heuvelink, G. B. M., and Kempen, B. (2017). Multivariate mapping of soil with structural equation modelling. *European Journal of Soil Science*, 68(5):575–591.
- Araya-López, R., Lopatin, J., Fassnacht, F., and Hernández, H. (2018). Monitoring Andean high altitude wetlands in central Chile with seasonal optical data: A comparison between Worldview-2 and Sentinel-2 imagery. *ISPRS Journal of Photogrammetry and Remote Sensing*, 145(Part B).
- Baena, S., Moat, J., Whaley, O., and Boyd, D. S. (2017). Identifying species from the air: UAVs and the very high resolution challenge for plant conservation. *PLoS ONE*, 12(11):1–21.
- Barker, M. and Rayens, W. (2003). Partial least squares for discrimination. *Journal of Chemometrics*, 17(3):166–173.
- Beilman, D. W., Vitt, D. H., Bhatti, J. S., and Forest, S. (2008). Peat carbon stocks in the southern Mackenzie River Basin: Uncertainties revealed in a high-resolution case study. *Global Change Biology*, 14(6):1221–1232.
- Binggeli, P. (1996). A taxonomic, biogeographical and ecological overview of invasive woody plants. *Journal of Vegetation Science*, 7:121–124.
- Booth, D. T. and Cox, S. E. (2008). Image-based monitoring to measure ecological change in rangeland. *Frontiers in Ecology and the Environment*, 6(4):185–190.

- Breckenridge, R. P., Dakins, M., Bunting, S., Harbour, J. L., and White, S. (2011). Comparison of Unmanned Aerial Vehicle Platforms for Assessing Vegetation Cover in Sagebrush Steppe Ecosystems. *Rangeland Ecology & Management*, 64(5):521–532.
- Breiman, L. (2001). Random Forests. *Machine Learning*, 45:5–32.
- Brodu, N. and Lague, D. (2012). 3D terrestrial lidar data classification of complex natural scenes using a multi-scale dimensionality criterion: Applications in geomorphology. *ISPRS Journal of Photogrammetry and Remote Sensing*, 68(1):121–134.
- Burges, C. (1998). A tutorial on support vector machines for pattern recognition. *Data Mining and Knowledge Discovery*, 2:121–167.
- Cabezas, J., Galleguillos, M., and Perez-Quezada, J. F. (2016). Predicting Vascular Plant Richness in a Heterogeneous Wetland Using Spectral and Textural Features and a Random Forest Algorithm. *IEEE Geoscience and Remote Sensing Letters*, 13(5):646–650.
- Cabezas, J., Galleguillos, M., Valdés, A., Fuentes, J. P., Pérez, C., and Perez-Quezada, J. F. (2015). Evaluation of impacts of management in an anthropogenic peatland using field and remote sensing data. *Ecosphere*, 6(12):1–24.
- Cacho, J. O., Spring, D., Pheloung, P., and Hester, S. (2006). Evaluating the Feasibility of Eradicating an Invasion. *Biological Invasions*, 8(4):903–917.
- Camargo, J. (1992). New Diversity Index for Assessing Structural Alterations in Aquatic Communities. *Bulletin of Environment Contamination and Toxicology*, (428-434):428–434.
- Cao, J., Leng, W., Liu, K., Liu, L., He, Z., and Zhu, Y. (2018). Object-Based mangrove species classification using unmanned aerial vehicle hyperspectral images and digital surface models. *Remote Sensing*, 10(89).
- Carter, G. A. (1993). Responses of Leaf Spectral Reflectance to Plant Stress. *American Journal of Botany*, 80(3):239–243.
- Castillo-Riffart, I., Galleguillos, M., Lopatin, J., and Perez-Quezada, J. F. (2017). Predicting Vascular Plant Diversity in Anthropogenic Peatlands: Comparison of Modeling Methods with Free Satellite Data. *Remote Sensing*, 9(7):681.
- Chase, J. M. and Knight, T. M. (2013). Scale-dependent effect sizes of ecological drivers on biodiversity: Why standardised sampling is not enough. *Ecology Letters*, 16(SUPPL.1):17–26.
- Chen, H., Mommer, L., van Ruijven, J., de Kroon, H., Fischer, C., Gessler, A., Hildebrandt, A., Scherer-Lorenzen, M., Wirth, C., and Weigelt, A. (2017). Plant species richness negatively affects root decomposition in grasslands. *Journal of Ecology*, 105(1):209–218.
- Chen, S., Wang, W., Xu, W., Wang, Y., Wan, H., Chen, D., Tang, Z., Tang, X., Zhou, G., Xie, Z., Zhou, D., Shangguan, Z., Huang, J., He, J.-S., Wang, Y., Sheng, J., Tang, L., Li, X., Dong, M., Wu, Y., Wang, Q., Wang, Z., Wu, J., Chapin, F. S., and Bai, Y. (2018). Plant diversity enhances productivity and soil carbon storage. *Proceedings of the National Academy of Sciences*, 115(16):4027–4032.

- Clapp, R. A. (1995). The Unnatural History of the Monterey Pine. *Geographical Review*, 85(1):1–19.
- Clarke, K. (1993). Non-parametric multivariate analyses of changes in community structure. *Austral Ecology*, 18(1):117–143.
- Clewley, D., Bunting, P., Shepherd, J., Gillingham, S., Flood, N., Dymond, J., Lucas, R., Armston, J., and Moghaddam, M. (2014). A python-based open source system for Geographic Object-Based Image Analysis (GEOBIA) utilizing raster attribute tables. *Remote Sensing*, 6(7):6111–6135.
- Colomina, I. and Molina, P. (2014). Unmanned aerial systems for photogrammetry and remote sensing: A review. *ISPRS Journal of Photogrammetry and Remote Sensing*, 92:79–97.
- Cong, W.-F., van Ruijven, J., Mommer, L., De Deyn, G. B., Berendse, F., and Hoffland, E. (2014). Plant species richness promotes soil carbon and nitrogen stocks in grasslands without legumes. *Journal of Ecology*, 102(5):1163–1170.
- Dallimer, M., Tinch, D., Acs, S., Hanley, N., Southall, H. R., Gaston, K. J., and Armsworth, P. R. (2009). 100 years of change: examining agricultural trends, habitat change and stakeholder perceptions through the 20th century. *Journal of Applied Ecology*, 46:334–343.
- Dalponte, M., Bruzzone, L., and Gianelle, D. (2012). Tree species classification in the Southern Alps based on the fusion of very high geometrical resolution multispectral/hyperspectral images and LiDAR data. *Remote Sensing of Environment*, 123:258–270.
- Dandois, J. P. and Ellis, E. C. (2010). Remote Sensing of Vegetation Structure Using Computer Vision. *Remote Sensing*, 2(4):1157–1176.
- Dandois, J. P. and Ellis, E. C. (2013). High spatial resolution three-dimensional mapping of vegetation spectral dynamics using computer vision. *Remote Sensing of Environment*, 136:259–276.
- Dargie, G. C., Lewis, S. L., Lawson, I. T., Mitchard, E. T. A., Page, S. E., Bocko, Y. E., and Ifo, S. A. (2017). Age, extent and carbon storage of the central Congo Basin peatland complex. *Nature*, 542(7639):86–90.
- Darvishzadeh, R., Skidmore, A., Schlerf, M., and Atzberger, C. (2008). Inversion of a radiative transfer model for estimating vegetation LAI and chlorophyll in a heterogeneous grassland. *Remote Sensing of Environment*, 112(5):2592–2604.
- de Groot, R., Brander, L., van der Ploeg, S., Costanza, R., Bernard, F., Braat, L., Christie, M., Crossman, N., Ghermandi, A., Hein, L., Hussain, S., Kumar, P., McVittie, A., Portela, R., Rodriguez, L. C., ten Brink, P., and van Beukering, P. (2012). Global estimates of the value of ecosystems and their services in monetary units. *Ecosystem Services*, 1(1):50–61.
- de Sá, N. C., Castro, P., Carvalho, S., Marchante, E., López-Núñez, F. A., and Marchante, H. (2018). Mapping the Flowering of an Invasive Plant Using Unmanned Aerial Vehicles: Is There Potential for Biocontrol Monitoring? *Frontiers in Plant Science*, 9(March):1–13.
- de Vries, F. T. and Bardgett, R. D. (2016). Plant community controls on short-term ecosystem nitrogen retention. *New Phytologist*, 210(3):861–874.

- Díaz, M. F., Larraín, J., Zegers, G., and Tapia, C. (2008). Caracterización florística e hidrológica de turberas de la Isla Grande de Chiloé, Chile. *Revista chilena de historia natural*, 81:455–468.
- Dorrepaal, E., Cornelissen, J. H. C., and Aerts, R. (2007). Changing leaf litter feedbacks on plant production across contrasting sub-arctic peatland species and growth forms. *Oecologia*, 151(2):251–261.
- Dorrepaal, E., Cornelissen, J. H. C., Aerts, R., Wallén, B., and Van Logtestijn, R. S. P. (2005). Are growth forms consistent predictors of leaf litter quality and decomposability across peatlands along a latitudinal gradient? *Journal of Ecology*, 93(4):817–828.
- Draper, F. C., Roucoux, K. H., Lawson, I. T., Mitchard, E. T. A., Honorio Coronado, E. N., Lähteenoja, O., Torres Montenegro, L., Valderrama Sandoval, E., Zaráte, R., and Baker, T. R. (2014). The distribution and amount of carbon in the largest peatland complex in Amazonia. *Environmental Research Letters*, 9(12):124017.
- Duque-Lazo, J., van Gils, H., Groen, T., and Navarro-Cerrillo, R. M. (2016). Transferability of species distribution models: The case of *Phytophthora cinnamomi* in Southwest Spain and Southwest Australia. *Ecological Modelling*, 320(JUNE 2013):62–70.
- Dvořák, P., Müllerová, J., Bartaloš, T., and Brůna, J. (2015). Unmanned Aerial Vehicles for Alien Plant Species Detection and Monitoring. In *ISPRS - International Archives of the Photogrammetry, Remote Sensing and Spatial Information Sciences*, volume XL-1/W4, pages 83–90.
- Dyrmann, M., Karstoft, H., and Midtby, H. S. (2016). Plant species classification using deep convolutional neural network. *Biosystems Engineering*, 151(2005):72–80.
- Evans, J., Murphy, M., Holden, Z., and Cushman, S. (2011). Predictive species and habitat modeling in landscape ecology. chapter Modeling s, pages 139–159. Springer.
- Fairbanks, D. H. K. and McGwire, K. C. (2004). Patterns of floristic richness in vegetation communities of California: regional scale analysis with multi-temporal NDVI. *Global Ecology and Biogeography*, 13(3):221–235.
- Fassnacht, F. E., Latifi, H., Stereńczak, K., Modzelewska, A., Lefsky, M., Waser, L. T., Straub, C., and Ghosh, A. (2016). Review of studies on tree species classification from remotely sensed data. *Remote Sensing of Environment*, 186(August):64–87.
- Fassnacht, F. E., Mangold, D., Schäfer, J., Immitzer, M., Kattenborn, T., Koch, B., and Latifi, H. (2017). Estimating stand density, biomass and tree species from very high resolution stereo-imagery – towards an all-in-one sensor for forestry applications? *Forestry: An International Journal of Forest Research*, pages 1–19.
- Fassnacht, F. E., Neumann, C., Förster, M., Buddenbaum, H., Ghosh, A., Clasen, A., Joshi, P. K., and Koch, B. (2014). Comparison of Feature Reduction Algorithms for Classifying Tree Species With Hyperspectral Data on Three Central European Test Sites. *IEEE Journal of Selected Topics in Applied Earth Observation and remote Sensing*, 7(6):2547–2561.

- Feilhauer, H., Asner, G. P., Martin, R. E., and Schmidtlein, S. (2010). Brightness-normalized Partial Least Squares Regression for hyperspectral data. *Journal of Quantitative Spectroscopy and Radiative Transfer*, 111(12-13):1947–1957.
- Feilhauer, H., Faude, U., and Schmidtlein, S. (2011). Combining Isomap ordination and imaging spectroscopy to map continuous floristic gradients in a heterogeneous landscape. *Remote Sensing of Environment*, 115(10):2513–2524.
- Feilhauer, H. and Schmidtlein, S. (2011). On variable relations between vegetation patterns and canopy reflectance. *Ecological Informatics*, 6(2):83–92.
- Fenner, N. and Freeman, C. (2011). Drought-induced carbon loss in peatlands. *Nature Geosci*, 4(12):895–900.
- Ferner, J., Schmidtlein, S., Guuroh, R. T., Lopatin, J., and Linstädter, A. (2018). Disentangling effects of climate and land-use change on West African drylands' forage supply. *Global Environmental Change*, 53(August):24–38.
- Filella, I., Peñuelas, J., Llorens, L., and Estiarte, M. (2004). Reflectance assessment of seasonal and annual changes in biomass and CO₂ uptake of a Mediterranean shrubland submitted to experimental warming and drought. *Remote Sensing of Environment*, 90(3):308–318.
- Foody, G. M. (2010). Assessing the accuracy of land cover change with imperfect ground reference data. *Remote Sensing of Environment*, 114(10):2271–2285.
- Franklin, S. E., Ahmed, O. S., and Williams, G. (2017). Northern Conifer Forest Species Classification Using Multispectral Data Acquired from an Unmanned Aerial Vehicle. *Photogrammetric Engineering & Remote Sensing*, 83(7):501–507.
- Fuentes-Ramírez, A., Pauchard, A., Cavieres, L. A., and García, R. A. (2011). Survival and growth of *Acacia dealbata* vs. native trees across an invasion front in south-central Chile. *Forest Ecology and Management*, 261(6):1003–1009.
- Fung, T., Ma, F. Y., and Siu, W. L. (1998). Hyperspectral data analysis for subtropical tree species recognition. In *IGARSS '98, sensing and managing the environment*, pages 1298 – 1300.
- Gamon, J. A., Somers, B., Malenovsky, Z., Middleton, E. M., Rascher, U., and Schaepman, M. E. (2019). Assessing vegetation function with imaging spectroscopy. *Surveys in Geophysics*.
- Ganapol, B. D., Johnson, L. F., Hlavka, C. A., Peterson, D. L., and Bond, B. (1999). LCM2: A coupled leaf/canopy radiative transfer model. *Remote Sensing of Environment*, 70:153–166.
- Gebhardt, S., Schellberg, J., Lock, R., and Kühbauch, W. (2006). Identification of broad-leaved dock (*Rumex obtusifolius* L.) on grassland by means of digital image processing. *Precision Agriculture*, 7(3):165–178.
- Getzin, S., Wiegand, K., and Schöning, I. (2012). Assessing biodiversity in forests using very high-resolution images and unmanned aerial vehicles. *Methods in Ecology and Evolution*, 3(2):397–404.

- Gislason, P. O., Benediktsson, J. A., and Sveinsson, J. R. (2006). Random forests for land cover classification. *Pattern Recognition Letters*, 27(4):294–300.
- Gorham, E. (1991). Northern peatlands: role in the carbon cycle and probable responses to climatic warming. *Ecological Applications*, 1.
- Gough, L., Grace, J. B., and Taylor, K. L. (1994). The Relationship between Species Richness and Community Biomass: The Importance of Environmental Variables. *Oikos*, 70(2):271–279.
- Grace, J. and Bollen, K. (2005). Interpreting the results from multiple regression and structural equation models. *Bulletin of the Ecological Society of America*, 9623(October):296–300.
- Grace, J. B., Anderson, T. M., Olf, H., and Scheiner, S. M. (2010). On the specification of structural equation models for ecological systems. *Ecological Monographs*, 80(1):67–87.
- Grace, J. B., Anderson, T. M., Seabloom, E. W., Borer, E. T., Adler, P. B., Harpole, W. S., Hautier, Y., Hillebrand, H., Lind, E. M., Pärtel, M., Bakker, J. D., Buckley, Y. M., Crawley, M. J., Damschen, E. I., Davies, K. F., Fay, P. A., Firn, J., Gruner, D. S., Prober, S. M., and Smith, M. D. (2016). Integrative modelling reveals mechanisms linking productivity and plant species richness. *Nature*, 529(7586):1–10.
- Grace, J. B. and Keeley, J. E. (2006). A structural equation model analysis of postfire plant diversity in California shrublands. *Ecological Applications*, 16(2):503–514.
- Grace, J. B., Michael Anderson, T., Smith, M. D., Seabloom, E., Andelman, S. J., Meche, G., Weiher, E., Allain, L. K., Jutila, H., Sankaran, M., Knops, J., Ritchie, M., and Willig, M. R. (2007). Does species diversity limit productivity in natural grassland communities? *Ecology Letters*, 10(8):680–689.
- Green, A., Berman, M., Switzer, P., and Craig, M. (1988). A transformation for ordering multispectral data in terms of image quality with implications for noise removal. *IEEE Transactions on Geoscience and Remote Sensing*, 26:65–74.
- Gu, L. and Robles-Kelly, A. (2014). Shadow modelling based upon Rayleigh scattering and Mie theory. *Pattern Recognition Letters*, 43:89–97.
- Gumbrecht, T., Roman-Cuesta, R. M., Verchot, L., Herold, M., Wittmann, F., Householder, E., Herold, N., and Murdiyarto, D. (2017). An expert system model for mapping tropical wetlands and peatlands reveals South America as the largest contributor. *Global Change Biology*, (November 2016).
- Harris, A., Charnock, R., and Lucas, R. M. (2015). Hyperspectral remote sensing of peatland floristic gradients. *Remote Sensing of Environment*, 162:99–111.
- He, K. S., Rocchini, D., Neteler, M., and Nagendra, H. (2011). Benefits of hyperspectral remote sensing for tracking plant invasions. *Diversity and Distributions*, 17(3):381–392.
- Hendrickson, E. C., Weinstein, B. G., Thompson, P. G., Arredondo, T. M., Grasty, M. R., Kohn, B. F., and Cruzan, M. B. (2016). Small Unmanned Aerial Vehicles (Micro-Uavs, Drones) in Plant Ecology. *Applications in Plant Sciences*, 4(9):1600041.

- Hernández-Stefanoni, J. L., Gallardo-Cruz, J. A., Meave, J. a., Rocchini, D., Bello-Pineda, J., and López-Martínez, J. O. (2012). Modeling α - and β -diversity in a tropical forest from remotely sensed and spatial data. *International Journal of Applied Earth Observation and Geoinformation*, 19:359–368.
- Hill, D. J., Tarasoff, C., Whitworth, G. E., Baron, J., Bradshaw, J. L., and Church, J. S. (2017). Utility of unmanned aerial vehicles for mapping invasive plant species: a case study on yellow flag iris (*Iris pseudacorus* L.). *International Journal of Remote Sensing*, 38(8-10):2083–2105.
- Holmgren, J. and Persson, Å. (2004). Identifying species of individual trees using airborne laser scanner. *Remote Sensing of Environment*, 90(4):415–423.
- Hribljan, J. A., Suarez, E., Bourgeau-Chavez, L., Endres, S., Lilleskov, E. A., Chimbolema, S., Wayson, C., Serocki, E., and Chimner, R. A. (2017). Multidate, multisensor remote sensing reveals high density of carbon-rich mountain peatlands in the páramo of Ecuador. *Global Change Biology*, 23(12):5412–5425.
- Hruska, R., Mitchell, J., Anderson, M., and Glenn, N. F. (2012). Radiometric and Geometric Analysis of Hyperspectral Imagery. *Remote Sensing*, 4(9):2736–2752.
- Huang, C.-y. and Asner, G. P. (2009). Applications of Remote Sensing to Alien Invasive Plant Studies. *Sensors*, 9(6):4869–4889.
- Husson, E., Lindgren, F., and Ecke, F. (2014). Assessing Biomass and Metal Contents in Riparian Vegetation Along a Pollution Gradient Using an Unmanned Aircraft System. *Water, Air, & Soil Pollution*, 225(6):1957.
- Immitzer, M., Böck, S., Einzmann, K., Vuolo, F., Pinnel, N., Wallner, A., and Atzberger, C. (2018). Fractional cover mapping of spruce and pine at 1 ha resolution combining very high and medium spatial resolution satellite imagery. *Remote Sensing of Environment*, 204(February):690–703.
- Irwin, R. E. (2006). The consequences of direct versus indirect species interactions to selection on traits: pollination and nectar robbing in *Ipomopsis aggregata*. *The American naturalist*, 167(3):315–328.
- Ishida, T., Kurihara, J., Viray, F. A., Namuco, S. B., Paringit, E. C., Perez, G. J., Takahashi, Y., and Marciano, J. J. (2018). A novel approach for vegetation classification using UAV-based hyperspectral imaging. *Computers and Electronics in Agriculture*, 144(August 2017):80–85.
- Ishii, H. and Asano, S. (2010). The role of crown architecture, leaf phenology and photosynthetic activity in promoting complementary use of light among coexisting species in temperate forests. *Ecological Research*, 25(4):715–722.
- Jacquemoud, S., Verhoef, W., Baret, F., Bacour, C., Zarco-tejada, P. J., Asner, G. P., François, C., and Ustin, S. L. (2009). PROSPECT + SAIL models : A review of use for vegetation characterization. *Remote Sensing of Environment*, 113:S56–S66.
- Jaenicke, J., Rieley, J. O., Mott, C., Kimman, P., and Siegert, F. (2008). Determination of the amount of carbon stored in Indonesian peatlands. *Geoderma*, 147(3-4):151–158.

- Jandt, U., von Wehrden, H., and Bruelheide, H. (2011). Exploring large vegetation databases to detect temporal trends in species occurrences. *Journal of Vegetation Science*, 22(6):957–972.
- Jobe, T. R. and White, P. S. (2009). A new cost-distance model for human accessibility and an evaluation of accessibility bias in permanent vegetation plots in Great Smoky Mountains National Park, USA. *Journal of Vegetation Science*, 20(6):1099–1109.
- Jones, G., Pearlstine, G., and Percival, P. (2006). An Assessment of Small Unmanned Aerial Vehicles for Wildlife Research. *Wildlife Society Bulletin*, 34:750–758.
- Jones, H. and Vaughan, R. (2010). *Remote Sensing of Vegetation*. Oxford University Press, U.S.A.
- Jonsson, M. and Wardle, D. A. (2009). Structural equation modelling reveals plant community drivers of carbon storage in boreal forest ecosystems. *Biology Letters*, (August 2009):116–119.
- Jueterbock, A., Smolina, I., Coyer, J. A., and Hoarau, G. (2016). The fate of the Arctic seaweed *Fucus distichus* under climate change: an ecological niche modeling approach. *Ecology and Evolution*, 6(6):1712–1724.
- Kaplan, H., van Niekerk, A., Le Roux, J. J., Richardson, D. M., and Wilson, J. R. (2014). Incorporating risk mapping at multiple spatial scales into eradication management plans. *Biological Invasions*, 16(3):691–703.
- Kattenborn, T., Fassnacht, F., Pierce, S., Lopatin, J., Grime, J. P., and Schmidtlein, S. (2017). Linking plant strategies and plant traits derived by radiative transfer modelling. *Journal of Vegetation Science*, 38(1):42–49.
- Kattenborn, T., Fassnacht, F. E., and Schmidtlein, S. (2018a). Differentiating plant functional types using reflectance: which traits make the difference? *Remote Sensing in Ecology and Conservation*, pages 1–15.
- Kattenborn, T., Lopatin, J., Förster, M., Braun, A. C., and Fassnacht, F. E. (2019). UAV data as alternative to field sampling to map woody invasive species based on combined Sentinel-1 and Sentinel-2 data. *Remote Sensing of Environment*, 227(January):61–73.
- Kattenborn, T., Lopatin, J., Kattenborn, G., and Fassnacht, F. E. (2018b). Pilot study on the retrieval of DBH and diameter distribution of deciduous forest stands using cast shadows in UAV-based ortomosaics. In *ISPRS Annals of the Photogrammetry, Remote Sensing and Spatial Information Sciences*, volume IV-1, pages 10–12.
- Kattenborn, T., Maack, J., Fassnacht, F. E., Enssle, F., Ermert, J., and Koch, B. (2015). Mapping forest biomass from space - Fusion of hyperspectral EO1-hyperion data and Tandem-X and WorldView-2 canopy height models. *International Journal of Applied Earth Observation and Geoinformation*, 35:359–367.
- Kattenborn, T., Sperlich, M., Bataua, K., and Koch, B. (2014). Automatic single palm tree detection in plantations using UAV-based photogrammetric point clouds. In *International Archives of the Photogrammetry, Remote Sensing and Spatial Information Sciences - ISPRS Archives*, volume 40, pages 139–144.

- Kattge, J., Díaz, S., Lavorel, S., Prentice, I. C., Leadley, P., Bönisch, G., Garnier, E., Westoby, M., Reich, P. B., Wright, I. J., Cornelissen, J. H. C., Violle, C., Harrison, S. P., Van Bodegom, P. M., Reichstein, M., Enquist, B. J., Soudzilovskaia, N. A., Ackerly, D. D., Anand, M., Atkin, O., Bahn, M., Baker, T. R., Baldocchi, D., Bekker, R., Blanco, C. C., Blonder, B., Bond, W. J., Bradstock, R., Bunker, D. E., Casanoves, F., Cavender-Bares, J., Chambers, J. Q., Chapin, F. S., Chave, J., Coomes, D., Cornwell, W. K., Craine, J. M., Dobrin, B. H., Duarte, L., Durka, W., Elser, J., Esser, G., Estiarte, M., Fagan, W. F., Fang, J., Fernández-Méndez, F., Fidelis, A., Finegan, B., Flores, O., Ford, H., Frank, D., Freschet, G. T., Fyllas, N. M., Gallagher, R. V., Green, W. A., Gutierrez, A. G., Hickler, T., Higgins, S. I., Hodgson, J. G., Jalili, A., Jansen, S., Joly, C. A., Kerkhoff, A. J., Kirkup, D., Kitajima, K., Kleyer, M., Klotz, S., Knops, J. M. H., Kramer, K., Kühn, I., Kurokawa, H., Laughlin, D., Lee, T. D., Leishman, M., Lens, F., Lenz, T., Lewis, S. L., Lloyd, J., Llusià, J., Louault, F., Ma, S., Mahecha, M. D., Manning, P., Massad, T., Medlyn, B. E., Messier, J., Moles, A. T., Müller, S. C., Nadrowski, K., Naeem, S., Niinemets, U., Nöllert, S., Nüske, A., Ogaya, R., Oleksyn, J., Onipchenko, V. G., Onoda, Y., Ordoñez, J., Overbeck, G., Ozinga, W. A., Patiño, S., Paula, S., Pausas, J. G., Peñuelas, J., Phillips, O. L., Pillar, V., Poorter, H., Poorter, L., Poschlod, P., Prinzing, A., Proulx, R., Rammig, A., Reinsch, S., Reu, B., Sack, L., Salgado-Negret, B., Sardans, J., Shiodera, S., Shipley, B., Siefert, A., Sosinski, E., Soussana, J. F., Swaine, E., Swenson, N., Thompson, K., Thornton, P., Waldram, M., Weiher, E., White, M., White, S., Wright, S. J., Yguel, B., Zaehle, S., Zanne, A. E., and Wirth, C. (2011). TRY - a global database of plant traits. *Global Change Biology*, 17(9):2905–2935.
- Keenan, T. F., Gray, J., Friedl, M. A., Toomey, M., Bohrer, G., Hollinger, D. Y., Munger, J. W., O’Keefe, J., Schmid, H. P., Wing, I. S., Yang, B., and Richardson, A. D. (2014). Net carbon uptake has increased through warming-induced changes in temperate forest phenology. *Nature Climate Change*, 4:598.
- Keil, P., Storch, D., and Jetz, W. (2015). On the decline of biodiversity due to area loss. *Nature Communications*, 6:8837.
- Key, T., Warner, T. A., McGraw, J. B., and Fajvan, M. A. (2001). A Comparison of Multispectral and Multitemporal Information in High Spatial Resolution Imagery for Classification of Individual Tree Species in a Temperate Hardwood Forest. *Remote Sensing of Environment*, 75(1):100–112.
- Klimeš, L., Dančák, M., Hájek, M., Jongepierová, I., and Kučera, T. (2001). Scale-Dependent Biases in Species Counts in a Grassland. *Journal of Vegetation Science*, 12(5):699–704.
- Kohavi, R. (1995). A study of cross-validation and bootstrap for accuracy estimation and model selection. *Proceedings of International joint conference on artificial intelligence*, 2:1137–1143.
- Korpela, I. (2004). *Individual tree measurements by means of digital aerial photogrammetry*. PhD thesis.
- Kumar, L. and Sinha, P. (2014). Mapping salt-marsh land-cover vegetation using high-spatial and hyperspectral satellite data to assist wetland inventory. *Giscience & Remote Sensing*, 51(5):483–497.

- Lange, M., Eisenhauer, N., Sierra, C. A., Bessler, H., Engels, C., Griffiths, R. I., Mellado-Vázquez, P. G., Malik, A. A., Roy, J., Scheu, S., Steinbeiss, S., Thomson, B. C., Trumbore, S. E., and Gleixner, G. (2015). Plant diversity increases soil microbial activity and soil carbon storage. *Nature Communications*, 6.
- Lawson, I. T., Kelly, T. J., Aplin, P., Boom, A., Dargie, G., Draper, F. C. H., Hassan, P. N. Z. B. P., Hoyos-Santillan, J., Kaduk, J., Large, D., Murphy, W., Page, S. E., Roucoux, K. H., Sjögersten, S., Tansey, K., Waldram, M., Wedeux, B. M. M., and Wheeler, J. (2014). Improving estimates of tropical peatland area, carbon storage, and greenhouse gas fluxes. *Wetlands Ecology and Management*, pages 1–20.
- Lepš, J. and Hadincová, V. (1992). How reliable are our vegetation analyses? *Journal of Vegetation Science*, 3(1):119–124.
- Levin, N., Shmida, A., Levanoni, O., Tamari, H., and Kark, S. (2007). Predicting mountain plant richness and rarity from space using satellite-derived vegetation indices. *Diversity and Distributions*, 13:692–703.
- Levy, E. and Madden, E. (1933). The point method of pasture analysis. *New Zealand Journal of Crop and Horticultural Science/Experimental Agriculture*, 46(267-269).
- Li, Y., Zhang, H., Xue, X., Jiang, Y., and Shen, Q. (2018). Deep learning for remote sensing image classification: A survey. *Data Mining and Knowledge Discovery*, (December 2017):1–17.
- Liaw, A. and Wiener, M. (2002). Classification and regression by randomForest. *R News*, 2:18–22.
- Little, C., Cuevas, J. G., Lara, A., Pino, M., and Schoenholtz, S. (2015). Buffer effects of streamside native forests on water provision in watersheds dominated by exotic forest plantations. *Ecohydrology*, 8(7):1205–1217.
- Liu, W. and Yamazaki, F. (2012). Object-based shadow extraction and correction of high-resolution optical satellite images. *IEEE Journal of Selected Topics in Applied Earth Observations and Remote Sensing*, 5(4):1296–1302.
- Lopatin, J., Dolos, K., Hernández, H. J., Galleguillos, M., and Fassnacht, F. E. (2016). Comparing Generalized Linear Models and random forest to model vascular plant species richness using LiDAR data in a natural forest in central Chile. *Remote Sensing of Environment*, 173:200–210.
- Lopatin, J., Dolos, K., Kattenborn, T., and Fassnacht, F. E. (2019). How canopy shadow affects invasive plant species classification in high spatial resolution remote sensing. *Remote Sensing in Ecology and Conservation*, pages 1–16.
- Lopatin, J., Fassnacht, F. E., Kattenborn, T., and Schmidtlein, S. (2017). Mapping plant species in mixed grassland communities using close range imaging spectroscopy. *Remote Sensing of Environment*, 201(January):12–23.

- Lopatin, J., Galleguillos, M., Fassnacht, F. E., Ceballos, A., and Hernandez, H. J. (2015). Using a Multistructural Object-Based LiDAR Approach to Estimate Vascular Plant Richness in Mediterranean Forests With Complex Structure. *IEEE Geoscience and Remote Sensing Letters*, 12(5):1008–1012.
- Lu, B. and He, Y. (2017). Species classification using Unmanned Aerial Vehicle (UAV)-acquired high spatial resolution imagery in a heterogeneous grassland. *ISPRS Journal of Photogrammetry and Remote Sensing*, 128:73–85.
- Lu, S., Shimizu, Y., Ishii, J., Funakoshi, S., Washitani, I., and Omasa, K. (2009). Estimation of abundance and distribution of two moist tall grasses in the Watarase wetland, Japan, using hyperspectral imagery. *ISPRS Journal of Photogrammetry and Remote Sensing*, 64(6):674–682.
- Luebert, F. and Pliscoff, P. (1999). *Sinopsis Bioclimática y Vegetacional de Chile*. Editorial Universitaria.
- Ma, Q., Cui, L., Song, H., Gao, C., Hao, Y., Luan, J., Wang, Y., and Li, W. (2017). Aboveground and Belowground Biomass Relationships in the Zoige Peatland, Eastern Qinghai–Tibetan Plateau. *Wetlands*, 37(3):461–469.
- Maack, J., Kattenborn, T., Sperlich, M., Bataua, K., and Koch, B. (2015). Modeling forest biomass using Very-High-Resolution data - Combining textural, spectral and photogrammetric predictors derived from spaceborne stereo images. *Remote Sensing*, 6(11):1–26.
- Mack, B., Roscher, R., Stenzel, S., Feilhauer, H., Schmidlein, S., and Waske, B. (2016). Mapping raised bogs with an iterative one-class classification approach. *ISPRS Journal of Photogrammetry and Remote Sensing*, 120:53–64.
- Mafanya, M., Tsele, P., Botai, J., Manyama, P., Swart, B., and Monate, T. (2017). Evaluating pixel and object based image classification techniques for mapping plant invasions from UAV derived aerial imagery: *Harrisia pomaniensis* as a case study. *ISPRS Journal of Photogrammetry and Remote Sensing*, 129:1–11.
- Malenovský, Z., Lucieer, A., King, D. H., Turnbull, J. D., and Robinson, S. A. (2017). Unmanned aircraft system advances health mapping of fragile polar vegetation. *Methods in Ecology and Evolution*, 8(12):1842–1857.
- McClellan, M., Comas, X., Benschoter, B., Hinkle, R., and Sumner, D. (2017). Estimating Belowground Carbon Stocks in Isolated Wetlands of the Northern Everglades Watershed, Central Florida, Using Ground Penetrating Radar and Aerial Imagery. *Journal of Geophysical Research: Biogeosciences*, 122(11):2804–2816.
- McGaughey, R. (2018). FUSION/LDV: Software for LIDAR Data Analysis and Visualization.
- McIntyre, S., Lavorel, S., Landsberg, J., and Forbes, T. D. A. (1999). Disturbance response in vegetation – towards a global perspective on functional traits. *Journal of Vegetation Science*, 10(5):621–630.
- Melaas, E. K., Friedl, M. A., and Zhu, Z. (2013). Detecting interannual variation in deciduous broadleaf forest phenology using Landsat TM/ETM+ data. *Remote Sensing of Environment*, 132:176–185.

- Mercer, J. J. and Westbrook, C. J. (2016). Ultrahigh-resolution mapping of peatland microform using ground-based structure from motion with multiview stereo. *Journal of Geophysical Research: Biogeosciences*, 121(11):2901–2916.
- Merow, C., Smith, M. J., and Silander, J. A. (2013). A practical guide to MaxEnt for modeling species' distributions: What it does, and why inputs and settings matter. *Ecography*, 36(10):1058–1069.
- Michez, A., Piégay, H., Jonathan, L., Claessens, H., and Lejeune, P. (2016). Mapping of riparian invasive species with supervised classification of Unmanned Aerial System (UAS) imagery. *International Journal of Applied Earth Observation and Geoinformation*, 44:88–94.
- Mielke, P. W., Berry, K. J., and Brier, G. W. (1981). Application of Multi-Response Permutation Procedures for Examining Seasonal Changes in Monthly Mean Sea-Level Pressure Patterns. *Monthly Weather Review*, 109:120–126.
- Milas, A. S., Arend, K., Mayer, C., Simonson, M. A., and Mackey, S. (2017). Different colours of shadows: classification of UAV images. *International Journal of Remote Sensing*, 38(8–10):3084–3100.
- Möckel, T., Dalmayne, J., Schmid, B. C., Prentice, H. C., and Hall, K. (2016). Airborne hyperspectral data predict fine-scale plant species diversity in grazed dry grasslands. *Remote Sensing*, 8(2):1–19.
- Müllerová, J., Brůna, J., Bartaloš, T., Dvořák, P., Vítková, M., and Pyšek, P. (2017). Timing Is Important: Unmanned Aircraft vs. Satellite Imagery in Plant Invasion Monitoring. *Frontiers in Plant Science*, 8(May):1–13.
- Müllerová, J., Pergl, J., and Pyšek, P. (2013). Remote sensing as a tool for monitoring plant invasions: Testing the effects of data resolution and image classification approach on the detection of a model plant species *Heracleum mantegazzianum* (giant hogweed). *International Journal of Applied Earth Observation and Geoinformation*, 25(1):55–65.
- Myers, N., Mittermeier, R. A., Mittermeier, C. G., da Fonseca, G. A. B., and Kent, J. (2000). Biodiversity hotspots for conservation priorities. *Nature*, 403(6772):853–858.
- Nagendra, H. (2001). Using remote sensing to assess biodiversity. *International Journal of Remote Sensing*, 22(12):2377–2400.
- Nagendra, H. and Rocchini, D. (2008). High resolution satellite imagery for tropical biodiversity studies: The devil is in the detail. *Biodiversity and Conservation*, 17:3431–3442.
- Nagendra, H., Rocchini, D., Ghate, R., Sharma, B., and Pareeth, S. (2010). Assessing plant diversity in a dry tropical forest: comparing the utility of Landsat and IKONOS satellite images. *Remote Sensing*, 2:478–496.
- Neumann, C., Förster, M., Kleinschmit, B., and Itzerott, S. (2016). Utilizing a PLSR-Based Band-Selection Procedure for Spectral Feature Characterization of Floristic Gradients. *IEEE Journal of Selected Topics in Applied Earth Observations and Remote Sensing*, 9(9):3982–3996.

- Neumann, C., Weiss, G., Schmidlein, S., Itzerott, S., Lausch, A., Doktor, D., and Brell, M. (2015). Gradient-Based Assessment of Habitat Quality for Spectral Ecosystem Monitoring. *Remote Sensing*, 7(3):2871–2898.
- Nevalainen, O., Honkavaara, E., Tuominen, S., Viljanen, N., Hakala, T., Yu, X., Hyypä, J., Saari, H., Pölönen, I., Imai, N. N., and Tommaselli, A. M. (2017). Individual tree detection and classification with UAV-Based photogrammetric point clouds and hyperspectral imaging. *Remote Sensing*, 9(3).
- Norambuena, H., Escobar, S., and Rodríguez, F. (2000). The Biocontrol of Gorse , *Ulex europaeus* , in Chile : A Progress Report.
- Oksanen, J., Blanchet, F. G., Friendly, M., Kindt, R., Legendre, P., McGlinn, D., Minchin, P. R., O’Hara, R. B., Simpson, G. L., Solymos, P., Stevens, M. H. H., Szoecs, E., and Wagner, H. (2017). *vegan: Community Ecology Package*.
- Ollinger, S. V. (2011). Sources of variability in canopy reflectance and the convergent properties of plants. *New Phytologist*, 189(2):375–394.
- Olsen, A. R., Sedransk, J., Edwards, D., Gotway, C. A., Liggett, W., Rathbun, S., Reckhow, K. H., and Yyoung, L. J. (1999). Statistical Issues for Monitoring Ecological and Natural Resources in the United States. *Environmental Monitoring and Assessment*, 54(1):1–45.
- Ørka, H. O. and Hauglin, M. (2016). Use of remote sensing for mapping of non-native conifer species. Technical report.
- Parish, F., Sirin, A., Charman, D., Joosten, H., Minayeva, T., Silvius, M., and Stringer, L. (2008). Assessment on peatlands, biodiversity and climate change: main report. Technical report, Global Environment Centre, Kuala Lumpur, Malaysia.
- Pedregosa, F., Varoquaux, G., Gramfort, A., Michel, V., Thirion, B., Grisel, O., Blondel, M., Prettenhofer, P., Weiss, R., Dubourg, V., Vanderplas, J., Passos, A., Cournapeau, D., Brucher, M., Perrot, M., and Duchesnay, E. (2011). Scikit-learn: Machine Learning in Python. *Journal of Machine Learning Research*, 12:2825–2830.
- Pettorelli, N., Safi, K., and Turner, W. (2014). Satellite remote sensing, biodiversity research and conservation of the future. *Philosophical Transactions of the Royal Society of London B Biological Sciences*, 369:20130190.
- Phillips, R. and Beerli, O. (2008). The role of hydro-pedologic vegetation zones in greenhouse gas emissions for agricultural wetland landscapes. *Catena*, 72(3):386–394.
- Phillips, S. J., Anderson, R. P., and Schapire, R. E. (2006). Maximum entropy modeling of species geographic distributions. *Ecological Modelling*, 190:231–259.
- Posada, J. M., Lechowicz, M. J., and Kitajima, K. (2009). Optimal photosynthetic use of light by tropical tree crowns achieved by adjustment of individual leaf angles and nitrogen content. *Annals of Botany*, 103(5):795.
- Przybilla, H. and Wester-Ebbinghaus, W. (1979). Bildflug mit ferngelenktem Kleinflugzeug. *Bildmessung und Luftbildwesen*, 47:137–142.

- Puttonen, E., Suomalainen, J., Hakala, T., Räikkönen, E., Kaartinen, H., Kaasalainen, S., and Litkey, P. (2010). Tree species classification from fused active hyperspectral reflectance and LIDAR measurements. *Forest Ecology and Management*, 260(10):1843–1852.
- Ricciardi, A., Palmer, M. E., and Yan, N. D. (2011). Should Biological Invasions Be Managed as Natural Disasters? *BioScience*, 61(4):312–317.
- Richardson, D. M., Hui, C., Nuñez, M. A., and Pauchard, A. (2014). Tree invasions: Patterns, processes, challenges and opportunities. *Biological Invasions*, 16(3):473–481.
- Rocchini, D., Andreo, V., Förster, M., Garzon-Lopez, C. X., Gutierrez, A. P., Gillespie, T. W., Hauffe, H. C., He, K. S., Kleinschmit, B., Mairota, P., Marcantonio, M., Metz, M., Nagendra, H., Pareeth, S., Ponti, L., Ricotta, C., Rizzoli, A., Schaab, G., Zebisch, M., Zorer, R., and Neteler, M. (2015). Potential of remote sensing to predict species invasions: A modelling perspective. *Progress in Physical Geography*, 39(3):283–309.
- Rocchini, D., Bacaro, G., Chirici, G., Re, D. D., Feilhauer, H., Foody, G. M., Galluzzi, M., Garzon-Lopez, C. X., Gillespie, T. W., He, K. S., Lenoir, J., Marcantonio, M., Nagendra, H., Ricotta, C., Rommel, E., Schmidtlein, S., Skidmore, A. K., Kerchove, R. V. D., Wegmann, M., and Rugani, B. (2018). Remotely sensed spatial heterogeneity as an exploratory tool for taxonomic and functional diversity study. *Ecological Indicators*, 85:983–990.
- Rosenzweig, M. L. (1995). *Species Diversity in Space and Time*. Cambridge University Press.
- Rudiyanto, Minasny, B., Setiawan, B. I., Saptomo, S. K., and McBratney, A. B. (2018). Open digital mapping as a cost-effective method for mapping peat thickness and assessing the carbon stock of tropical peatlands. *Geoderma*, 313(August 2017):25–40.
- Saha, A. K., Arora, M. K., Csaplovics, E., and Gupta, R. P. (2005). Land Cover Classification Using IRS LISS III Image and DEM in a Rugged Terrain: A Case Study in Himalayas. *Geocarto International*, 20(2):33–40.
- Sanchez, G., Trinchera, L., and Russolillo, G. (2017). plspm: Tools for Partial Least Squares Path Modeling (PLS-PM).
- Sardà-Palomera, F., Bota, G., Viñolo, C., Pallarés, O., Sazatornil, V., BROTONS, L., Gomáriz, S., and Sardà, F. (2012). Fine-scale bird monitoring from light unmanned aircraft systems. *Ibis*, 154(1):177–183.
- Schaepman-Strub, G., Limpens, J., Menken, M., Bartholomeus, H. M., and Schaepman, M. E. (2008). Towards spatial assessment of carbon sequestration in peatlands: spectroscopy based estimation of fractional cover of three plant functional types. *Biogeosciences Discussions*, 5(2):1293–1317.
- Schmidt, K. S. and Skidmore, A. K. (2003). Spectral discrimination of vegetation types in a coastal wetland. *Remote Sensing of Environment*, 85(1):92–108.
- Schmidtlein, S., Feilhauer, H., and Bruelheide, H. (2012). Mapping plant strategy types using remote sensing. *Journal of Vegetation Science*, 23(3):395–405.
- Schmidtlein, S. and Sassin, J. (2004). Mapping of continuous floristic gradients in grasslands using hyperspectral imagery. *Remote Sensing of Environment*, 92(1):126–138.

- Schmidtlein, S., Zimmermann, P., Schupferling, R., and Weiss, C. (2007). Mapping the floristic continuum: Ordination space position estimated from imaging spectroscopy. *Journal of Vegetation Science*, 18(1):131–140.
- Shepard, R. N. (1962). The analysis of proximities: Multidimensional scaling with an unknown distance function. I. *Psychometrika*, 27(2):125–140.
- Silva, B., Lehnert, L., Roos, K., Fries, A., Rollenbeck, R., Beck, E., and Bendix, J. (2014). Mapping Two Competing Grassland Species from a Low-Altitude Helium Balloon. *IEEE Journal of Selected Topics in Applied Earth Observation and Remote Sensing*, 7(7):3038–3049.
- Silvan-Cardenas, J. and Wang, L. (2010). Retrieval of subpixel Tamarix canopy cover from Landsat data along the Forgotten River using linear and nonlinear spectral mixture models. *Remote Sensing of Environment*, (114):1777–1790.
- Singh, K. K., Pal, K., and Nigam, M. J. (2012). Shadow Detection and Removal from Remote Sensing Images using NDI and Morphological Operators. *International Journal of Computer Applications*, 42(10):37–40.
- Sismanidis, P., Karathanassi, V., and Kolokoussis, P. (2014). De-shadowing of airborne imagery using at-sensor downwelling irradiance data. *International Journal of Remote Sensing*, 35(19):6973–6992.
- Skowronek, S., Asner, G., and Feilhauer, H. (2017a). Performance of one-class classifiers for invasive species mapping using airborne imaging spectroscopy. *Ecological Indicators*, 37:66–76.
- Skowronek, S., Ewald, M., Isermann, M., Van De Kerchove, R., Lenoir, J., Aerts, R., Warrie, J., Hattab, T., Honnay, O., Schmidtlein, S., Rocchini, D., Somers, B., and Feilhauer, H. (2017b). Mapping an invasive bryophyte species using hyperspectral remote sensing data. *Biological Invasions*, 19(1):239–254.
- Smart, S., Thompson, K., Marrs, R., Duc, M. L., Maskell, L., and LG., F. (2006). Biotic homogenization and changes in species diversity across human-modified eco- systems. *Proceedings of the Royal Society B: Biological Sciences*, 273:2659–2665.
- Smith, L. C., MacDonald, G. M., Velichko, A. A., Beilman, D. W., Borisova, O. K., Frey, K. E., Kremenetski, K. V., and Sheng, Y. (2004). Siberian Peatlands a Net Carbon Sink and Global Methane Source since the Early Holocene. *Science*, 303(5656):353–356.
- Somers, B. and Asner, G. (2014). Tree species mapping in tropical forests using multi-temporal imaging spectroscopy: Wavelength adaptive spectral mixture analysis. *International Journal of Applied Earth Observation and Geoinformation*, 31:57–66.
- Stenzel, S., Fassnacht, F. E., Mack, B., and Schmidtlein, S. (2017). Identification of high nature value grassland with remote sensing and minimal field data. *Ecological Indicators*, 74:28–38.
- Stocker, C., Bennett, R., Nex, F., Gerke, M., and Zevenbergen, J. (2017). Review of the Current State of UAV Regulations. *Remote Sensing*, 9(5):459.

- Svejcar, L. N., Bestelmeyer, B. T., Duniway, M. C., and James, D. K. (2015). Scale-Dependent Feedbacks Between Patch Size and Plant Reproduction in Desert Grassland. *Ecosystems*, 18(1):146–153.
- Svetnik, V., Liaw, A., Tong, C., Culberson, J., Sheridan, and R. Feuston, B. (2003). Random forest: A classification and regression tool for compound classification and QSAR modeling. *Journal of Chemical Information and Computer Sciences*, 43(6):1947–1958.
- Sykes, J. M., Horrill, A. D., and Mountford, M. D. (1983). Use of Visual Cover Assessments as Quantitative Estimators of Some British Woodland Taxa. *Journal of Ecology*, 71(2):437–450.
- TEEB (2010). *The Economics of Ecosystems and Biodiversity Ecological and Economic Foundations*. Rensselaer Working Papers in Economics.
- Tenenhaus, M., Esposito, V., Chatelin, T.-M., and Lauro, C. (2005). PLS path modeling. *Computational Statistics & Data Analysis*, 48:159–205.
- Thackway, R. and Lesslie, R. (2008). Describing and Mapping Human-Induced Vegetation Change in the Australian Landscape. *Environmental Management*, 42(4):572–590.
- Torres-Sánchez, J., Peña, J. M., de Castro, a. I., and López-Granados, F. (2014). Multi-temporal mapping of the vegetation fraction in early-season wheat fields using images from UAV. *Computers and Electronics in Agriculture*, 103:104–113.
- Turetsky, M. R., Kane, E. S., Harden, J. W., Ottmar, R. D., Manies, K. L., Hoy, E., Kasischke, E. S., and 5 (2011). Recent acceleration of biomass burning and carbon losses in Alaskan forests and peatlands. *Nature Geoscience*, 4:27–31.
- Turner, W. (2014). Sensing biodiversity. *Science*, 346:301–302.
- Turner, W., Spector, S., Gardiner, N., Fladeland, M., Sterling, E., and Steininger, M. (2003). Remote sensing for biodiversity science and conservation. *Trends in Ecology and Evolution*, 18(6):306–314.
- Ustin, S. L., Wessman, C. A., Curtiss, B., Kasischke, E., Way, J., and Vanderbilt, C. (1991). Opportunities for Using the Eos Imaging Spectrometers and Synthetic Aperture Radar in Ecological Models. *Ecology*, 72(6):1934–1945.
- Üstün, B., Melssen, W. J., and Buydens, L. M. C. (2007). Visualisation and interpretation of Support Vector Regression models. *Analytica Chimica Acta*, 595(1–2):299–309.
- Valbuena, R., Mauro, F., Rodriguez-Solano, R., and Manzanera, J. A. (2010). Accuracy and precision of GPS receivers under forest canopies in a mountainous environment. *Spanish Journal of Agricultural Research*, 8:1047–1057.
- van der Walt, S., Schönberger, J. L., Nunez-Iglesias, J., Boulogne, F., Warner, J. D., Yager, N., Gouillart, E., and Yu, T. (2014). Scikit-image: image processing in Python. *PeerJ*, 2:e453.
- van Wesenbeeck, B., Van De Koppel, J., M. J. Herman, P., and J. Bouma, T. (2008). Does scale-dependent feedback explain spatial complexity in salt-marsh ecosystems? *Oikos*, 117(1):152–159.

- Vapnik, V. (2000). *The Nature of Statistical Learning Theory*. New York, Springer edition.
- Verrelst, J., Camps-Valls, G., Muñoz-Marí, J., Rivera, J. P., Veroustraete, F., Clevers, J. G., and Moreno, J. (2015). Optical remote sensing and the retrieval of terrestrial vegetation biogeophysical properties - A review. *ISPRS Journal of Photogrammetry and Remote Sensing*, 108:273–290.
- Vilà, M., Espinar, J. L., Hejda, M., Hulme, P. E., Jarošík, V., Maron, J. L., Pergl, J., Schaffner, U., Sun, Y., and Pyšek, P. (2011). Ecological impacts of invasive alien plants: A meta-analysis of their effects on species, communities and ecosystems. *Ecology Letters*, 14(7):702–708.
- Vittoz, P. and Guisan, a. (2007). How reliable is the monitoring of permanent vegetation plots? A test with multiple observers. *Journal of Vegetation Science*, 18(2007):413–422.
- Vuolo, F., Neugebauer, N., Bolognesi, S. F., Atzberger, C., and D’Urso, G. (2013). Estimation of Leaf Area Index Using DEIMOS-1 Data: Application and Transferability of a Semi-Empirical Relationship between two Agricultural Areas. *Remote Sensing*, 5(3):1274–1291.
- Weinacker, H., Koch, B., and Weinacker, R. (2004). TREESVIS—a software system for simultaneous 3D-realtime visualization of DTM, DSM, laser raw data, multispectral data, simple tree and building models. *International Archives of Photogrammetry, Remote Sensing and Spatial Information Sciences*, XXXVI:90–95.
- Wesche, K., Krause, B., Culmsee, H., and Leuschner, C. (2012). Fifty years of change in Central European grassland vegetation: Large losses in species richness and animal-pollinated plants. *Biological Conservation*, 150(1):76–85.
- Westoby, M. J., Brasington, J., Glasser, N. F., Hambrey, M. J., and Reynolds, J. M. (2012). ‘Structure-from-Motion’ photogrammetry: A low-cost, effective tool for geoscience applications. *Geomorphology*, 179:300–314.
- Whittaker, R. J., Arañójo, M. B., Jepson, P., Ladle, R. J., Watson, J. E. M., and Willis, K. J. (2005). Conservation Biogeography: assessment and prospect. *Diversity and Distributions*, 11(1):3–23.
- Wiens, J. A. (1989). Spatial Scaling in Ecology. *Functional Ecology*, 3(4):385–397.
- Wold, S., Sjöström, M., and Eriksson, L. (2001). PLS-regression: a basic tool of chemometrics. *Chemometrics and Intelligent Laboratory Systems*, 58(2):109–130.
- Yu, Q., Gong, P., Clinton, N., Biging, G., Kelly, M., and Schirokauer, D. (2006). Object-based detailed vegetation classification with airborne high spatial resolution remote sensing imagery. *Photogrammetric Engineering and Remote Sensing*, 72(7):799–811.
- Zahawi, R. a., Dandois, J. P., Holl, K. D., Nadwodny, D., Reid, J. L., and Ellis, E. C. (2015). Using lightweight unmanned aerial vehicles to monitor tropical forest recovery. *Biological Conservation*, 186:287–295.
- Zaman, B., Jensen, A. M., and McKee, M. (2011). Use of high-resolution multispectral imagery acquired with an autonomous unmanned aerial vehicle to quantify the spread of an invasive wetlands species. In *International Geoscience and Remote Sensing Symposium (IGARSS)*, pages 803–806.

- Zarco-Tejada, P. J., Camino, C., Beck, P. S. A., Calderon, R., Hornero, A., Hernández-Clemente, R., Kattenborn, T., Montes-Borrego, M., Susca, L., Morelli, M., Gonzalez-Dugo, V., North, P. R. J., Landa, B. B., Boscia, D., Saponari, M., and Navas-Cortes, J. A. (2018). Previsual symptoms of *Xylella fastidiosa* infection revealed in spectral plant-trait alterations. *Nature Plants*, 4(7):432–439.
- Zarco-Tejada, P. J., Hornero, A., Beck, P. S., Kattenborn, T., Kempeneers, P., and Hernández-Clemente, R. (2019). Chlorophyll content estimation in an open-canopy conifer forest with Sentinel-2A and hyperspectral imagery in the context of forest decline. *Remote Sensing of Environment*, 223(February 2018):320–335.
- Zhang, J., Rivard, B., Sánchez-Azofeifa, A., and Castro-Esau, K. (2006). Intra- and inter-class spectral variability of tropical tree species at La Selva, Costa Rica: Implications for species identification using HYDICE imagery. *Remote Sensing of Environment*, 105(2):129–141.
- Zhang, L., Sun, X., Wu, T., and Zhang, H. (2015). An Analysis of Shadow Effects on Spectral Vegetation Indexes Using a Ground-Based Imaging Spectrometer. *IEEE Geoscience and Remote Sensing Letters*, 12(11):2188–2192.

A Appendices

Appendix paper 1

Appendix 1.1: Classification and cover prediction per species Classification

Classification accuracies (producer and user accuracies) and cover predictions (r^2 , RMSE and bias) of each species is presented in Table A1.

Table A.1: List of species along with respective producer (PA) and user (UA) accuracies and their r^2 , RMSE and bias from the cover estimation. Median values of the bootstrap iteration procedure are listed.

Species	PA	UA	r^2	RMSE [%]	bias
Bryophyte					
<i>Rhytidiadelphus squarrosus (Hedw.) Warnst.</i>	0.9	0.84	0.83	6.53	-0.39
Graminoids					
<i>Echinochloa crus-galli</i>	0.96	0.86	0.46	24.68	0.17
<i>Elymus repens</i>	0.89	0.84	0.46	9.87	0.31
<i>Nardus stricta</i>	1	0.84	0.8	14.29	0.06
<i>Panicum capillare</i>	0.83	0.84	0.84	5.74	-0.49
<i>Setaria pumila</i>	0.9	0.84	0.67	14.18	-0.36
Forbs					
<i>Achillea millefolium</i>	1	0.84	0.69	8.72	-0.04
<i>Anagallis arvensis</i>	-	0.84	-	-	-
<i>Anthemis arvensis</i>	0.92	0.85	0.43	20.66	0.47
<i>Artemisia vulgaris</i>	1	0.83	0.42	20.82	0.97
<i>Bellis perennis</i>	0.91	0.86	0.9	7.94	-0.15
<i>Crepis capillaris</i>	0.91	0.85	0.83	20.77	-0.52
<i>Cichorium intybus</i>	0.99	0.89	0.57	31.09	0.45

<i>Convolvulus sepium</i>	0.79	0.84	0.67	2.44	-0.12
<i>Conyza canadensis</i>	0.8	0.85	0.31	51.59	-0.03
<i>Daucus carota</i>	0.94	0.86	0.93	8.92	0.14
<i>Echium vulgare</i>	0.87	0.84	0.54	35.27	0.32
<i>Erigeron annuus</i>	0.99	0.84	0.43	17.58	0
<i>Filago arvensis</i>	0.85	0.84	0.36	22.49	0.12
<i>Geranium pusillum</i>	0.9	0.84	0.9	4.21	-0.18
<i>Glechoma hederacea</i>	0.95	0.84	0.52	3.67	-0.32
<i>Hypochaeris radicata</i>	0.81	0.85	0.68	6.67	-0.25
<i>Medicago arabica</i>	1	0.85	0.65	19.77	0.27
<i>Medicago lupulina</i>	1	0.85	0.41	28.63	0.91
<i>Medicago sativa</i>	0.9	0.86	0.5	3.97	0.69
<i>Minuartia hybrida</i>	0.75	0.85	0.73	4.2	-0.38
<i>Oenothera biennis</i>	-	0.84	0.42	0.96	0.42
<i>Oxalis stricta</i>	1	0.84	0.77	3.67	-0.19
<i>Plantago lanceolata</i>	0.89	0.85	0.42	15.92	0.05
<i>Plantago major</i>	0.91	0.87	0.52	3.18	0.23
<i>Polygonum persicaria</i>	-	0.83	-	-	-
<i>Potentilla reptans</i>	0.85	0.85	0.68	23.07	-0.25
<i>Prunella vulgaris</i>	1	0.87	1	1.45	-0.34
<i>Rumex obtusifolius</i>	0.93	0.84	0.52	23.06	0.49
<i>Senecio vulgaris</i>	0.74	0.86	0.83	3.5	0.65
<i>Solidago gigantea</i>	1	0.81	0.55	0.96	-0.15
<i>Taraxacum officinale</i>	0.85	0.86	0.41	9.78	-0.06
<i>Trifolium pratense</i>	0.87	0.85	0.68	4.65	-0.29
<i>Trifolium repens</i>	0.86	0.85	0.42	27.31	-0.27
<i>Urtica dioica</i>	1	0.9	0.44	29.91	-0.09
<i>Verbena officinal</i>	1	0.84	0.59	11.06	0.99
<i>Veronica persica</i>	0.97	0.86	0.83	8.79	-0.08

Appendix 1.2: Source codes of the paper

R and Python codes used in the analysis can be accessed at: <https://github.com/JavierLopatin/Grassland-Species-Classification>.

Appendix 1.3: Supplementary data

Images for model calibration: pot versus isolation methods

We tested two methods for collecting independent species spectra outside the plots: 1) a pot sample method, and 2) an isolation method (presented in the main manuscript):

1. For the pot method, complete individuals of species (i.e. roots included) were dug out and transplanted into small pots to maintain the structure of the individual plants. We used the same soil as present in the plots to minimize background effects. We increased the spectral heterogeneity of the samples by measuring them twice and rotate the pots 90° before the second scan. This ensured that differences in relative angles between leaf surface and the sensor were accounted for. For small species, several individuals were located in the same pot to maximize the canopy cover area. Three to five pots were obtained for each species – except for a few cases where the species individuals were too rare in the surrounding of the plots.
2. In the isolation approach, samples of each species were first identified in the areas neighboring the plots. Then surrounding canopies of other species that may interfere in the reflectance were removed prior to the AISA+ scans to isolate the target species. No scan-repetitions to change the view angles were performed in this case, because this procedure would have notably increased the sampling effort (too many movements of the scanner system), which would make the approach less suitable for operational applications.

In total 122 calibration reference image scans were taken, with 81 corresponding to the pot method and 41 to the isolation method.

The classification and cover estimations results based on the two sampling strategies are presented in Figure A1. In general, the isolation collection method obtained higher classification accuracies and better agreements with the field-estimated cover values than the pot method. For the classification results (Figure 2.3 A; overall accuracy and kappa), the accuracies of the isolation method were significantly higher ($\alpha = 0.05$) than the accuracies obtained with the pot

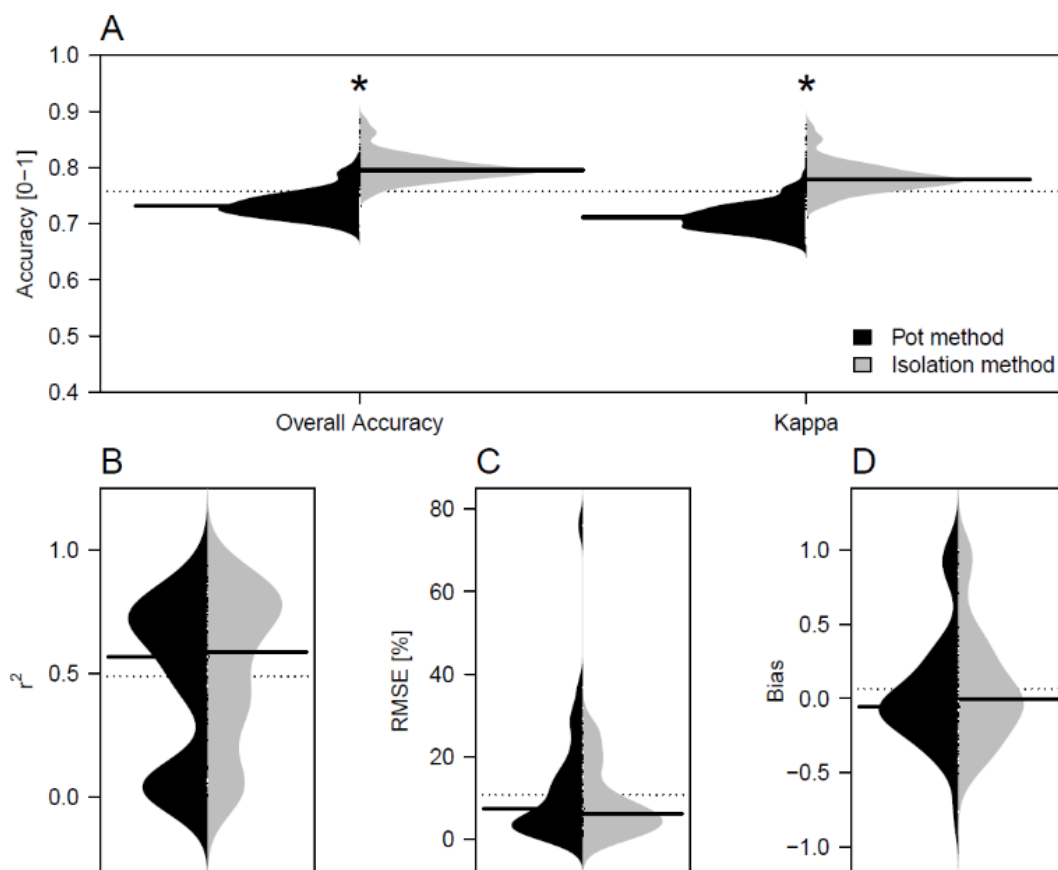


Figure A.1: Bootstrap distribution of classification results using all sub-plots. In (A), the overall accuracy and kappa of the SVM classification are presented, while in (B-D) the prediction accuracies (r^2 , RMSE and bias) of the measured against the predicted species covers are displayed. Distributions for the pot (black) and the isolation (gray) methods (for collecting training data) are depicted. Beanplots show the relative distribution of the bootstrap results with the width indicating the frequency of a given value, while black horizontal lines indicate the median values of the distribution and * indicates a significant difference of the distributions ($\alpha = 0.05$; Lopatin et al., 2016).

method, while non-significant differences were found for the correlations with field-estimated covers (Figure 2.3 B-D; r^2 , RMSE and bias).

In terms of practicability, both methods have advantages and disadvantages. The pot method requires fewer scans and no movement of the AISA+ sensor, as the samples are moved in their pots. This makes the sampling procedure more effective. Likewise, several individuals from species with small leaves can be put together in the same pot to generate more consistent sampling areas. On the negative side, the scans must be performed quickly, otherwise the samples – particularly forbs – lose turgidity due to the stress caused by the transplantation. This is mostly apparent in the visible and the short-wave infrared spectral regions (Carter, 1993). In contrast, scans for the isolation approach are taken without stress problems (as the individuals

remain untouched), but more scans and scanner movements are required to obtain a scan of all occurring species and obtaining scans from smaller individuals can be challenging. In some environments, removal of plants with a destructive sampling method (isolation method) may be problematic due to for example conservation regulations, while the pot method may allow for individuals to be returned to their environment.

In the pot sampling method, we increased the spectral heterogeneity of the samples by measuring them twice and turning the pots for 90° before the second scan. Here, we found two scans with a 90° shift of the pot between the two scans a sound compromise between maximizing the canopy view perspectives while keeping the method simple and fast. More efforts will be needed to fully understand how directional information affects species classification on such a detailed scale.

Wavelength importance analysis

A wavelength relevance analysis procedure was performed to link biochemical (e.g. pigments, leaf water and leaf area per area) and structural properties (e.g. leaf area, angle, and leaf structure) that enable the discrimination of species and functional types. For this purpose, we analyzed the relative importance of each band separately applying the Multiple Response Permutation Procedure (MRPP) algorithm. MRPP is a non-parametric procedure to test the hypothesis of no differences between two or more groups of entities (Mielke et al., 1981). The algorithm calculates a dissimilarity matrix (we used the Mahalanobis distance), obtains an average distance within groups, and estimates a weighted mean within group distance (δ). Smaller values of δ indicate a tendency for clustering while larger δ values indicate a lack of clustering. MRPP determines the probability of δ to be 'small' or 'large' by a brute force approach (test all possible partitions in the dataset; recommended for small datasets) or by a continuous distribution (e.g. Pearson type III). Finally, RMPP estimates a chance-corrected within-group agreement (A), describing the proportion of the distances explained by group identity (a value analogous to a coefficient of determination in a linear model). A is independent of the sample size of the groups (classes), and varies between zero (no explanation) and one (all observations identical

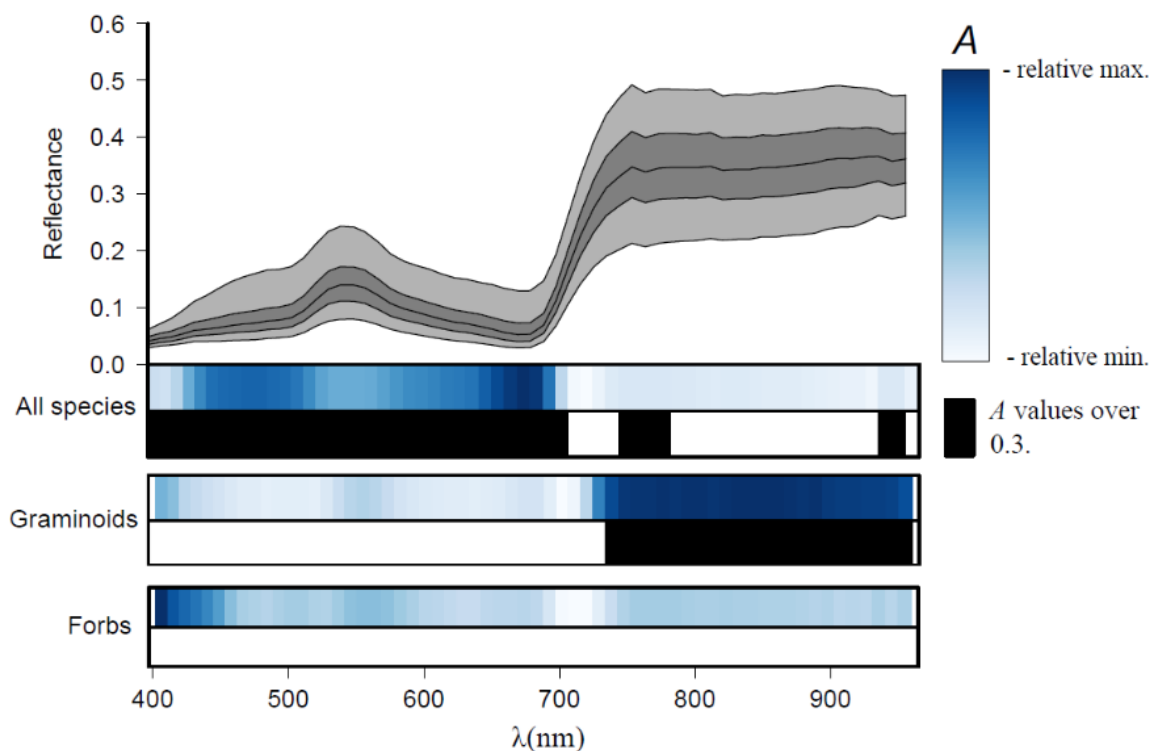


Figure A.2: MRPP wavelength distance analysis of single spectral bands. Results using all species, only graminoids and only forbs are presented. A describes the proportion of the distances explained by group identity. Values of A over 0.3 are shown as black areas. In the presented spectral signatures, the 5, 25, 50, 75 and 95 percentiles of all analyzed spectra are displayed.

within-groups), where normally values over 0.3 are considered high. Finally, MRPP determines the probability of A by Monte Carlo permutation (we applied 500 permutations) and by randomly assigning sample observations to the classes. See Mielke et al. (1981) for more insights into the MRPP algorithm.

Figure A2 shows the ability of single bands to differentiate between species using MRPP. We used the spectra obtained from the isolation training data to perform the analysis. According to MRPP, the visible region allowed for good differentiation between species. Some additional features in the near infrared (NIR; ~ 750 nm-800 nm and 980 nm) also showed high discrimination power.

Differences in plant characteristics, such as leaf thickness, tissue density, presence or absence of waxes, hairs, and/or air spaces, as well as plant-chemical characteristics including pigment composition and secondary plant materials, and canopy architecture all have an effect on the reflectance properties of single species (Jones and Vaughan, 2010). The review of Fassnacht

et al. (2016) showed that for tree species classification, selected spectral regions of the full-range optical region provide valuable information for species discrimination. For grassland species, Schmidt and Skidmore (2003) found that 75% of the bands (mainly the NIR) of the full spectrum were significant in the discrimination of 27 saltmarsh vegetation types (at $\alpha = 0.01$).

In agreement with the findings for tree species, the visible region showed a high discrimination potential for grassland species along with some spectral regions of the NIR. The VIS spectral region is commonly related to leaf pigments and biochemical characteristics of plants while the NIR is usually related to canopy structure (e.g. leaf area index and leaf angles; Ollinger (2011)). The VIS spectral region represents complex interactions of leaf and canopy traits, with strong influences of the leaf internal structure parameter (N) (Ollinger, 2011), leaf angle and leaf orientation (Ganapol et al., 1999; Jacquemoud et al., 2009; Posada et al., 2009). As in our study the number of forbs is greater than the number of graminoids and bryophytes, the selected wavelength may be biased towards forb species discrimination. With other species configurations the selected wavelength may change due to, for example, a higher relative importance of the NIR (i.e. structure) to discriminate graminoids. More research toward this direction is needed to obtain more detailed information.

Forbs discrimination follows similar patterns, however, no band reached an A value greater than 0.3 (the level above which a variable is considered to largely explain within-group discrimination (Mielke et al., 1981)). In contrast, the bands located in the NIR plateau showed a better ability for discriminating within graminoids. The main driver of NIR reflectance differences are the leaf-area index (LAI) and the leaf angle (Darvishzadeh et al., 2008). This may reveal that the structural information explains the majority of the graminoid species' spectral variance.

Algorithm comparison

We tested three classification approaches known for their capability to deal with highly heterogeneous data: Partial Least Squares Discriminant Analysis (PLS), Random Forest (RF) and Support Vector Machines (SVM).

PLS is a linear parametric algorithm that generates statistically independent latent vectors (LVs) as a linear combination of the spectral bands to cope with inter-correlation of spectral data. Unlike other ordination algorithms, PLS takes into account the observed variable (or the classification classes) in the LVs generation, making the LVs more efficient than other ordination methods (e.g. principal component analysis) when applied to discrimination of classes (Barker and Rayens, 2003). To obtain the variable importance of the PLS model the coefficients obtained in the cross-validated procedure are used. When applied with standardized variables, the sign of the coefficients in PLS indicates a positive or negative relationship, while the absolute value is a measure of the variable importance (Wold et al., 2001).

RF is a non-parametric classification and regression algorithm that uses bagging (i.e. based on bootstrapping) to form an ensemble of classification or regression (CART) like trees (Breiman, 2001). In classification, each tree cast a unit vote for the most popular class at the inputs. The majority votes of trees will determine the output of the classifier. This method can handle high dimensional datasets (Gislason et al., 2006), with more predictor variables than observations (Evans et al., 2011). Here, we used the Gini decrease in node impurity measure to obtain the variable importance, which is computed by permuting the predictor variables with the out-of-bag data in the RF validation approach (Liaw and Wiener, 2002).

SVM is also a non-parametric classifier. SVM work by constructing an optimal hyperplane separating two classes within a multidimensional feature space. When the linear separability of the two classes is not possible, SVM successively maps the data into a higher dimensional feature space via a kernel function until it finds a linear relationship. More information on the concept of SVMs can be found in Burges (1998). Here, we use the variable importance proposed by Üstün et al. (2007), where the inner product of the spectral bands and the α -vectors are used to incorporate the support vectors. These values can be interpreted as coefficients, where the sign of the coefficients indicates either a positive or negative relationship, and the absolute value is the measure for the variable importance.

Furthermore, we tested four different datasets that use either the full spectra of the hyperspectral images, or the minimum noise fraction transformation (MNF) with the first 10 compo-

nents. MNF is an ordination method similar to Principal Components Analysis, but instead of maximizing the variance, MNF creates new components based on their signal-to-noise ratio. This allows for obtaining always the components in decreasing order of importance (Green et al., 1988)(Green et al., 1988) and it has showed to be one of the preferred data transformations to classify hyperspectral images (Fassnacht et al., 2014). The MNF components vary between scans due to differences in the spectral composition of each scan. Hence, we calculated the MNF components of each plot and then applied these components to the reference scans containing the training samples for the corresponding plot. Before calculating the MNF components we applied a NDVI mask to eliminate non vegetated areas and thereby maximize vegetation-related information. In this way we made sure that the MNF components had the same composition along the scans. Furthermore, due to the high spatial resolution of the scans we applied a brightness normalization (Feilhauer et al., 2010) to cope with the differences of spectra caused by shadowing. The normalization transforms a spectrum to a uniform value of one as $X_{bn} = x_i / (\sum_{i=1} x_i^2)^{1/2}$, where x_i is the hyperspectral data and x_{bn} is the normalize spectra. Therefore, the four datasets were: *Spectra*, *Spectra_{bn}*, *MNF* and *MNF_{bn}*. These datasets were tested using the pot and the rip-it-off reference methods and with the algorithms PLS, RF and SVM, resulting in 24 models. All image processing were done using the Python 3 programming language.

Results of all models can be seen in Figure A3. In general, the pot and the isolation methods to collect the reference spectra obtained similar accuracies, with a small tendency of the isolation method to reach better classification accuracies (Kappa). PLS showed lower classification accuracies and higher errors and biases in predictions, while RF and SVM show similar performances. One major difference is that RF obtains the best performances with the MNF datasets, while SVM reached highest performances with the spectral datasets. A slight improvement of accuracies was observed when applying the brightness normalization to the datasets.

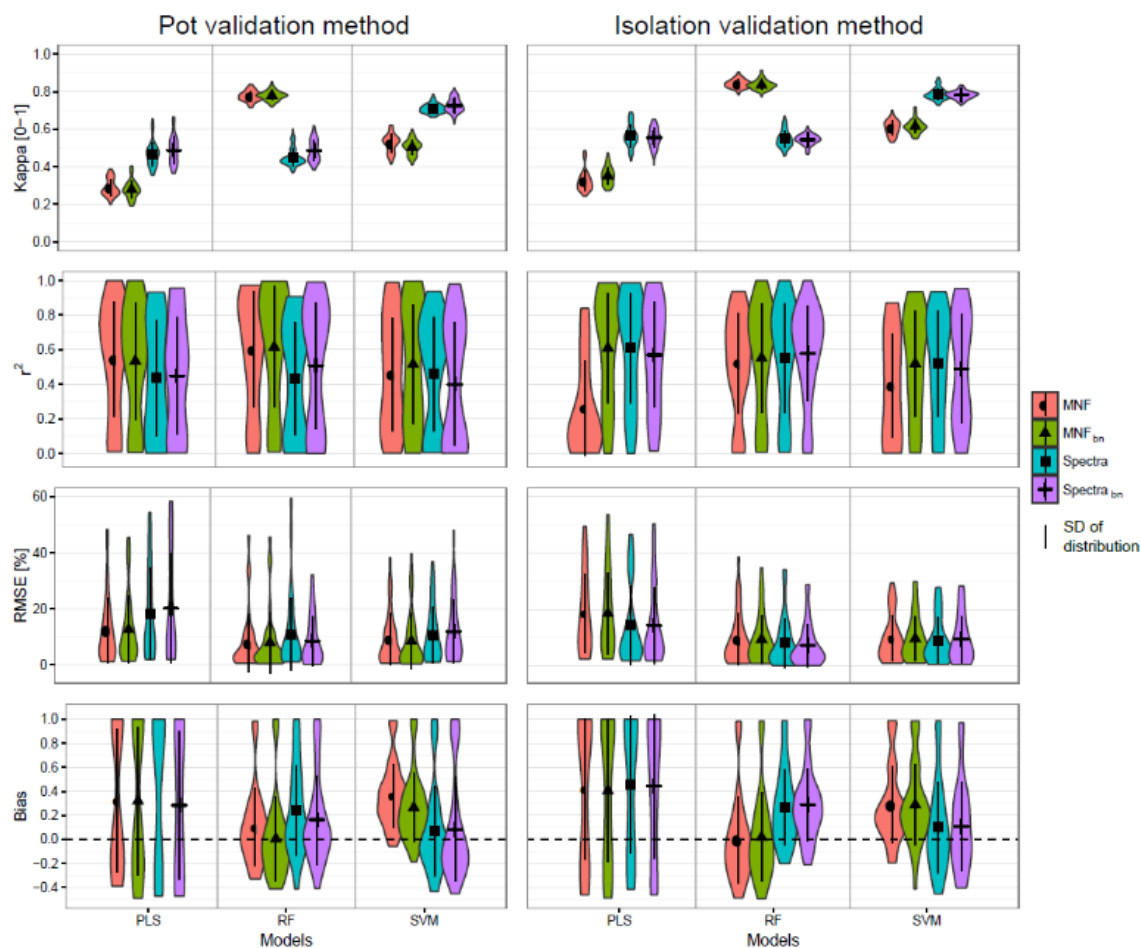


Figure A.3: Bootstrap distributions of classification and cover prediction (%) accuracies of all models. Model symbols (\circ , \triangle , \square , $+$) shows the mean value of the bootstrap distribution while the vertical line depict the standard deviation of the bootstrap distribution. Wider areas represent a higher frequency. Spectra = spectral bands as input; MNF = minimum noise fraction transformation as input; bn = preprocessing using brightness normalization of the spectral (Feilhauer et al., 2010).

Appendix paper 2

Appendix 2.1: Data accessibility

R and Python codes used in the analysis can be accessed at: <https://github.com/JavierLopatin/UAV-InvasiveSp>.

Appendix 2.2: Supporting information

Supporting information for paper 2 include Table A.2 and Figure A.4 and A.5.

Table A.2: Parameterization of Agisoft Photoscan. Settings not included in the table were set as default.

Module	Parameter	Selection
Alignment	Quality	High
	Mode	Reference
Dense cloud	Quality	High
	Depth filtering	Mild
Mesh	Surface type	Height field
Orthomosaic	Source	Mesh
	Blending mode	Mosaic
	Brightness correction	Enabled

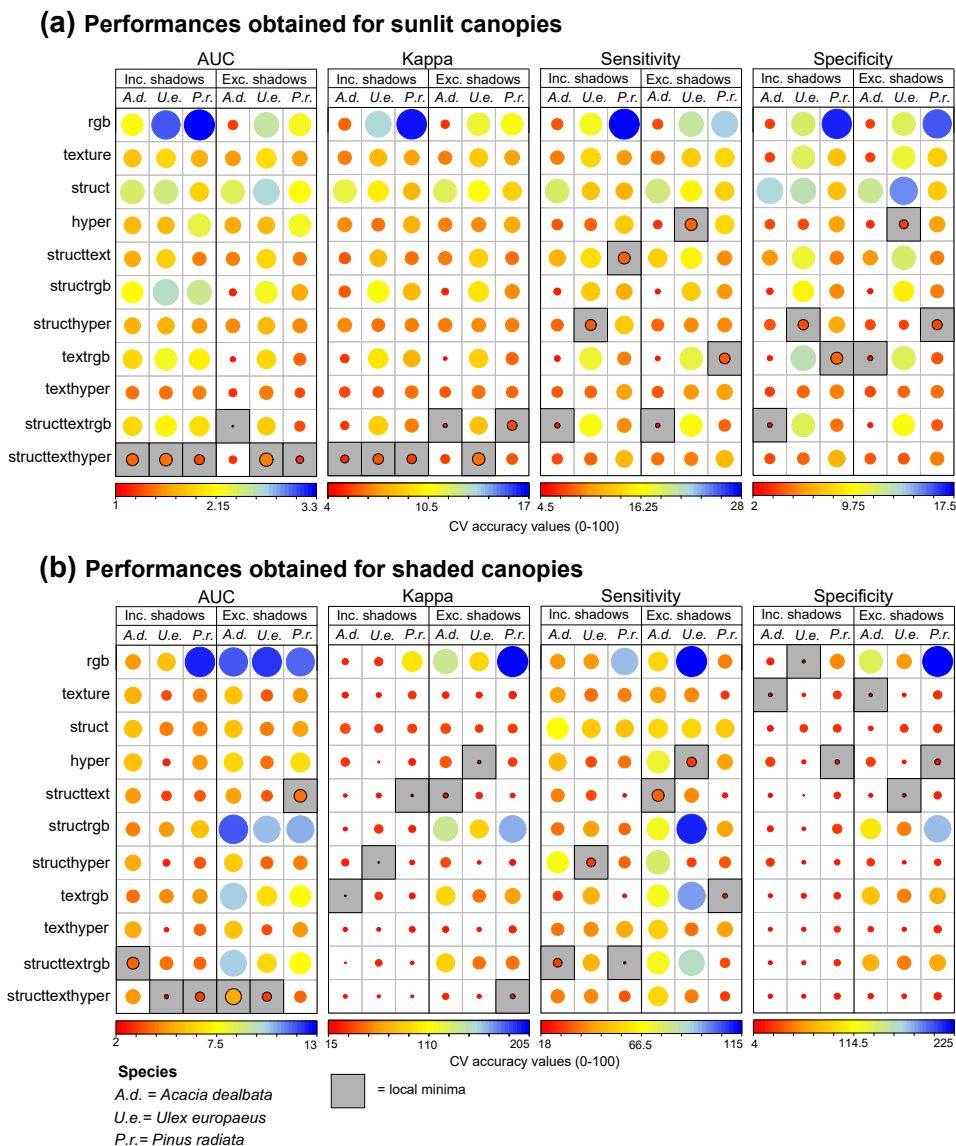


Figure A.4: Model performances for sunlit (A) and shaded (B) canopies using models that include (incl.) and exclude (excl.) shadows in the calibration data. The coefficient of variation (CV) iterative values are presented, with dot size scaled to the values. A.d. = *Acacia dealbata*; U.e. = *Ulex europaeus*; P.r. = *Pinus radiata*. * depicts significant ($\alpha = 0.05$) improvements of the models excluding shaded canopies over the models including shaded canopies (A) and of the models including shaded canopies over the models excluding shaded canopies (B).

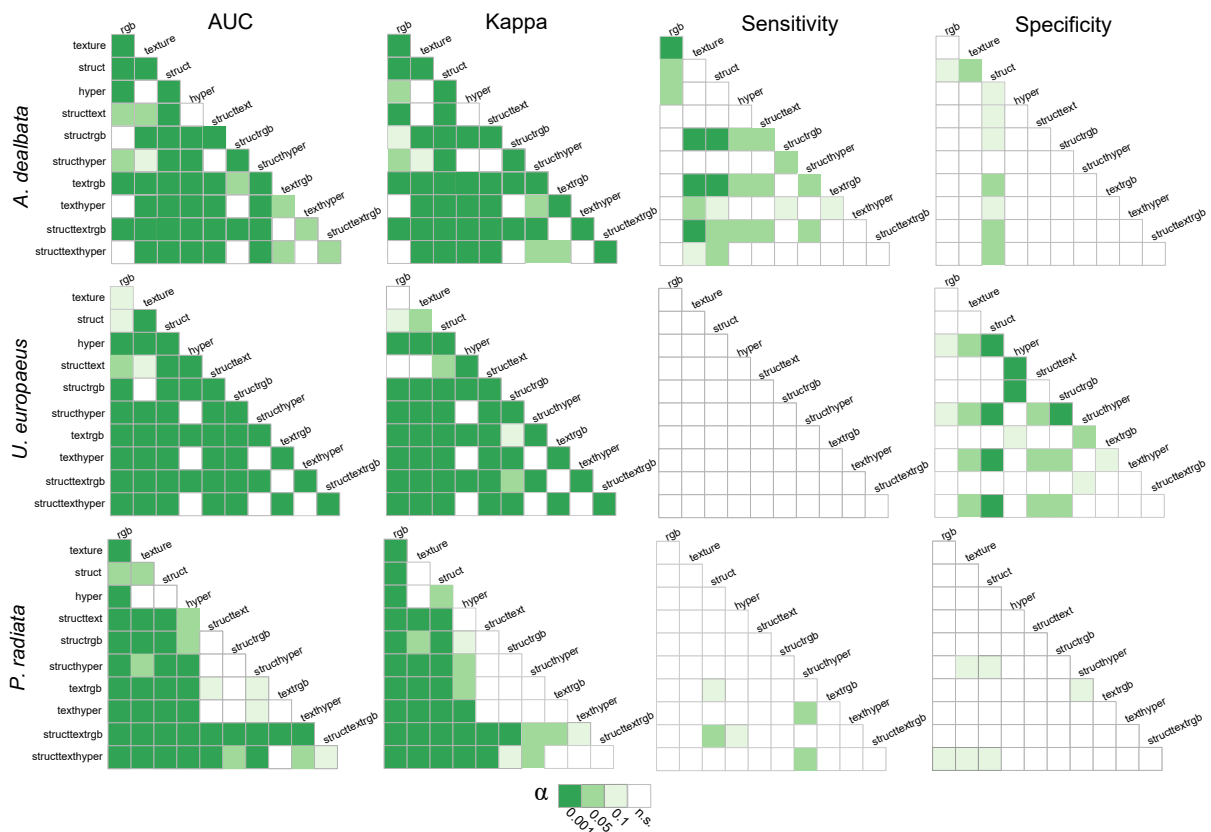


Figure A.5: Significant differences in terms of model performance among models using models excluding shadows in the calibration data.

Appendix paper 3

Appendix 3.1: Applied scripts

The R and Python scripts applied in this investigation can be found in the following repository:
<https://github.com/JavierLopatin/Peatland-carbon-stock>.

Appendix 3.2: PLS path modeling extra information

Extra information regarding the used PLS path model in paper 3 can be found in table A.3. Meanwhile, Figure A.6. shows the structural architecture of the PLS-PM used to predict below ground *C* stock with UAV-based data (Figure 4.3b).

Table A.3: PLS-PM outer model specifications. The weights correspond to the outer model coefficients while the loading are similar to the correlations in regression analysis. Non-significant predictors (n.s.) are highlighted in gray.

Latent variables	Predictor	Weight (ω)	Loading (l)
Vascular vegetation height	Vegetation height	1	1
Floristic composition	NMDS 1	1	1
	NMDS 2	n.s.	n.s.
	NMDS 3	n.s.	n.s.
Vascular aboveground biomass	Bryophytes biomass	n.s.	n.s.
	Herbaceous biomass	0.65	0.94
	Shrubs biomass	0.45	0.87
Vascular species richness	Graminoid richness	0.5	0.9
	Forbs richness	0.59	0.93
	Shrub richness	n.s.	n.s.
SOM	Soil organic matter depth	1	1
C stock	Belowground C stock	1	1

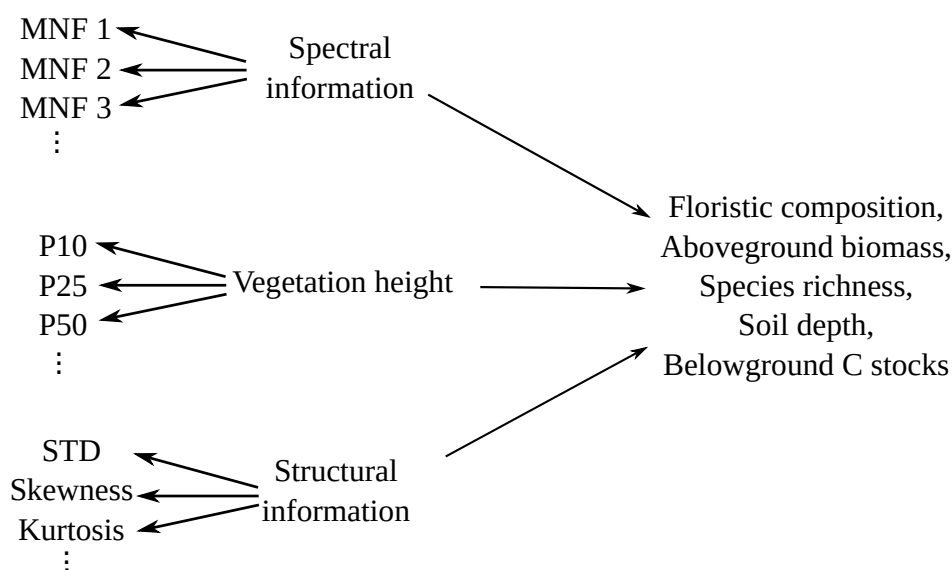


Figure A.6: PLS-PM structural model for the estimation of vegetation proxies, soil depth and belowground C stock using UAV-based predictors (Fig. 3b).

Appendix 3.3: Floristic composition information

Figure A.7 depicts the floristic gradient obtained from the ordination procedure and its interpretation. Compare Supplementary information below for a description of the procedure.

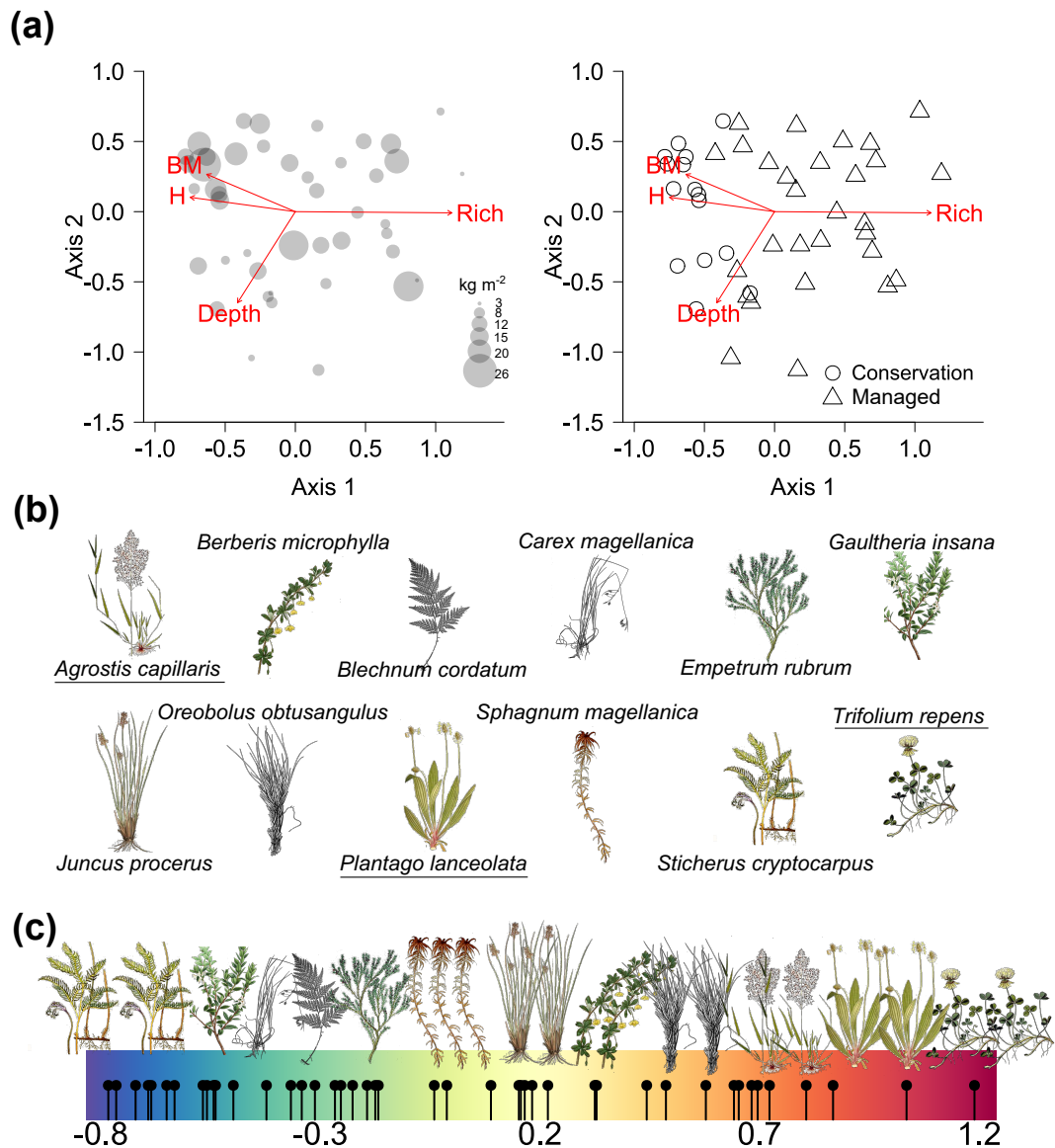


Figure A.7: Results of the floristic gradient. (a) Distribution of plots (sample points) in the two-dimensional ordination space of NMDS, showing the distribution of the belowground C stock (left) and the management types (right) along the gradients. Close plots feature a similar species composition, while remote plots are more dissimilar. Vectors illustrate the correlations of the axes with the PLS-PM latent variables (H = vascular vegetation height, BM = vascular aboveground biomass, Rich = vascular species richness and Depth = soil depth). (b) Typical species identified with the isopam clustering algorithms in the NMDS first axis. Underlined species names indicate exotic species. (c) Floristic gradient obtained in the NMDS first axis with the plot locations (black dots) and the placement of the common species on it.

Appendix 3.4: Supplementary information

Floristic composition

To estimate the floristic composition, we assessed the most important floristic gradients in the species-by-plot matrix using Nonmetric Multidimensional Scaling (NMDS; Shepard, 1962). NMDS has been related successfully to remote sensing data before (e.g. Feilhauer et al., 2011; Schmidtlein et al., 2007) and is one of the most used algorithms in vegetation ordination. NMDS arranged vegetation plots based dissimilarities ranked by the Euclidean distance in the ordination space. Similar to principal component analysis, NMDS rotate the ordination space so the first axis describes the highest floristic variation (Clarke, 1993). To avoid local minima, the best solution out of 500 iterations was selected. NMDS estimations were carried using the ‘vegan’ R-package (Oksanen et al., 2017).

Two ordination axes were found to contribute the most to the gradient. We analyzed the distribution of the plot-based vegetation traits - i.e. vegetation heights, species richness, aboveground biomass – and soil depth and C stock in the ordination space to obtain initial information towards their distribution in the floristic gradient. Likewise, management types were plotted to display floristic differences (see Figure A.7).

Photogrammetric point cloud structural information

The structural metrics derived from the CloudMetrics function of FUSION (McGaughey, 2018). The estimated variables were: the minimum, maximum, mean, median, mode, standard deviation, variance, interquartile distance, skewness, kurtosis, ADD (average absolute deviation), percentiles, MADMedian (median of the absolute deviations from the overall median), MAD-Mode (median of the absolute deviations from the overall mode), L-moments (L1, L2, L3, L4), L-moment skewness, L-moment kurtosis, canopy relief ratio $((\text{mean} - \text{min}) / (\text{max} - \text{min}))$ and generalized means for the 2nd and 3rd power (elev. Quadratic mean and elev. Cubic mean).

Random forest variable importance using the UAV-based predictors

Figure A.8 shows the variable importance of random forest regressions applying the UAV-based data (Figure 4.3b).

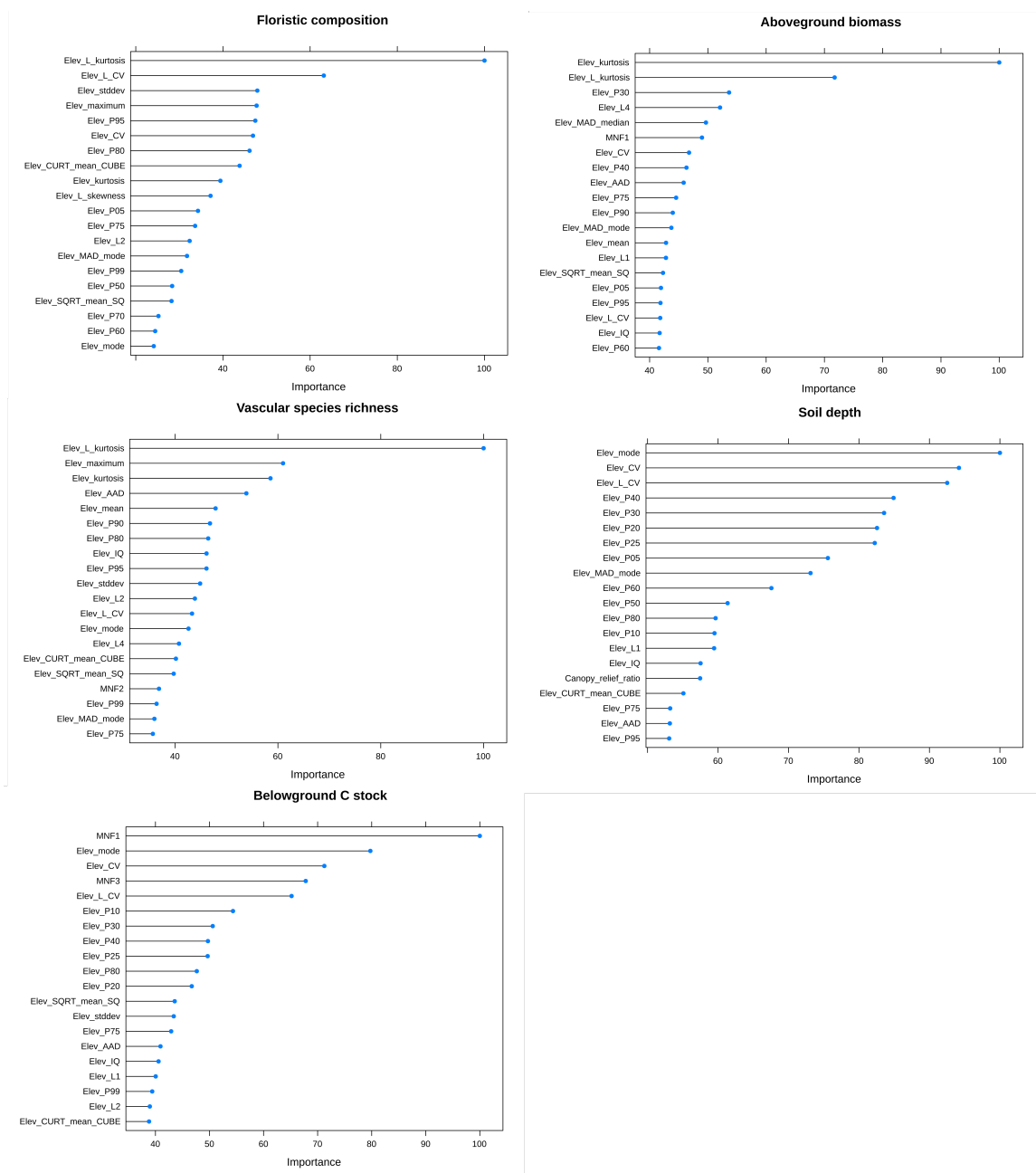


Figure A.8: Variable importance of the random forest models using the UAV-based predictors

Eidesstattliche Versicherung

Eidesstattliche Versicherung gemäß § 6 Abs. 1 Ziff. 4 der Promotionsordnung des Karlsruher Instituts für Technologie für die Fakultät für Bauingenieur-, Geo- und Umweltwissenschaften

1. Bei der eingereichten Dissertation zu dem Thema Unmanned Aerial Vehicles for Vegetation Monitoring: Opportunities and Challenges handelt es sich um meine eigenständig erbrachte Leistung.

2. Ich habe nur die angegebenen Quellen und Hilfsmittel benutzt und mich keiner unzulässigen Hilfe Dritter bedient. Insbesondere habe ich wörtlich oder sinngemäß aus anderen Werken übernommene Inhalte als solche kenntlich gemacht.

3. Die Arbeit oder Teile davon habe ich wie folgt/ bislang nicht an einer Hochschule des Inoder Auslands als Bestandteil einer Prüfungs- oder Qualifikationsleistung vorgelegt.

- Titel der Arbeit: *Unmanned Aerial Vehicles for Vegetation Monitoring: Opportunities and Challenges*

- Hochschule und Jahr: *Karlsruher Institute für Technologie, 2019*

- Art der Prüfungs- oder Qualifikationsleistung: Dissertation

4. Die Richtigkeit der vorstehenden Erklärungen bestätige ich.

5. Die Bedeutung der eidesstattlichen Versicherung und die strafrechtlichen Folgen einer unrichtigen oder unvollständigen eidesstattlichen Versicherung sind mir bekannt.

Ich versichere an Eides statt, dass ich nach bestem Wissen die reine Wahrheit erkläre und nichts verschwiegen habe.

Ort und Datum

Unterschrift

Eidesstattliche Versicherung

Belehrung

Die Universitäten in Baden-Württemberg verlangen eine Eidesstattliche Versicherung über die Eigenständigkeit der erbrachten wissenschaftlichen Leistungen, um sich glaubhaft zu versichern, dass der Promovend die wissenschaftlichen Leistungen eigenständig erbracht hat.

Weil der Gesetzgeber der Eidesstattlichen Versicherung eine besondere Bedeutung beimisst und sie erhebliche Folgen haben kann, hat der Gesetzgeber die Abgabe einer falschen eidesstattlichen Versicherung unter Strafe gestellt. Bei vorsätzlicher (also wissentlicher) Abgabe einer falschen Erklärung droht eine Freiheitsstrafe bis zu drei Jahren oder eine Geldstrafe.

Eine fahrlässige Abgabe (also Abgabe, obwohl Sie hätten erkennen müssen, dass die Erklärung nicht den Tatsachen entspricht) kann eine Freiheitsstrafe bis zu einem Jahr oder eine Geldstrafe nach sich ziehen.

Die entsprechenden Strafvorschriften sind in § 156 StGB (falsche Versicherung an Eides Statt) und in § 161 StGB (fahrlässiger Falscheid, fahrlässige falsche Versicherung an Eides Statt) wiedergegeben.

§ 156 StGB: Falsche Versicherung an Eides Statt

Wer vor einer zur Abnahme einer Versicherung an Eides Statt zuständigen Behörde eine solche Versicherung falsch abgibt oder unter Berufung auf eine solche Versicherung falsch aussagt, wird mit Freiheitsstrafe bis zu drei Jahren oder mit Geldstrafe bestraft.

§ 161 StGB: Fahrlässiger Falscheid, fahrlässige falsche Versicherung an Eides Statt

Abs. 1: Wenn eine der in den § 154 bis 156 bezeichneten Handlungen aus Fahrlässigkeit begangen worden ist, so tritt Freiheitsstrafe bis zu einem Jahr oder Geldstrafe ein. Abs. 2: Strafflosigkeit tritt ein, wenn der Täter die falsche Angabe rechtzeitig berichtigt. Die Vorschriften des § 158 Abs. 2 und 3 gelten entsprechend.

Ort und Datum

Unterschrift